RADON-222 POTENTIAL IN TILLS OF HALIFAX, NOVA SCOTIA

by

Kelsey Elizabeth O'Brien

Submitted in partial fulfillment of the
requirements for the degree of
Master of Science

at

Dalhousie University
Halifax, Nova Scotia
August 2013

My thesis is dedicated to my best friend and partner: Nigel.
This project could never have been completed without your unwavering love and support.
Thank you for coming on this adventure with me.

Table of Contents

List of Tables

List of Figures

Abstract

The relative contributions of bedrock geology, radiometric uranium, till permeability and surficial geology were assessed as predictors of radon in indoor air in the Halifax Regional Municipality (HRM), NS, Canada. Bedrock geology and radiometric uranium were statistically significant predictors (14.4%) of indoor radon, based on available indoor radon data. Permeability was not among the predictors, which was surprising given its importance in past studies. In a follow up field analogue study done in laboratory columns, the permeability and diffusivity, as gas transport mechanisms, were found, as suspected, to be important drivers on the concentrations of radon-222 detected. Given the variable thickness of till in the HRM (< 0.5 m to > 3 m), these experiments highlighted the significance of till thickness, composition, and permeability in predicting the radioactive radon-222 potential.

List of Abbreviations and Symbols Used

°C	Degree celsius
%	Percent
©	Copyrighted
1D	One dimensional
2UW	Two un-weighted
2W	Two weighted
4UW	Four un-weighted
4W	Four weighted
AGRS	Airborne gamma ray spectrometry
ANOVA	Analysis of variance analysis
Bq	Becquerel
BRT	Beaver River Till
CCFZ	Cobequid-Chedabucto fault zone
cm	Centimetre
CO_2	Carbon dioxide
DA	Dissemination area
DNA	Deoxyribonucleic acid
eU	Equivalent Uranium
FGL	Fine-grained leucomonzogranite
GIS	Geographic Information Systems
GPS	Global positioning system

GS	Green Street
He	Helium
HRM	Halifax Regional Municipality
IDW	Inverse distance weighted
IS	Inert sand
kBq	Kilobecquerel
km	Kilometre
m	Metre
mg	Milligram
mL	Millilitre
mol	Mole
mV	Millivolt
N	Nitrogen
n	Number of samples
nA	Nanoampere
NASGLP	North American soil geochemical landscape project
NRCan	Natural Resources Canada
NS	Nova Scotia
NSDNR	Nova Scotia Department of Natural Resources
OLS	Ordinary least squares
per. com.	Personal communication
Po	Polonium
ppm	Parts per million

PSI	Pound per square inch
PVC	Polyvinyl choride
Q1	Quartile 1
Q3	Quartile 3
Rn	Radon
s	Second
SMB	South Mountain Batholith
SRP	Soil radon potential
st dev	Standard deviation
U	Uranium
VIF	Variance inflation factor
VOI	Variable of interest

Acknowledgements

I am extremely grateful to the following people and organizations: Terry Goodwin (formerly Nova Scotia Department of Natural Resources, currently Imperial Soil Limited, Fort McMurray) for continuous support, expert advice, and paper reviews. George O'Reilly (Nova Scotia Department of Natural Resources) for uranium expertise and assistance collecting bedrock samples. John Gosse (Dalhousie University) for expertise and assistance collecting till samples. Ken Ford, Peter Friske, and Rick McNeil (Geological Survey of Canada) for the generous use of the soil sampling equipment, and the Radon JOK Portable Permeability Machine. Nick Nickerson (St Francis Xavier) for invaluable modeling help and guidance. Charlie Walls (Dalhousie University) for GIS help, and an introduction to interpolation. Jennifer Grek Martin (Dalhousie University) for cartography suggestions and map reviews. Paul Hill (Dalhousie University) for assistance and use of soil sieving facilities. Yoko Yoshida (Dalhousie University) for statistics consulting and input. Ian Spooner (Acadia University) and Rebecca Jamieson (Dalhousie University) for constructive reviews and edits. And, of course, my supervisors: Dave Risk and Daniel Rainham, and my committee member: Anne Marie O'Beirne-Ryan.

I would also like to thank my friends for providing me with much needed distraction during my thesis, and helping me keep my sanity.

Finally, and most importantly, a big thank you goes out to my family. I am so appreciative of the constant encouragement and love you have shown me through this whole process.

Chapter 1

Introduction

1.1 General Introduction

As Nova Scotia has been documented as having some of the highest radon potential category within Canada (Chen et al., 2008a), there is a need for statistically weighted indoor radon potential maps for the Halifax Regional Municipality. This study optimizes and quantifies the radon potential predictors: bedrock geology, till geochemistry, airborne radiometric uranium, and till permeability, with respect to an indoor radon database. Field analogue soil column experiments were created to quantify the permeability, diffusivity, and radon gas concentrations through a variety of moisture conditions within the fine-grained leucomonzogranite phase of the South Mountain Batholith. As a result, this thesis measures radon gas trends on both a local scale (through till) and on a county scale (across the HRM).

1.2 What is Radon?

Radioactive radon-222 (half-life 3.82 days) is a daughter product in the uranium-238 decay series. Radon is a naturally occurring colourless, odorless, and tasteless noble gas. As uranium-238 (half-life 703.80 million years) decays through the series, it produces many daughter products, emitting either alpha, or beta, or gamma radiation in the process. One of the daughters, radium-226 (half-life 1590 years), decays to the inert radon-222, which in turn decays to polonium-218 (3.05 minutes), releasing an alpha particle. The uranium-238 chain ends in stable lead-206. (Figure 1.1). Under specific conditions, both radium and radon are soluble in water.

Radioactive radon-220 gas, known as thoron (half-life 55.60 seconds), is a direct daughter product from the thorium-232 series (half-life 14.05 billion years). Thoron is a daughter product of radium-224 (half-life 3.60 days), and decays to polonium-216 (half-life 0.14 seconds) releasing an alpha particle in the process. The final stable

lead-208 ends the thorium-232 chain. (Figure 1.2).

Radon and thoron are produced wherever uranium and thorium are naturally present: in rocks, till, and groundwater. As a result of thoron's extremely short half-life, it often decays before reaching the surface to be detected. Because of this, radon-222 is a more significant source of radon than radon-220, and is therefore the focus of this study.

1.3 Why is Radon an Issue?

Radon-222 gas is a major health issue; long-term inhalation of radon gas is the second highest cause of lung cancer in North America after smoking (WHO, 2005). The alpha particle released during the decay of both radon-222 and polonium-218 damages the lung tissue's DNA (Selinus et al., 2005). As there is limited research on the health effects of short-term radon-222 on the body, radon is primarily a health issue when it accumulates over time. Concentrations of radon gas in ambient air (the atmosphere) are insignificant (average of roughly 10.8 Bq m^{-3}, (ASTDR, 2012)). However, radon gas can accumulate indoors, and for this reason, Health Canada has established an indoor guideline of 200 Bq m^{-3} (where a Bq is an SI unit of measurement describing the number of disintegrations per second). The World Health Organization has an indoor radon guideline of 100 Bq m^{-3}, with an upper limit of 300 Bq m^{-3} (WHO, 2005). The reference level in the United States of America is 150 Bq m^{-3}, and internationally, individual countries in the European Union have guidelines ranging from 200 Bq m^{-3} to 400 Bq m^{-3}.

While radon gas inhalation is a major human health risk, radon can also affect human health through other pathways. Radon dissolves in water, and can potentially pose a health threat in drinking water (HC, 2012); high levels in drinking water are found in regions of high radon soil gas (as explained by Parsons (2007)). Recent studies from Health Canada suggest that the main health risk associated with radon comes from inhalation (radon in air) not from ingestion (radon in drinking water) (HC, 2012).

1.4 Radon's Connection to Geology

The radon gas present in indoor air comes predominantly from the underlying geological materials: for example, the bedrock, and/or the glacial till (Miles and Ball, 1996; Miles and Appleton, 2005; Kemski et al., 2006). Many different factors can affect the radon gas concentrations within a building, including: the building age, construction details (e.g. insulation and finished vs. unfinished basement), and time of year. However, regardless of home construction, a dominant predictor is the underlying geology (Shi et al., 2006).

There are many ways that radon soil gas can infiltrate a building (Figure 1.3). Radon soil gas can enter through cracks in foundations or walls, dirt floors, and any gaps around windows or piping (Friske et al., 2010; HC, 2012). As radon is soluble in water, it can also travel through the groundwater and seep into wells. The gas enters the home through the water supply (i.e. shower, tap, washing machines, kitchen sinks). Because it is *more* soluble in air, radon becomes airborne once it leaves the faucet. The process is accelerated if the water is 'agitated' (e.g. shower faucet) (Je, 1998b). Though concentrations of radon in the water may not be high, this can significantly increase concentrations of radon in indoor air (HC, 2010a).

All rocks contain varying levels of naturally occurring uranium. Certain rock types, predominantly granites, organic-rich slates/shales, and organic-rich sandstones have been documented as having elevated measured uranium (Je, 1998a); shale is considered organic-rich when there is a greater than 2% organic carbon content (Otton et al., 1993). In igneous rocks, higher silica content can correlate with higher uranium content (Keppler and Wyllie, 1990). Therefore, granites generally have higher uranium values than diorites or basalts. Uranium in rocks and tills is typically found as oxides (such as uranite), as well as in apatite and zircon (Selinus et al., 2005). The dominant expelling force of radon from a radium mineral is the alpha recoil from the grain surface. As radium decays to radon, the alpha particle and newly created radon nucleus are ejected in opposite directions (Otton et al., 1993). That recoil ejection pushes the radon daughter atom away with force (Figure 1.4). Both the location of the radium atom within the mineral and the direction of recoil can determine if radon is released from the grain into a pore space.

Secular equilibrium occurs in a radioactive system when the production rate is

equal to the decay rate. The ultimate parent of radon, uranium-238, has a 'much longer half-life than the intermediate nuclides (Bourdon, 2003). For the uranium decay series to be in secular equilibrium, the decay chain must be undisturbed for a period that is 6 times longer than the 'longest half-lived intermediate nuclide' (Bourdon, 2003). There are many ways a system can be disturbed. Chemical processes can disrupt a system, such as: 'phase change, partial melting, crystallization, partitioning, dissolution, adsorption, degassing, oxidation/reduction, and complexation' (Bourdon, 2003). Radioactive decay (such as recoil effects) can also impact the system's equilibrium.

Because of its relatively short half-life, the presence and concentration of radon in indoor air is dictated by gas transport mechanisms. Diffusivity and convection are the two major processes for general gaseous transport (Hillel, 1998). Though they are both key contributors, it has been shown that diffusion (or permeability), rather than convection, is the primary mechanism of soil aeration (Keen, 1931; Penman, 1940; Russell, 1952; Ball et al., 1999). Therefore, for radon soil gas movement, the most significant control is the diffusivity of the tills. As a result of the solubility of radon, the moisture content can also affect transit of the gas (Selinus et al., 2005, 254).

Diffusivity is characterized by diffusive flux moving particles from areas of high concentrations to areas of low concentrations. It essentially describes the amount of substance (radon gas) moving over a given area in a set period of time. Diffusivity is defined by Fick's First Law, as seen in Hillel (1998):

$$J = -D\frac{\partial \phi}{\partial x} \tag{1.1}$$

Where:

J is the diffusion flux

D is the diffusion co-efficient, or diffusivity

ϕ is the concentration in dimension of [(amount of substance) length $^{-3}$]

x is the position [length]

Permeability has also been shown to predict the radon gas release from a source (Nazaroff, 1992). Typical permeability values for soils, silts, and sands can be seen in Figure 1.5 Nazaroff (1992).

Permeability describes the transport of a fluid (in this case gas) through a body

by advection. It can be defined by Darcy's Law as (Nazaroff, 1992):

$$v_D = -\frac{k}{\mu}\nabla P \tag{1.2}$$

Where:

v_D is the superficial flow velocity vector

k is the soil permeability

μ is the dynamic viscosity of the fluid

∇P is the gradient of the dynamic pressure

There have been several ways to measure the in-situ permeability. The most commonly used across Canada is a soil probe (Ford et al., 2001; Friske et al., 2010; Goodwin et al., 2009; Chen et al., 2008b). The radon gas permeability of the till at depth can be defined in terms of probe measurements (Damkjaer and Korsbech, 1992):

$$Q = F\frac{k}{\mu}P \tag{1.3}$$

Where:

Q is the air flow from the probe

F is the shape factor of the probe (dependent on the probe head and depth below surface)

k is the soil permeability

μ is the dynamic viscosity of the air

P is the pressure difference between probe head and surface

Though soil gas transport is not known to be directly controlled by permeability, diffusivity and permeability are proxies for one another, and are proportional (Washington et al., 1994). As both are a measure of air-filled pore spaces, the co-efficients of bulk diffusivity and gas permeability have a strong positive linear relationship; this relationship can be defined by the equation (Washington et al., 1994):

$$logD_{b,g} = 2.47 + 0.53logk - logM_g^{0.5} \tag{1.4}$$

Where: D is the diffusion co-efficient

k is the permeability

M is the mass of the gas of interest

This equation provides a way to estimate the gas diffusivity given the permeability, as diffusivity is difficult to measure in the field (Risk et al., 2008). As both diffusivity and permeability are rarely measured at the same site, this equation provides a reasonable alternative to direct measurement.

The moisture content of tills has a less significant impact on the radon gas transport (Washington and Rose, 1990). Adding water to a till body effectively blocks available air filled pore spaces in which radon travels. In low-moisture tills, the water is predominantly found on the grain surfaces and filling small pore spaces. In high-moisture tills, however, water fills the larger pore spaces, thus reducing the diffusion co-efficient of the tills (Nazaroff, 1992). Holkko and Liukkonen (1992) showed that the diffusive co-efficient increases in moist tills compared to dry tills. Further work needs to be done to refine the exact relationship between radon diffusion and soil moisture, as there is conflicting previous work (e.g. Nazaroff (1992) and Holkko and Liukkonen (1992)). The moisture content of till has been shown to affect the concentration of radon measured (as well as the diffusivity and permeability values), therefore it important to consider the water content of the till.

Gas transport mechanisms and underlying geology are key predictors of radon gas concentrations in indoor air. Where the underlying rocks or soils have superimposed features that enhance radon gas transport (i.e. fractures in bedrock), not only are gaseous transport mechanisms acting on the till, but they are also affecting the bedrock. It has been shown that there are higher concentrations of radon soil gas where the bedrock is fractured, as the gas can travel more easily through the cracks (Je, 1998a).

1.5 Why is Radon in Nova Scotia of Concern?

Nova Scotia has been identified as a high natural radon and/or equivalent uranium region as a result of the underlying bedrock geology (Chen et al., 2008a; Goodwin et al., 2010; O'Reilly, 2008; Jackson, 1990; Lewis et al., 1998; Grantham, 1986; Dyck et al., 1976). Nova Scotia's geology can be divided into the northern Avalon Supergroup and the southern Meguma Supergroup, separated by the Cobequid-Chedabucto fault zone (CCFZ) (summarized by (MacHattie and O'Reilly, 2008)).

Radon gas can be found in measurable quantities throughout Nova Scotia, especially in the Meguma terrane (Goodwin et al., 2008); this study will focus on the Halifax Regional Municipality (HRM) region (part of the Meguma terrane), as this is where approximately 42% of Nova Scotia's population resides.

The most commonly documented regions of high radon gas concentration occur south of the CCFZ. These regions are underlain by granite intrusions, slates, and metasandstones - units similar to those suggested by Je as being elevated in uranium (Je, 1998a).

HRM is underlain by four important geological formations: the Carboniferous Windsor Group, the Late Devonian South Mountain Batholith (SMB), and the Cambrian-Ordovician Halifax and Goldenville Groups (vs formations) (MacDonald and Horne, 1987; Keppie, 2006; White, 2010).

The Lower Carboniferous Windsor Group is dominated by marine evaporites (Lavoie et al., 1995); halite, anhydrite, dolomite and gypsum are the most common lithologies. The group is divided into five formations: the Macumber Formation at the base, Carrolls Corner Formation, Stewiacke Formation, MacDonald Road Formation, and the Green Oaks Formation at the top (Boehner et al., 2002).

The Devonian South Mountain Batholith is a granitic plutonic complex that intruded the Meguma Terrane around 380 - 373 Ma (White et al., 2007). The SMB can be subdivided, based on its composition, into early monzogranite, coarse-grained leucomonzogranite and fine-grained leucomonzogranite (MacDonald, 1994; MacDonald and Horne, 1987). The 'light grey' monzogranite phase has abundant micas present (muscovite and biotite) and a slightly megacrystic (mostly alkali feldspar with lesser plagioclase) texture. The coarse-grained leucomonzogranite phase is 'predominantly light orange' in colour with abundant megacrysts, and also has muscovite with lesser biotite. The 'light pink' fine-grained leucomonzogranite (FGL) phase is variably porphyritic and equigranular, again with muscovite and lesser biotite present (MacDonald, 1994).

The South Mountain Batholith is a significant source of radon gas because the pluton is enriched in uranium. The most evolved phase of the SMB, the fine-grained leucomonzogranite has even higher radon as it contains the concentrated incompatible trace elements (i.e. uranium) (MacDonald et al., 1992).

The Cambro-Ordovician Halifax Group is dominated primarily by mudstone and siltstone (and their metamorphic equivalent: slate). It can be divided into two formations: the Cunard formation, and the upper Bluestone formation (White et al., 2007). The Cunard unit, when weathered, is visibly 'rusty' looking because of pyrite, pyrrhotite and arsenopyrite. The Bluestone unit has distinctive calcareous concretions (White, 2002; Jamieson et al., 2012).

The Cambrian to Early Ordovician Goldenville Group is dominated by thick metasandstone beds. The group can be further subdivided into the Tancook formation, the New Harbour formation, and the upper Beaverbank formation (White, 2002, 2010). The Tancook member ranges from low to high metamorphic grade (Hicks et al., 1999). The low grade member is comprised of meta- silt and sandstones with calcareous nodules present; the higher grade member includes andalusite-staurolite to garnet-sillimanite schists (White, 2002). The New Harbour formation is defined by thick light grey beds of metasandstone and green metasiltstone. The uppermost Beaverbank formation has characteristic manganese nodules.

Some of the surficial units across the HRM are significant in terms of radon potential, as they are derived from the local bedrock. As the local bedrock has documented high radon potential, the till should be also critically analyzed. There are two major tills in the HRM: the Lawrencetown Till and the underlying Beaver River Till (BRT) (Stea and Fowler, 1979; Goodwin, 2002). The Lawrencetown Till (Stea and Fowler, 1979) is a distally derived clay-rich till that generally has a reddish colour and is found primarily in ground moraine (8-35 m thick) and drumlins (max: 25 m thick) through the HRM (Stea and Fowler, 1979). Foreign clasts are predominantly derived from the Antigonish Highlands and the Cobequid Mountains (Stea and Fowler, 1979). The Beaver River Till is derived from the local HRM bedrock. As such, it can be broken into three major phases associated with the bedrock assemblages: metasandstone phase, granite phase and slate phase (Stea and Fowler, 1979).

The metasandstone phase till (formerly named the quartzite till) is derived from the Goldenville Group metasandstone (Stea and Fowler, 1979). The till phase is therefore bluish-grey in colour and has abundant metasandstone clasts; it occurs generally as ground moraine overlying the associated Goldenville bedrock. Though it

can be up to 20 m thick, it averages 3 m thick around the HRM (Stea and Fowler, 1979). The granite phase till is derived from the local South Mountain Batholith; it is yellow-grey in colour and has angular SMB clasts throughout the stony matrix (Finck and Graves, 1987). The granite phase occurs predominantly as a thin hummocky ground moraine: the thickness is 2 m on average (Stea and Fowler, 1979). The slate phase till is light brown/grey in colour and has a sandy matrix. The angular clasts are from the associated Halifax Group slate, and the phase generally forms ground moraine over the local bedrock (Finck and Graves, 1987). The slate till is also thin with a maximum thickness of 4 m (Stea and Fowler, 1979). Local bedrock outcrops with ice flow indicators (i.e. striations) show that two dominant ice flow directions affected the HRM area: the older directed to the southwest and the younger directed to the southeast (Finck and Graves, 1987).

1.6 Radon Investigations in Nova Scotia

Radon soil gas had been studied extensively in Nova Scotia (Goodwin et al., 2009, 2010; O'Brien et al., 2011). There have also been many studies examining uranium levels across the province (Dyck et al., 1976; O'Reilly et al., 2009a; DPME, 1982; Grantham, 1986), but as the more recent work focuses specifically on radon, the recent work (Goodwin et al., 2009, 2010; O'Brien et al., 2011) comprises the dominant investigations. Some of the most recent radon research includes a provincial study undertaken in 2007 as part of the North American soil geochemical landscapes project (NASGLP) (Friske et al., 2010). Radon soil gas measurements across Nova Scotia (1 sample every 1600 km^2) showed the highest radon soil gas regions (60 - 207 kBq m^{-3}) associated with the SMB (Goodwin et al., 2008). Because part of the SMB is within the HRM, there was an interest in further understanding the radon gas distribution (Goodwin et al., 2009). In the summer 2009 field season, additional sites were sampled to increase the sampling density of 1 sample every 800 km^2 (Goodwin2009b). The results from the two studies showed that the highest radon-producing bedrock and associated overlying till in the HRM was the SMB (not broken into phases) and overlying till (mean: 54.1 kBq m^{-3}). The SMB also contained the highest soil radon potential (SRP) index (43.6); the SRP correlates the soil gas radon with the till permeability to predict indoor radon (Neznal et al., 2006).

However, there was significant variability within the measured radon values in the respective geological units (Goodwin et al., 2009). A follow up by O'Brien et al. (2011) included the sampling of additional sites within the HRM in which the SMB was subdivided into its three compositional phases: monzogranite, coarse-grained leucomonzogranite and fine-grained leucomonzogranite. The monzogranite had an average mean radon concentration of 44.3 kBq m^{-3}, the coarse-grained leucomonzogranite samples had an average of 50.2 kBq m^{-3}, and the fine-grained leucomonzogranite measured the highest concentration of radon averaging 51.0 kBq m^{-3} (O'Brien et al., 2011). These results indicate that the fine-grained leucomonzogranite phase is the highest radon-producing unit within the HRM.

There have been several recent till permeability studies in Nova Scotia (Goodwin et al., 2009, 2010; O'Brien et al., 2011). In-situ field permeability values were reportedly measured as part of the North American soil geochemical landscapes project (NASGLP) across the province (Goodwin et al., 2008). However, when the results of the sampling were released in 2009, the permeability values were not reported, only the soil radon potential index values (calculated from the permeability values). In Goodwin et al. (2010), permeability values for the surficial geology units of the HRM were released (Figure 1.9). The clay-rich Lawrencetown Till had the lowest mean permeability (3.73 x 10^{-12} m^2), and the sandy metasandstone phase till had the highest average permeability (8.61 x10-^{11} m^2; Goodwin et al. (2010)). O'Brien et al. (2011) presented the average permeability values for the till units of the HRM, this time sub-dividing the granite phase till into monzogranite, coarse-grained leucomonzogranite and fine-grained leucomonzogranite. Similar to the Goodwin et al. (2010) work, the Lawrencetown Till had the lowest geometric mean of permeability and metasandstone phase till had the highest permeability (O'Brien et al., 2011).

Though there are several suggested methods of calculating diffusivity (or diffusive constants) in the field (Jellick and Schnabel, 1986; Rolston et al., 1991), it is difficult to obtain accurate in situ measurements (Risk et al., 2008). The HRM is lacking field diffusivity measurements for the major surficial geology units. Recent diffusivity values were calculated using a one-dimensional (1D) model of the radon concentration profile through inert sands (Figure 1.10) (O'Brien et al., 2011). However, the limitations of this approach required that additional work should be done using

measured field analogue tills to provide more accurate values that account for radon production in the till.

Nova Scotia has been previously described as a region with high potential for radon in indoor air. A map of Canada was released in 2008 that showed Manitoba, Winnipeg, and Nova Scotia to be among the regions with the highest potential indoor radon concentrations in Canada (Chen et al., 2008a). This map (Figure 1.8) justified further radon potential mapping in the province.

A preliminary map of Nova Scotia divided the province into low-, medium-, and high-risk zones (Figure 1.11) (O'Reilly, 2008). The area of highest risk (according to population density and radon-producing potential) was the part of the HRM underlain by the South Mountain Batholith. This radon potential map was similar to previous airborne radiometric equivalent uranium survey maps (O'Reilly et al., 1988; Ford et al., 1998; Jackson, 1992), suggesting that the dominant control on the potential for indoor radon accumulation is the nature of the underlying rock and soil.

A more accurate radon prediction map might incorporate bedrock geology and airborne radiometric equivalent uranium, as well as the permeability and till potential. Such multi-variate maps (Kemski et al., 2009; O'Reilly et al., 2009b; Appleton and Miles, 2010; Appleton et al., 2011) overlay all the predictors, some even with weighting factors for each layer. The provincial government provides province-wide coverage for radon predictor layers such as bedrock geology, surficial geology, and airborne radiometric equivalent uranium.

Indoor radon values have also been used to predict radon potentials of a region within Nova Scotia (NS). 719 homes in NS were tested to better understand areas of high potential radon in indoor air; 12% of homes exceeded the United States environmental protection agency (US EPA) guideline (approximately 148 Bq m^{-3} in 1991) and 3% of homes exceeded approximately 740 Bq m^{-3} (Jackson, 1992). Some of the regions in Nova Scotia that were of interest included: Cheticamp (mean of 785.2 Bq m^{-3}; range of 14.8 - 5925.9 Bq m^{-3}), Halifax city (mean of 414.8 Bq m^{-3}; range of 14.8 - 814.8 Bq m^{-3}), Ingonish (mean of 429.6 Bq m^{-3}; range of 14.8 - 3629.6 Bq m^{-3}), and Lakeside (mean of 496.3 Bq m^{-3}; range of 14.8 - 1407.4 Bq m^{-3}) (all converted from pCi L^{-1}) (Jackson, 1990). In a one-year study across the country, Health Canada tested 296 homes throughout Nova Scotia; of those, 6.4% of homes

exceeded the 200 Bq m^{-3} guideline (HC, 2010b).

Twenty one workplaces across Nova Scotia were measured for indoor radon levels (Mersereau et al., 2013). The highest average indoor values occurred in St. Margaret's Bay (94.0 Bq m^{-3}; range of 39.1 - 169.1 Bq m^{-3}) and Coxhealth (98.6 Bq m^{-3}; range of 58.5 - 202.1 Bq m^{-3}; Mersereau et al. (2013)). The majority of indoor air studies identify the region of the HRM underlain by SMB bedrock as a region of high radon; these results correspond to the area underlain by rock and till with high radon production potential. As such, it appears to be possible to correlate bedrock geology and indoor radon in NS.

1.7 Gaps in Research

In June 2007, Health Canada reduced the indoor radon guideline from 800 to 200 Bq m^{-3}. Many homes that did not previously exceed the recommended guidelines now exceeded the limit. As a result, radon in Nova Scotia has been evaluated since 2007 and new maps are necessary to assess the potential for radon gas in indoor air.

The provincial government of Nova Scotia has accessible bedrock, surficial geology and airborne radiometric equivalent uranium surveys. However, there has yet to be a provincial study that statistically quantifies the importance of each predictor layer with respect to indoor radon values. A series of maps predicting the radon potential of a specific region using varying combinations of predictor layers and weighting factors would significantly improve the understanding of radon potential in Nova Scotia. There is a particular need for this type of integrative study in the HRM because of the population density, as it would provide the most beneficial radon exposure risk assessment for human health prediction.

There is also a lack of concurrent till permeability and diffusivity data for the HRM. As permeability and diffusivity have been proven to influence the transport of radon gas, they could be significant predictors in determining regions where radon has a high potential to infiltrate a building. Additionally, the effect of moisture on radon diffusion in tills in the HRM has yet to be studied, and could provide additional clarification into seasonal variations in indoor radon. Nova Scotia has a particularly rainy climate (approx. 90 mm / month of precipitation in the summer), and the effect of seasonal moisture on the local tills could significantly alter the amount of radon

gas that permeates to the surface.

1.8 Study Objectives

This study aims to satisfy the two overall goals, each with their own specific objectives:

1. To synthesize existing provincial datasets and create a series of radon prediction maps of the HRM based on statistically significant indicator layers.

   i) Quantify the statistical significance of each layer (bedrock geology, surficial geology, permeability, airborne radiometric equivalent uranium) with respect to indoor radon values within the HRM.

   ii) Identify trends in the spatial distributions between predicted potential high radon regions and available indoor radon data.

   iii) Compare findings and high risk regions with previous Nova Scotia potential radon maps.

2. To quantify radon gas transport mechanisms through field analogue models of the HRM's high radon geologic units

   i) Determine the controlling factor for the concentration of radon present at the till surface. Quantify the importance of till and production rate of the radon in HRM.

   ii) Determine if the radon measured at the till surface is produced predominantly in the overlying glacial sediments or the underlying bedrock.

   iii) Calculate experimental permeability and diffusivity values through the field analogues.

   iv) Examine if there is a positive linear correlation between permeability and diffusivity values (Washington et al., 1994).

   v) Compare the radon concentrations in 'dry' (field moisture before a rain event) tills to the radon concentration in 'wet' (field moisture after a rain event) tills to determine the effect of moisture regime on the HRM's tills.

1.9 Format of the Thesis

This thesis integrates aspects of geological, environmental, and human health perspectives.

Chapter 2 is entitled 'Optimizing the creation of radon potential maps using statistical analyses and GIS-based mapping of predictor layers'. It highlights four different approaches for creating a radon potential map of the HRM, and compares and contrasts these approaches. Chapter 3 is entitled 'Radon soil gas migration and transport through Halifax tills and bedrock, Nova Scotia', and characterizes the permeability, diffusivity, and radon gas levels through soil columns in the fine-grained leucomonzogranite phase of the South Mountain Batholith. Chapter 3 also represents a manuscript that is currently in review for publication with Environmental Earth Sciences, and therefore some repetition is unavoidable and acknowledged. Chapters 1 and 4 of the thesis are the overall introduction and overall conclusion, which introduce and synthesize the findings from Chapters 2 and 3, respectively.

The appendices present additional information regarding statistical analysis and sensitivity analyses results.

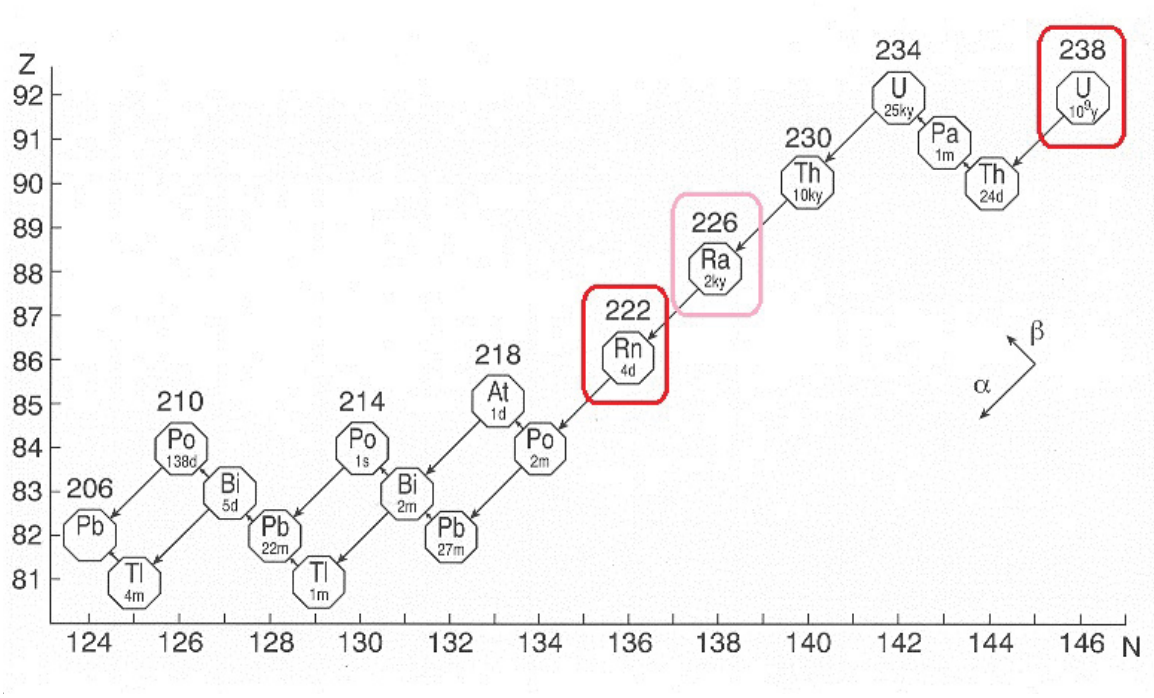

Figure 1.1: This figure depicts the uranium-238 decay chain, where Z is the atomic number and N is the number of neutrons. The half-life is also displayed in days (where 4d is equal to 3.82 days). Nuclides of interest are highlighted. Modified from the University of Maryland, Department of Physics. Source: `http://www.physics.umd.edu/lecdem/honr228q/notes/U238scheme.gif`.

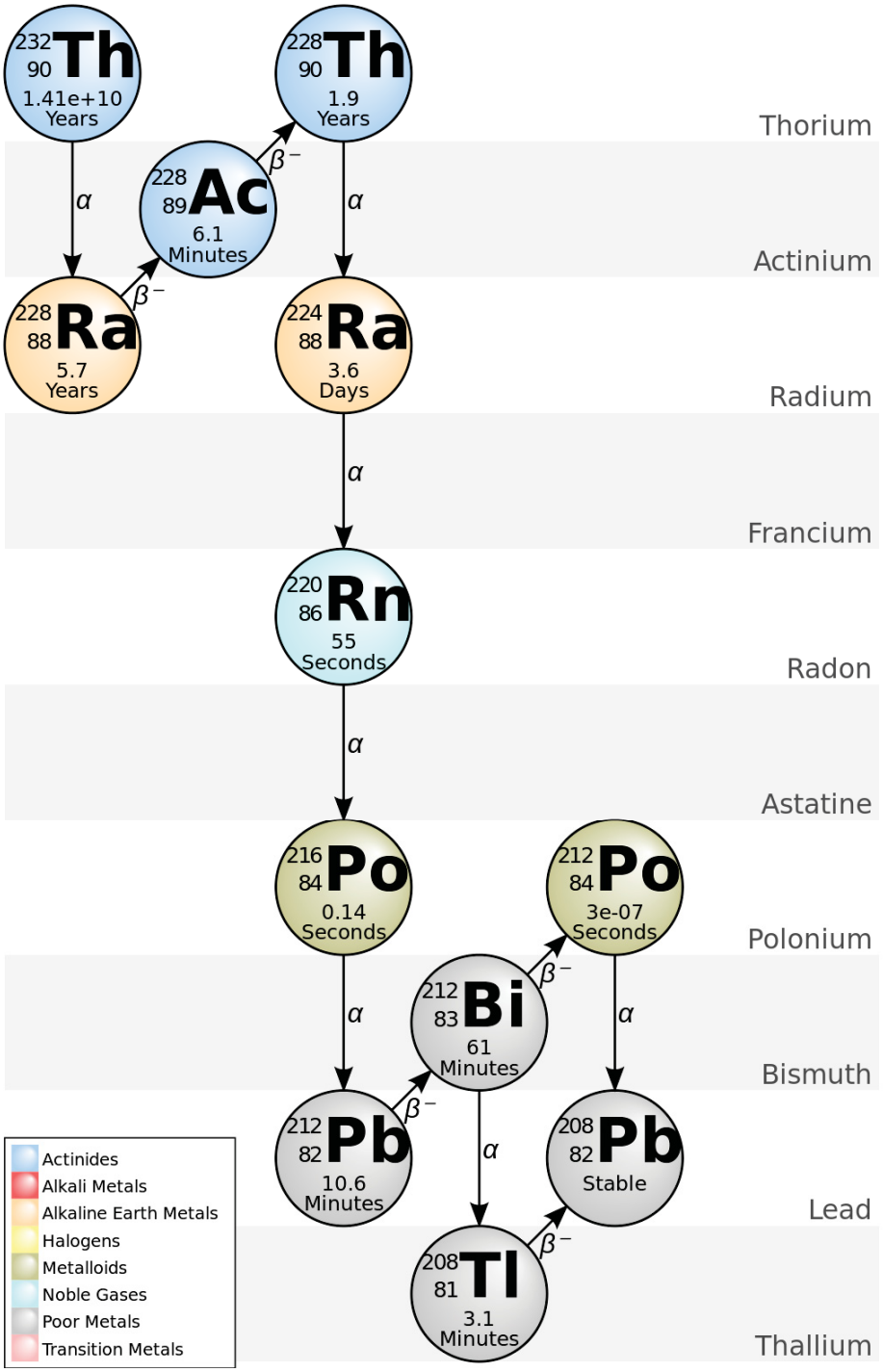

Figure 1.2: Thorium-232 decay series. Isotopes of note include: thorium-232, radium-224, radon-220, and polonium-216. Where a and b represent alpha and beta radiation. Source: `http://commons.wikimedia.org/wiki/File:Decay_chain(4n,Thorium_series).PNG`. Author: *BatesisBack*. Accessed: June 2013.

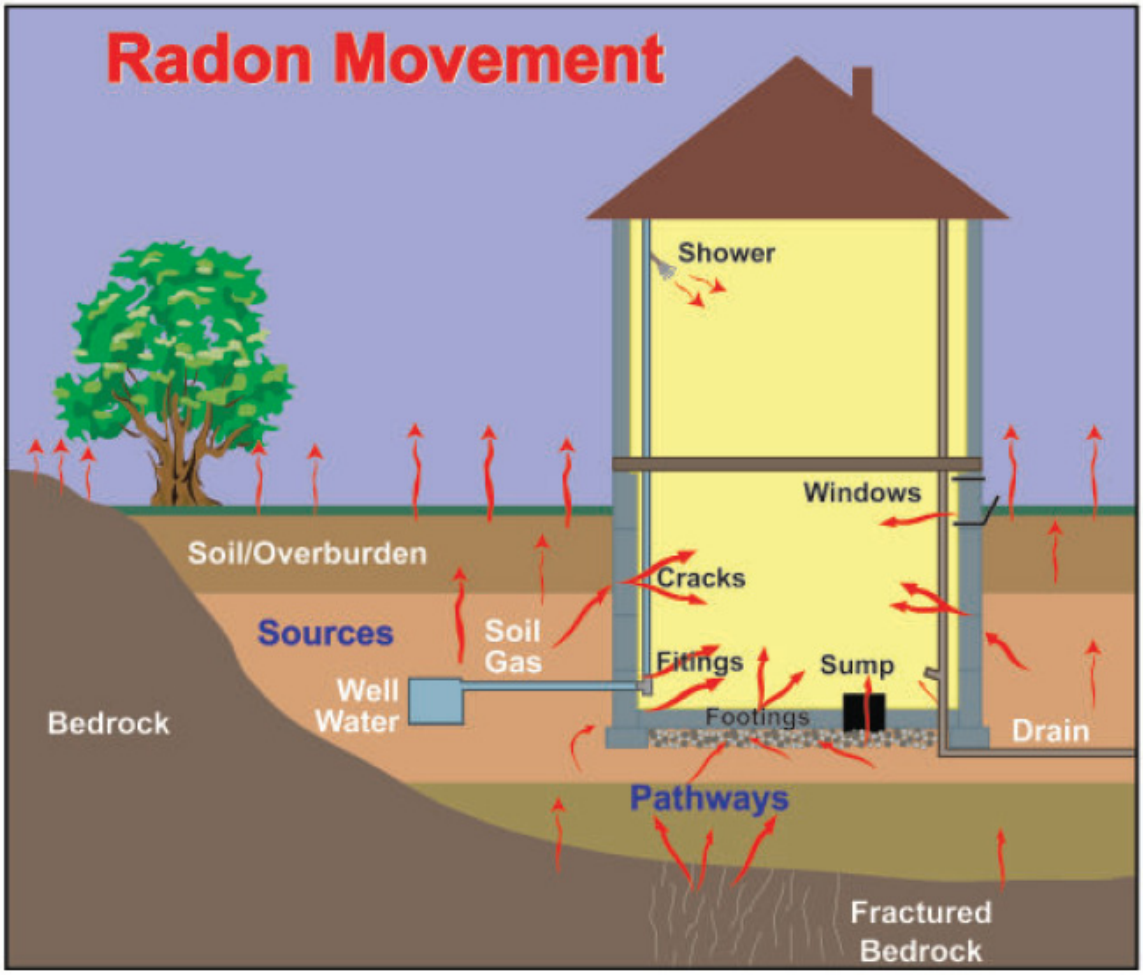

Figure 1.3: Radon pathways through the bedrock, till, overburden, and into indoor air. From Friske et al. (2010).

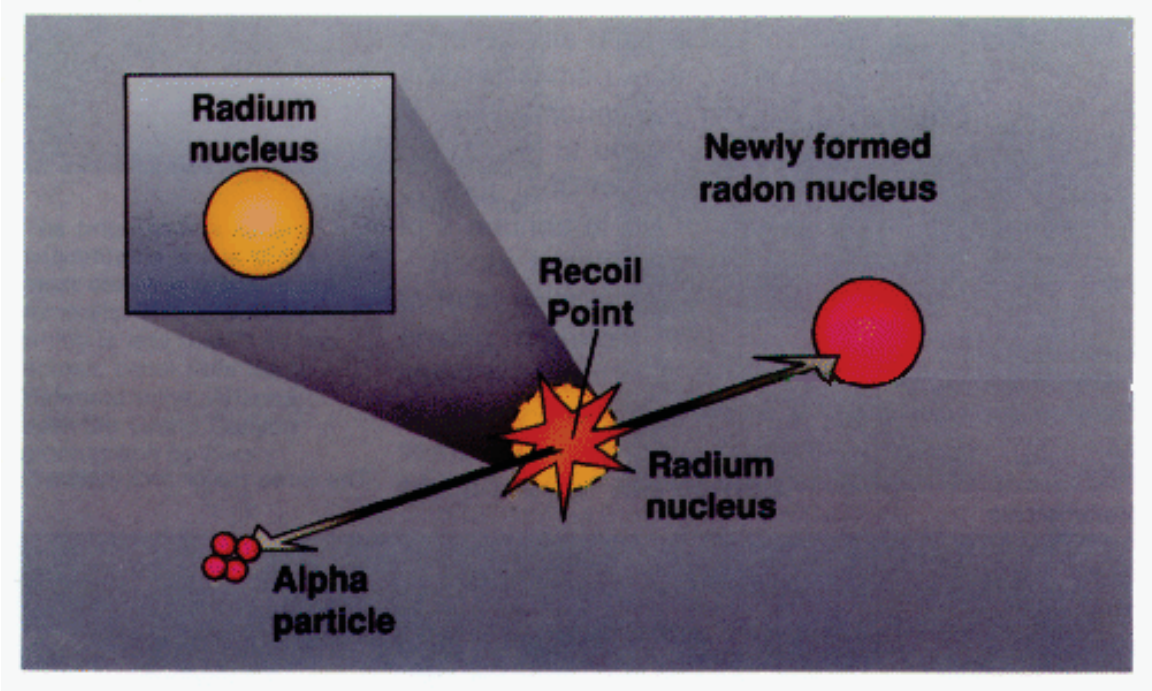

Figure 1.4: Alpha recoil of radon from the parent radium nucleus. From Otton et al. (1993).

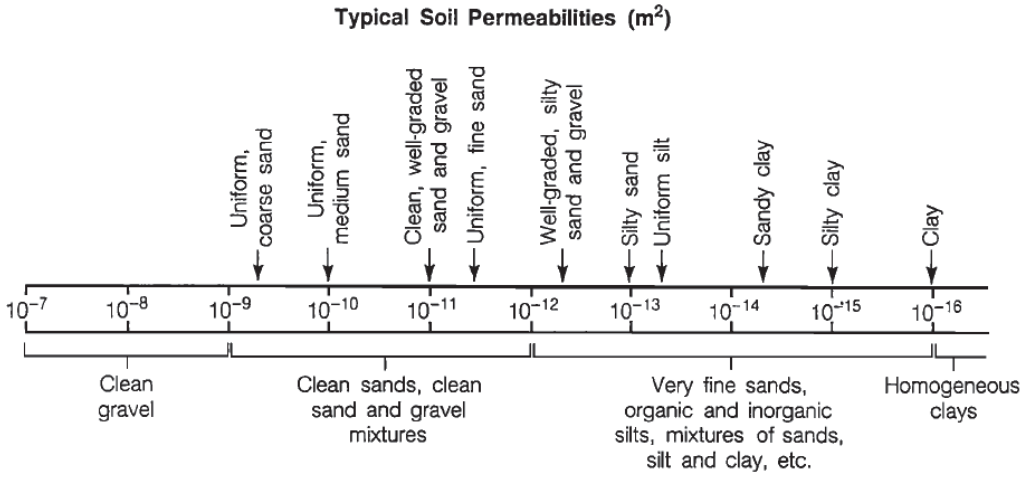

Figure 1.5: Permeabilities (m^2) for typical soil textures. From Nazaroff (1992).

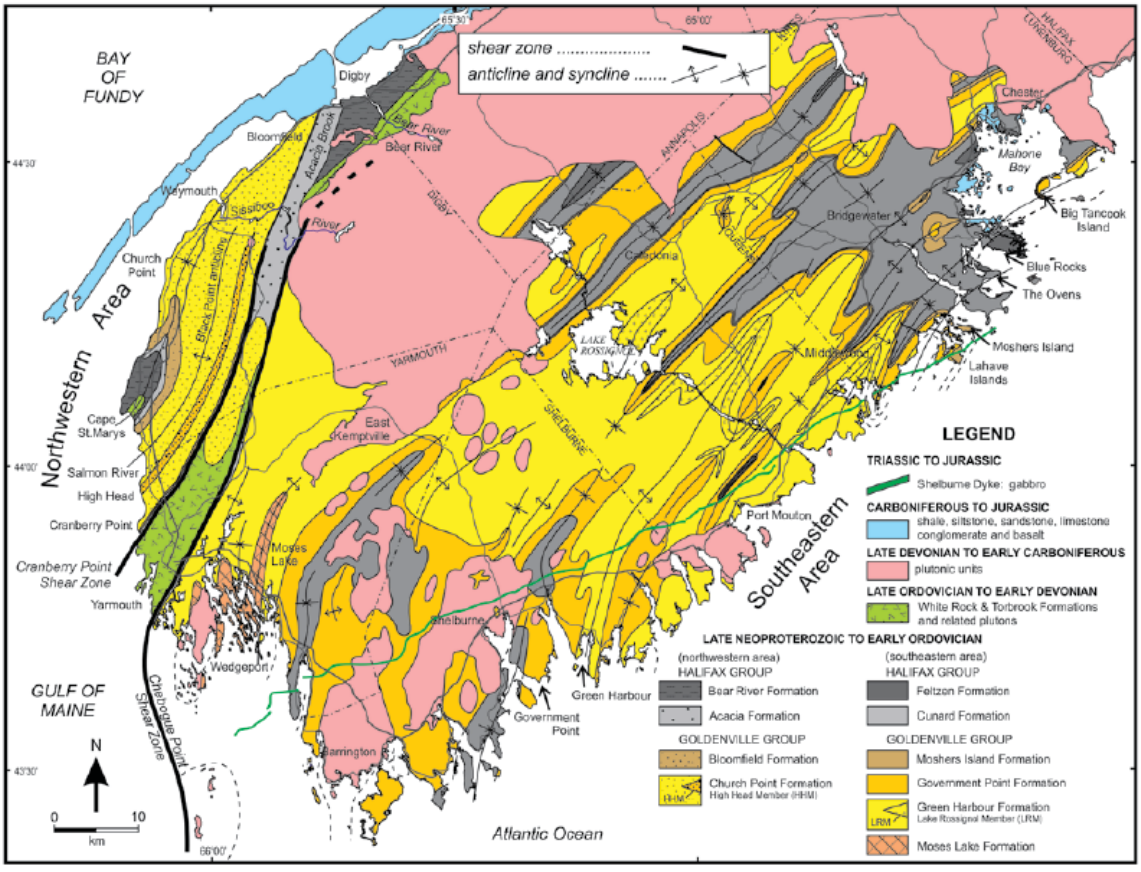

Figure 1.6: Bedrock geology of southern Meguma Terrane, Nova Scotia. From White (2010).

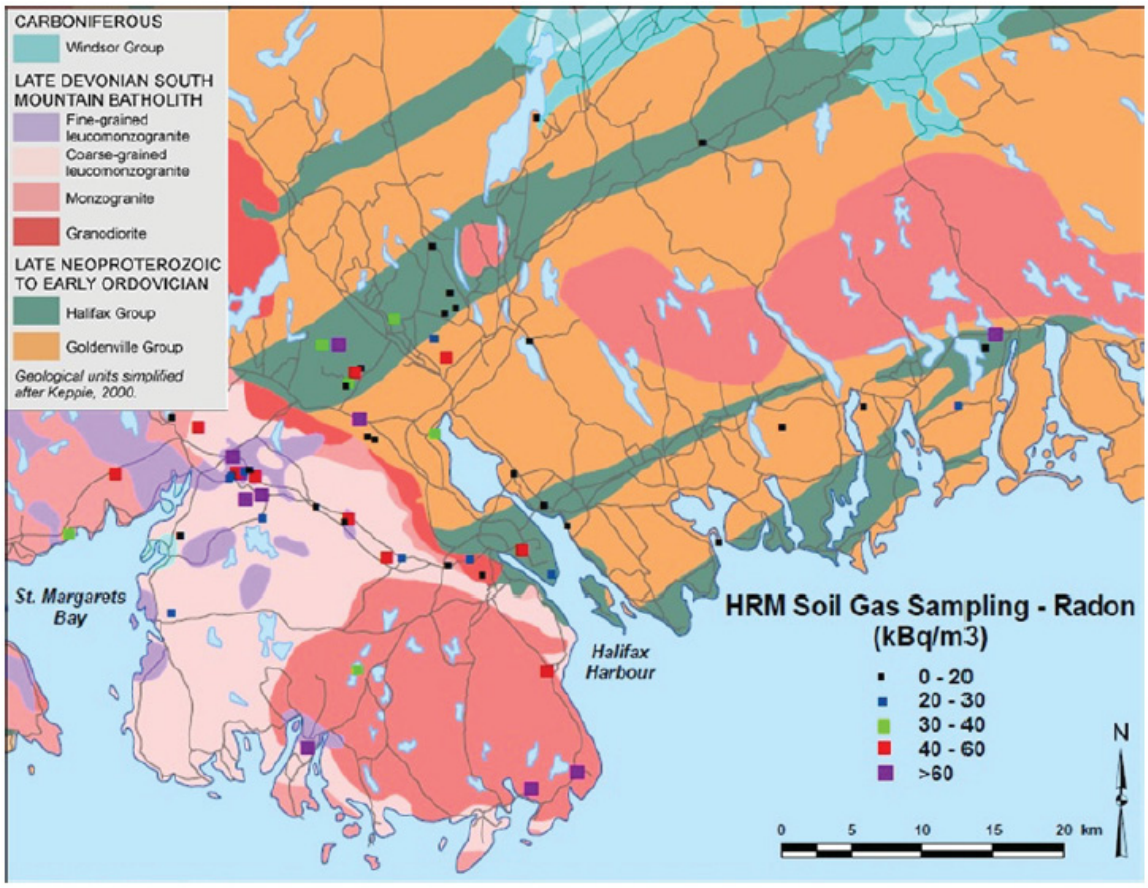

Figure 1.7: Radon soil gas sample locations and values (in kBq m^{-3}) within the HRM region. From O'Brien et al. (2011).

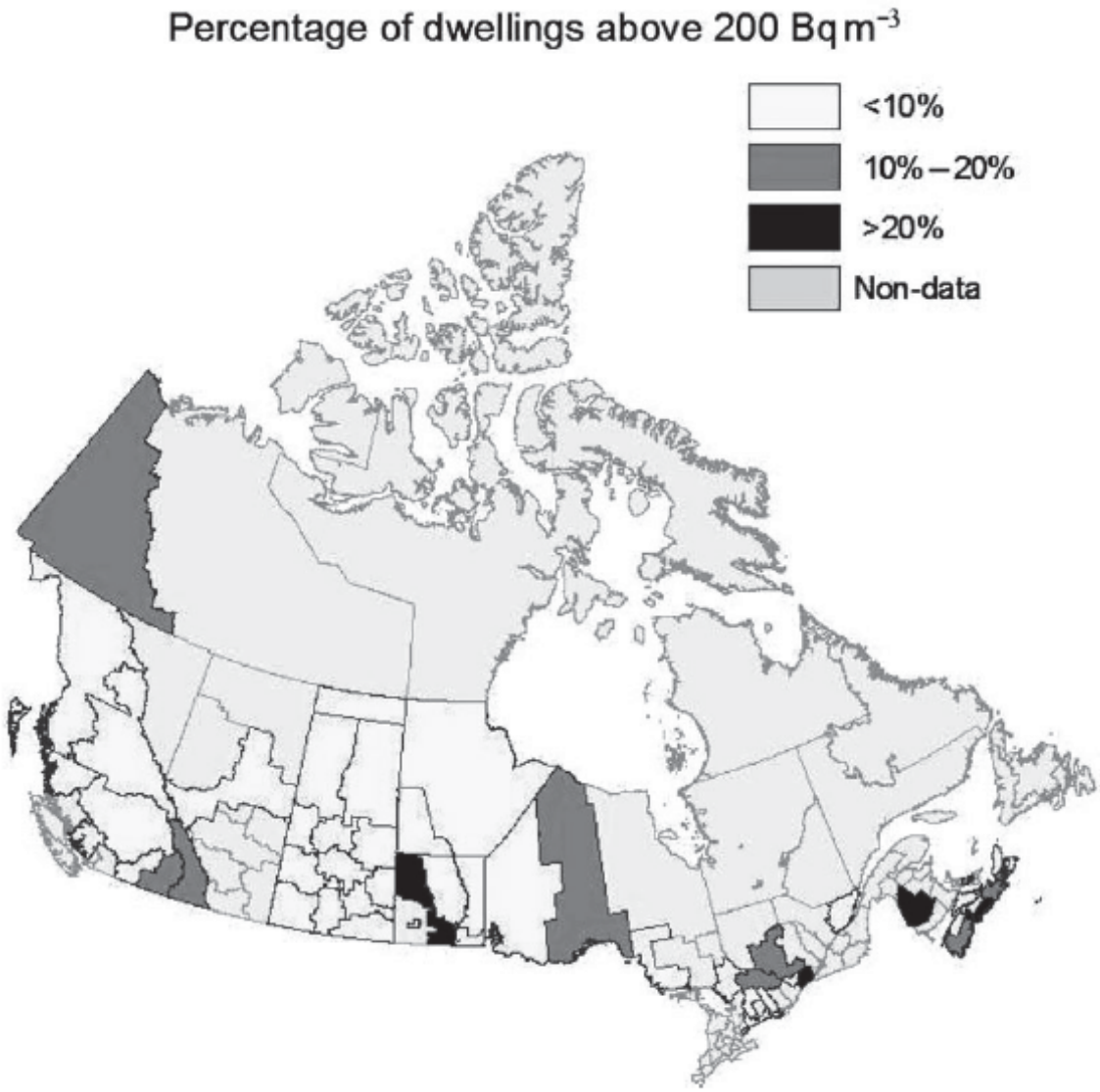

Figure 1.8: Potential map of Canada for radon-222 gas in indoor air. From Chen et al. (2008a).

Till Unit	n =	Min. (m^2)	Max. (m^2)	Mean (m^2)
Beaver River Till (BRT) (metasandstone facies)	10	1.455E-12	1.788E-11	8.61E-12
BRT (slate facies)	10	5.906E-13	1.561E-11	7.374E-12
BRT (granite facies)	30	4.490E-13	1.551E-11	5.770E-12
Lawrencetown Till	10	2.000E-14	1.1562E-11	3.729E-12

Figure 1.9: Permeability values for the major till units of the HRM (m^2). From Goodwin et al. (2010).

Diffusivity (m^2/s)	Production ($Bq/m^3/s$)	Concentration (0.6 m)
4.00E-07	10	2.39E+04
4.00E-07	25	5.98E+04
3.00E-07	50	2.14E+04
3.00E-07	100	4.28E+04
3.00E-07	1000	1.31E+04

Figure 1.10: Calculated diffusivities from 1D model of radon gas production (O'Brien et al., 2011). Production is of radon-222 for a reference depth of 0.6 m.

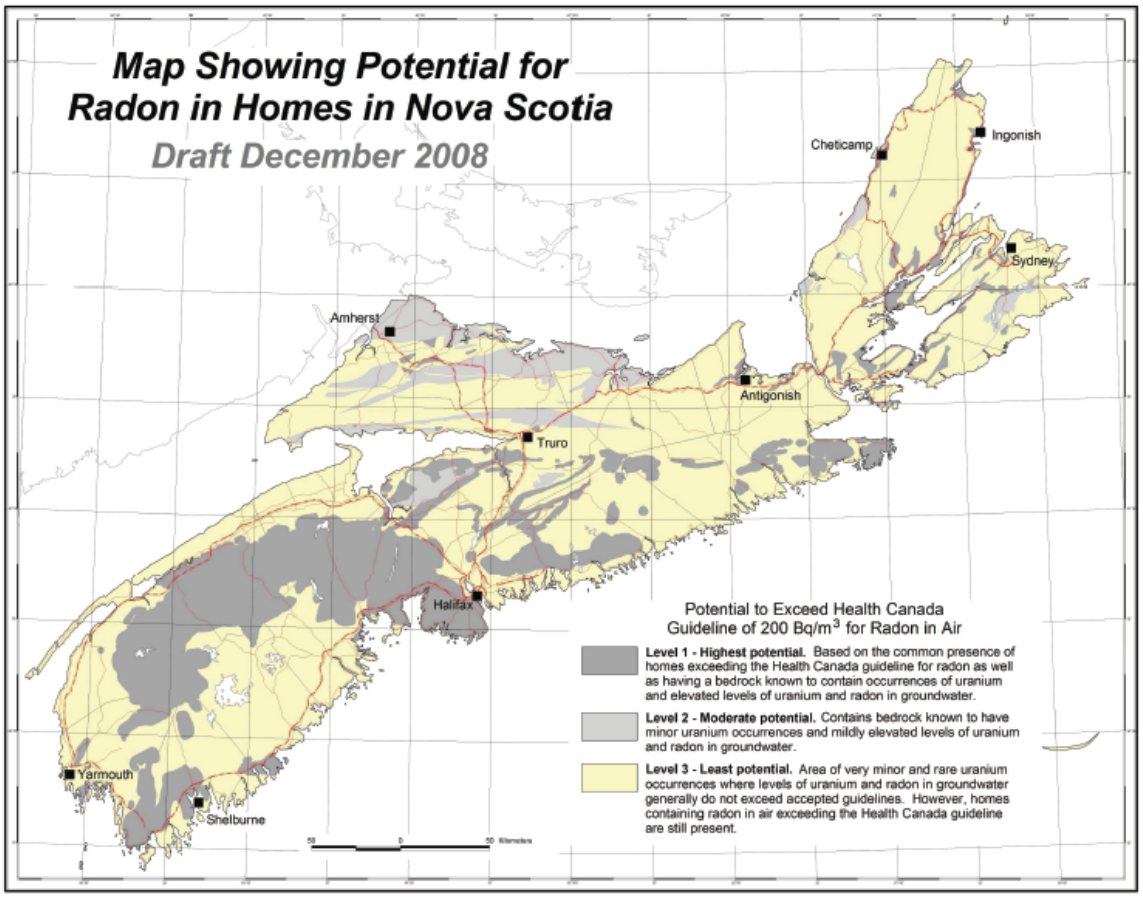

Figure 1.11: Radon potential map of Nova Scotia for indoor air. From O'Reilly (2008).

Chapter 2

Optimizing the Creation of Radon Potential Maps using Statistical Analyses and GIS-Based Mapping of Predictor Layers

2.1 Preamble

This chapter presents a series of radon prediction maps for consideration. I was the principal investigator for the project and did the literature review, synthesized previously collected data, conducted the Geographic Information Systems (GIS) , and ran and interpreted all statistical analyses.

2.2 Introduction

2.2.1 Radon as a Health Problem

Radon potential risk maps have been developed to identify locations with varying probabilities of radon exposure. Nova Scotia (NS), due to its bedrock geology, has been identified as having high radon and associated uranium concentrations (Dyck et al., 1976; O'Reilly et al., 2009a; Grantham, 1986; Chen et al., 2008a; Goodwin et al., 2009). High radon concentrations are of particular concern in the Halifax Regional Municipality (HRM) as it is the most populous region in Nova Scotia. Geology has been previously identified as being one of the controls on indoor radon concentrations (Miles and Ball, 1996; Miles and Appleton, 2005; Kemski et al., 2006). Though home construction can influence the infiltration and buildup of radon gas, the underlying surficial and bedrock geology is still the probable dominant control (Shi et al., 2006). Major predictors for radon in indoor air include, but are not limited to: bedrock geology, surficial geology, permeability, and airborne radiometric equivalent uranium (O'Reilly et al., 2009b; Kemski et al., 2009). However, there has been no map in Nova Scotia determining the statistical correlation of each of these predictors with

respect to a measured indoor radon database. Such a map would help to predict the relationship between geological measures of radon probability and concentrations of radon indoors.

2.2.2 Mapping Radon Potential

Radon potential maps exist for several countries (e.g. United States, Germany, Canada, and Northern Ireland) (USEPA, 1993; Dubois, 2005; Kemski et al., 2009; Chen et al., 2008a; Appleton et al., 2011). Methods for establishing indoor radon potential incorporate various data layers to predict the potential in the region. The predictor variable sets used include: i) indoor radon, geology, aerial radioactivity, soil parameters, and building foundation construction (United States; USEPA (1993)); ii) indoor radon and radon soil gas (Germany; Kemski et al. (2009)); iii) indoor radon (Canada; Chen et al. (2008a)); and iv) indoor radon, geology, airborne radiometrics and till permeability (Northern Ireland; Kemski et al. (2009)).

The most recent radon potential maps combine a variety of features to create the most inclusive risk potential map possible. The predictor layers most commonly used are: i) bedrock geology, ii) surficial geology (including permeability), iii) airborne radiometric uranium, and iv) radon in indoor air (Appleton, 2007; O'Reilly et al., 2009b; Appleton et al., 2011; Mose et al., 1992; Johner and Surbeck, 2001).

The importance of these predictors in estimating the radon potential has previously been recorded (USEPA, 1993; Dubois, 2005; Kemski et al., 2009; Chen et al., 2008a; Appleton et al., 2011). Bedrock geology maps have been used to identify potential regions of high indoor radon gas (Jackson, 1990; Chen et al., 2008a; Kemski et al., 2006). Significant correlations have been identified between bedrock geology and indoor radon, even without accounting for differing housing characteristics (Shi et al., 2006). Radon soil gas produced in till (glacial geology) can also be a significant contributor to the indoor radon potential of a region. Recent Canadian studies mapped the radon potential highs using soil gas measurements (Chen et al., 2008a; Friske et al., 2010). However, mapping based solely on bedrock geology has limited utility for predicting indoor radon concentrations; for example, recent studies show that unless the till cover is less than < 1.0 m, radon produced in bedrock decays before diffusing to the surface (O'Brien et al., 2011). Therefore, till thickness and

radon production can be just as important, if not more so, than bedrock geology as a predictor of radon exposure potential. The SRP index has been used across Canada to predict regions where indoor radon levels may exceed the guideline. A higher SRP index value indicates higher potential for radon to migrate through soil and enter buildings to concentrations exceeding 200 Bq m^{-3} (HC, 2012).

The soil radon potential index (SRP) incorporates measured radon soil gas, and soil permeability of a region (Neznal et al., 2006). The SRP index is defined as:

$$SRP = \frac{C - C_0}{-\log P + \log P_0} \tag{2.1}$$

Where:

C is the radon soil gas concentration for a field sample site in kBq m^{-3}.

P is the soil permeability of the field site in m^2.

C_0 is the radon concentration constant: 1 kBq m^{-3}

P_0 is the permeability constant: $1x10^{-10}$ m^2.

The SRP index has been the main tool used to quantify the potential indoor radon gas risk of a region in recent years, and has previously been used by the North American soil geochemical landscapes project (NASGLP; Chen et al. (2008b); Goodwin et al. (2008, 2009, 2010); Friske et al. (2010).

Airborne radiometric measurements have also been used as indicators of indoor radon potential. These gamma ray surveys (uranium, potassium, thorium) have been used to create radon potential maps for Canada (Ford et al., 2001), the United States (Otton et al., 1993), and Great Britain (Ball et al., 1993) (among others). Though indoor air radon measurements are important, they should not be used as the sole predictor of radon distribution in a region (Appleton, 2007). Airborne gamma ray spectrometry (AGRS) analysis has also been applied previously to classify regions of radon risk, as airborne radiometric equivalent uranium and indoor radon are highly correlated (Jackson, 1992; Shives et al., 1995; Appleton et al., 2008, 2011). In addition to airborne uranium, the till and bedrock permeability are also significant determinants of radon migration potential for indoor environments (Neznal and Neznal, 2005). Comprehensive radon potential maps incorporate data from: bedrock geology, surficial geology, airborne radiometric equivalent uranium, and till permeability. In this study, five independent layers (four indicators and the indoor

radon layer) all representing different aspects of uranium and radon potential were compiled to determine the radon exposure potential of a region.

2.2.3 Local Radon Potential Mapping

One of the first radon prediction maps to suggest that Nova Scotia has high potential radon regions (Cape Breton, Tantallon, and St Margaret's Bay, among others), likely as a result of the underlying bedrock geology (granite plutons), was that of Jackson (1990) based on geology. In a published radon map of the country, the highest indoor radon concentrations were found in Central Canada and Atlantic Canada (Chen et al., 2008a; Chen, 2009). In measurement campaigns, Nova Scotia had regions where $>$ 20% of the dwellings measured above the 200 Bq m^{-3} guideline (Chen et al., 2008a).

These results led to further work to identify the distribution of radon gas concentrations in NS. In 2008 O'Reilly created a map of Nova Scotia (Figure 1.11) ranking the potential for radon in homes. This potential map used indoor radon data, airborne radiometric surveys, uranium exploration surveys and 'personal knowledge' of the geological terrain (O'Reilly, 2008). The regions within Nova Scotia with the highest potential were located on ^{238}U rich bedrock (granitic plutons). Halifax was identified as a high potential indoor risk, because much of western HRM is underlain by the known high-radon emitting South Mountain Batholith (SMB) and thin overburden (O'Reilly, 2008).

This study by O'Reilly (2008) is limited as it shows only one possible map of the radon potential in Nova Scotia, based on the assumptions identified above. This thesis (Chapter 2) presents a series of radon potential maps that statistically optimizes the indoor radon potentials, focusing primarily on the HRM, where over 42% of Nova Scotia's population resides.

Incorporating multiple predictors of radon potential into a spatial model may improve prediction of radon variation and its relationship to measured indoor radon concentrations. Given the health impact of radon and its association with lung cancer, it is prudent to apply this approach to improve prediction in HRM.

2.2.4 Research Objectives

The following research objectives aim to fill the radon potential mapping knowledge gaps within Nova Scotia. This study will produce a geospatial representation of the probability of exposure to indoor radon. To achieve this aim, the study will:

1. Quantify the statistical significance of each currently available radon predictor dataset (bedrock geology, surficial geology, permeability, airborne radiometric equivalent uranium) with respect to a sample of indoor radon values within the HRM; then, synthesizing these recent provincial datasets, create a series of possible radon prediction maps of the HRM based on the statistical significance of the predictors using measured indoor values as the constraint on weighting factors..

2. Identify trends in the spatial distributions between potential environmental radon emissions and radon concentrations indoors, and compare the findings and high potential regions with previous Nova Scotia radon potential maps (O'Reilly, 2008; Jackson, 1990).

2.3 Methods

2.3.1 Data Sources

Using a mapping approach similar to the suggested platform by O'Reilly et al. (2009b), a series of radon potential maps were created in ArcGIS© using various predictor layers , including bedrock geology, airborne radiometric uranium, till geochemistry, till permeability, and indoor radon. Pre-existing provincial bedrock and surficial geology maps and till geochemistry datasets were acquired from the mineral resources branch of the Nova Scotia Department of Natural Resources (NSDNR). An equivalent uranium (eU) airborne gamma ray spectrometry compilation was obtained from Natural Resources Canada (NRCan) which is a measure of all uranium included from various isotopes in the top 30 cm of soil. Indoor radon datasets were obtained directly from local radon testing companies (sources 1 and 2), and an organization that provides free radon testing kits to the public and maintains a database of the results (source 3).

2.3.2 Geocoding Indoor Radon Data

Locations of indoor test sites were coded as civic addresses and required geocoding for inclusion in the ArcGIS© database. ESRI's North American Geocode Service was used to geocode the indoor radon data. Any addresses that could not be matched because of insufficient address information were excluded from the database. If the matched addresses were based on town or postal code, they were re-matched to rooftop or street. Radon data from previous studies, such as those by Jackson (1990), were not included as limited address information hindered the placement of the data within the HRM.

2.3.3 Study Area

The study area is roughly determined by the furthest spatial extent of the indoor radon dataset. Using the dissemination area (DA) data from the 2006 Nova Scotia Census Data (obtained from Statistics Canada), all the DAs that contained indoor radon points were selected. Adjacent polygons were also included in order to create a continuous study area of 1775 km^2.

2.3.4 Raster Risk Classification

Till geochemistry and airborne radiometric uranium datasets were stored in a numeric raster format with a resolution of 250 m x 250 m (minimum resolution). Data were rescaled to radon potential values (Tables 2.7 and 2.8) and were aligned spatially with the dissemination area.

The potential values were estimated on a 1 to 10 scale in terms of radon potential within the layer where 1 represented the lowest potential and 10 represented the highest potential of that unit. Estimates were determined for each unit within the layers based on published descriptions of the radon/uranium values (described further below). Data outside of the study area were removed. Data on bedrock geology, surficial geology, and permeability were converted from vector to raster format, adopting the same spatial extent and resolution of the till geochemistry and radiometric uranium. Similarly, geological bedrock types and permeability categories were re-classified to a numerical scale reflecting radon potential (Tables 2.3 and 2.5).

The provincial geology layer was classified based on previous work by Goodwin et al. (2009, 2010), Department of Mines and Energy (DPME, 1982), and O'Brien (2010); O'Brien et al. (2011). Intrusives (Late Devonian plutons such as the South Mountain Batholith) were measured as having the highest radon soil gas levels in the HRM (Goodwin et al., 2009, 2010; O'Brien et al., 2011). At 60 cm, the average SMB radon gas concentration for the 'primitive', 'middle', and 'evolved' granite phases are: 44.3 Bq m^{-3}, 50.2 Bq m^{-3}, and 51.0 Bq m^{-3}, respectively (Goodwin et al., 2010). The intrusive unit was therefore, classified in the highest potential category. The Cambro-Ordovician Slate was also measured for radon soil gas, and returned an average of 36.1 Bq m^{-3} (Goodwin et al., 2010); it was therefore the second highest unit. The average radon soil gas for the Cambro-Ordovician Greywacke (Metasandstone) was 22.4 Bq m^{-3} (Goodwin et al., 2010). The Early Carboniferous underlays less than 5 % of the HRM study area, and had yet to be measured in terms of then U/Rn potential; because of insufficient data, it was excluded from the potential risk classification (Table 2.3). As such, Early Carboniferous units on the map were given 'No Data' values; though they were not classified in this map, those regions still have the possibility to have high radon potential.

The ranking order for the indoor point shapefile (Table 2.4) was estimated based on indoor radon guidelines (Canadian: 200 Bq m^{-3}, World Health Organization: 100 - 300 Bq m^{-3}, United States: 150 Bq m^{-3}, and European Union: 200 - 400 Bq m^{-3}). Any values greater than 200 Bq m^{-3} exceed the Health Canada guideline for indoor radon.

Overall average indoor radon values from 0 - 50 Bq m^{-3} were given a low risk value of 0. Measurements between 50 - 100 Bq m^{-3} were given a risk value of 2 (as the values approach the World Health Organization's lower guideline of 100 Bq m^{-3}). Concentrations from 100 - 200 Bq m^{-3} were given a medium potential value of 5, as values within that range exceeded the World Health Organization's lower guideline of 100 Bq m^{-3}, and could exceed the United States indoor radon guideline of 150 Bq m^{-3}. Indoor radon gas measurements from 200 - 500 Bq m^{-3} were given a high potential value of 8, as they exceed both the Health Canada indoor radon guideline of 200 Bq m^{-3} and the European Union guideline range of 200 - 400 Bq m^{-3}. Gas concentrations between 500 -1000 Bq m^{-3} were given a potential estimate of 9, as

values within this range exceeded all current guidelines. Any concentrations greater than 1000 Bq m^{-3} again exceeded all guidelines by a large margin, and were given the highest potential value of 10.

The surficial geology units of the HRM were ranked in terms of permeability potential predictions (Table 2.5) using descriptions by Utting (2009), Goodwin (2002), Stea and Finck (2001), and the map unit drainage descriptions (Stea et al., 1992). The Lakes were classified in the lowest possible category for gas transport. The Bedrock was described as being of 'various types and ages' and mentioned no fracturing, therefore it was assumed to be nearly impermeable as well (Stea et al., 1992). However, in the previous surficial geology map (Finck and Graves, 1987), the bedrock unit description was 'weathered, shattered bedrock is common', therefore it was assigned a slightly higher potential than water. The Marine and Organic Deposits were both described as being 'clay' rich, with or locally overlain by, 'peat', indicating a low permeability and drainage condition (Stea et al., 1992). Alluvial Deposits were described as 'bedded gravel, sand, and mud' with 'poor drainage' (Stea et al., 1992). Kames and Eskers were composed of 'gravel, sand and silt' with 'rapid drainage' (Stea et al., 1992). Hummocky Ground Moraine is described as a 'mixture of gravel, sand, and mud'. It is 'often sandy and stony; loose' (Stea et al., 1992). Silty Drumlin has 'moderate drainage and stoniness', and can include distal 'red clay' (Stea et al., 1992). Because of the presence of clay, the silty drumlin is assigned a lower permeability potential than the silty till. The Silty Till Plain is described as 'silty, compact material' with 'moderate drainage and stoniness'. Stony till Plain has a 'stony matrix' and 'rapid drainage' conditions (Stea et al., 1992), and was classified as a high permeability potential. Stony drumlin has 'rapid drainage' and is prone to erosion (Stea et al., 1992), therefore it was also categorized as a high permeability potential.

Though units such as organic deposits or bedrock may have a potentially higher uranium risk (because of the elevated uranium), the surficial geology layer dealt with the permeability potential only; a till geochemistry layer was included to account for the uranium potential.

The till potentials were categorized based on the uranium concentration in ppm (Table 2.7). Potentials were estimated using worldwide natural uranium in soil values

(0.3 - 11.7 ppm), (UNSCLEAR, 2006), previous NS uranium in till studies from Stea and O'Reilly (1982), and in rock (DPME, 1982). Previous till geochemistry (DPME, 1982) measured the U in various till types across southern Nova Scotia. The granite phase of the BRT had the highest measured U concentrations of 8.2 ppm, the 'quartzite' (metasandstone) phase of the BRT measured 5.6 ppm, and the slate phase measured 4.1 ppm (DPME, 1982). As such, any values between 5 and 10 were classified with a higher potential value. The majority of the values greater than 10 ppm from this dataset was associated with granite phase till, and was therefore classified in the highest radon potential category. The group of points that returned '-99' ppm (error values) was not classified. Potentials were also compared to the natural average uranium range in soils; as the natural range was from 0.3 to 11.7 ppm, it supported the classification in the highest category for values in the database greater than 10 ppm. By classifying the till values in their natural breaks in ArcMap ©, they were well defined by the radon levels. The majority of the measurements below 5 ppm were spatially distributed on the east side of the HRM where there was less documented radon potential (Goodwin et al., 2009, 2010; O'Brien et al., 2011); they were therefore classified with lower potentials than values greater than 5 ppm.

The NRCan airborne radiometric potentials were classified based on the data cells' equivalent uranium value in ppm. Cells that returned uranium values of $<$ 0 ppm were classified as '0', as they were errors (seen in Table 2.8). The airborne radiometric uranium potentials were categorized every 1 ppm based on the available NRCan data. In the airborne radiometric uranium layer, the data ranged from 0 ppm up to 4.8 ppm. Spatially, the uranium values of greater than 2 were underlain by the previously documented high radon potential SMB (Goodwin et al., 2010). The highest airborne radiometric uranium values corresponded to areas underlain by the fine-grained leucomonzogranite phase of the SMB, previously documented as the highest radon potential phase (Goodwin et al., 2010; O'Brien et al., 2011); it was therefore classified in the highest potential category.

2.3.5 Converting Shapefiles to Raster Files

Inverse distance weighted (IDW) interpolation was used to create a continuous till geochemistry raster layer based on the actual uranium values. The newly created

raster was then re-classed based on the estimated risk factors and extracted to the study area. The surficial geology and bedrock geology shapefiles were converted to rasters based on the radon potential field (using 250 m resolution). The airborne radiometric raster was re-classed based on the radon potentials, with any negative values being re-classed as 0 (labeled as No Data).

Maps were created both with and without weighting. The 'Raster Calculator' tool was used to multiply several rasters together. To create the weighted maps, the raster layers were multiplied together, each with their given weight. The weights were derived from regression model co-efficients, and were used to quantify the weights for each map layers (See Appendix A).

2.3.6 Statistical Analyses

Descriptive Statistics

The variables of interest were: bedrock geology (*Bedrock*), surficial geology (*Till*), permeability (*Permeability*), airborne radiometric equivalent uranium (*Airborne*), and indoor radon (*Indoor*). The indoor air variable (Y) was the dependent variable, and the bedrock geology, surficial geology, permeability, and airborne radiometric equivalent uranium were the independent variables (X). Uni-variate analysis on the Y variable showed that *Indoor* was skewed to the right (skewness 4.5, kurtosis 26.1) indicating a non-normally distributed dataset. Further uni-variate analysis can be seen in Table 2.1. In order to look at the bi-variate relationships between all predictors, a correlation matrix was calculated to determine the correlation co-efficients and their significance (Table 2.9).

The main conclusions from the bi-variate relationships (Table 2.9) were as follows: indoor air and airborne uranium were significantly positively correlated (p=0.00, r=0.35), indoor air and bedrock were significantly positively correlated (p=0.00, r=0.31), bedrock and till were significantly positively correlated (p=0.00, r=0.63), and airborne uranium and bedrock were significantly positively correlated (p=0.00, r=0.55).

Regression Analysis Full Model

Given the nature of the statistical analysis (i.e. the need for all four variables to have a correlation co-efficient to re-weight the radon potential map layers), a multiple regression was run containing all of the independent (X) variables. The goal of running the full regression model was to create a comparative map using the suggested predictor layers from previous research, as the four indicators had all been shown to contribute to the potential in indoor air potential in past studies.

An alternate set of permeability data was developed (Table 2.6), given the proposed significance of permeability to radon transport. The permeability potential estimates (Table 2.5) were re-classified to see if changing the potentials significantly impacted the resulting permeability layer, as seen in Table 2.6. Eskers with 'rapid drainage' (Stea et al., 1992) were re-classified to the highest potential permeability (10). As well, Hummocky Ground Moraine was re-classified as a higher potential than the Silty Drumlin and Silty Till Plain, as the moraine was comprised of stony material, and the Silty Drumlin and Till Plain only had 'moderate drainage' (Stea et al., 1992). These changes were introduced to accommodate oversights in the original potentials that could have had an impact on the permeability layer generated.

A new permeability raster was created in ArcMap (Figure 2.3) with the updated potentials from Table 2.6. It was compared to the original permeability layer (Figure 2.2) from the original potentials in Table 2.5.

In the original permeability raster, 17,576 cells were classified in the top category and 86 in the second highest (Figure 2.2). Within the new permeability raster, 72 cells are classified in the top category and 17,576 in the second (Figure 2.3). The lowest permeability potentials - Lakes and Bedrock (classified as 1, and 1.5 respectively in both the old and new estimates (Tables 2.5 and 2.6) had the same number of raster cells in both maps; respectively 295 and 4,534 cells. Therefore, though the new potentials have switched the highest potential unit with the second highest there is not a noticeable difference when multiplying the permeability layer in the modified permeability designation (Figure 2.2 and 2.3). Given the overall similarity in the resultant permeability maps, it was decided to incorporate the original permeability potentials (those generated in Table 2.5) in the creation of the radon potential maps (Table 2.2). The permeability potential estimates are likely not the reason for the

lack of correlation to the indoor radon database. The indoor radon dataset has a number of poorly constrained variables and therefore is likely the major contributor to the poor correlation.

The dependent (Y) variable was *Indoor*, which represented the indoor radon values. The independent (X) variables were *Till* (the radon potential of the till, X_1), *Airborne* (the airborne radiometric equivalent uranium potential, X_2), *Permeability* (the original permeability potential of the surficial geology, X_3), and *Bedrock* (the radon potential of the bedrock, X_4). The model was run on values where the indoor data was available.

Because the dependent (Y) variable was not normally distributed, an ordinary least squares (OLS) regression model was used, as it was best suited for skewed dependent (Y) variable (per. com. Yoko Yoshida, 2013). The ordinary least squares regression equation (with 95% confidence interval) had the form:

$$Y = -63.58(Till)+67.05(Airborne)-14.44(Permeability)+150.61(Bedrock)-737.35 \tag{2.2}$$

The model significantly predicted 16.77% of the indoor radon variance (p=0.00). Variance inflation factor (VIF) was used to quantify the multicollinearity of the coefficients found in the regression, and the estimates were found to not be correlated with each other (Table 2.10).

Regression Analysis Significance Model

The second multiple regression used only the independent variables that were significantly correlated to the dependent variable. The goal of running the second model was to assess the apparent contribution of the significant variables in predicting the indoor radon variation. The OLS regression model (95% confidence interval) had the form:

$$Y = 80.09(Airborne) + 84.28(Bedrock) - 607.00 \tag{2.3}$$

The model significantly predicted 14.36% of the indoor variance (p=0.00), and multicollinearity was not found to be an issue because the VIF values were less than 10 (see VIF values in Table 2.10).

2.3.7 Categorizing the Maps into Potential Regions

After multiplying the rasters together (with or without OLS model weighting), the radon potential values were divided into five zones based on the Jenks natural breaks optimization of ArcGIS©. This geospatial optimization maximizes the heterogeneity between categories and minimizes the heterogeneity within categories. The resulting maps (see Table 2.2) were then compared to several known documented radon highs (e.g. Tantallon; Jackson (1990)) to ensure regions were represented correctly.

To assesses the difference between the zones, an analysis of variance between groups (ANOVA) was run on each map. The sensitivity analysis was performed on 12 different maps to determine if four-zone or three-zone maps returned zones with more significantly different means than the five-zone maps (per. com. Daniel Rainham, 2013). The 4UW, 4W, 2UW, and 2W maps were re-created and classified using the Jenks method into maps with 5 zones, 4 zones, and 3 zones. The ANOVA sensitivity analysis indicated that there is no statistically different variance between using five, four or three zones (see maps in Appendix B). The maps with four layers (4UW and 4W) had zonal means that were not significantly different from each other (using 5, 4, and 3 zones). The maps with two layers (2UW and 2W) had zonal means that were significantly different from each other (maps with 5, 4, and 3 zones). Therefore, because there was no difference, the original five-zone maps were kept to maximize the visual spatial variability (the colour scheme) in the map.

2.4 Results

2.4.1 Map Results

Four final maps, created using ArcGIS©, were presented to satisfy the first objective of creating a radon potential map of the HRM (Table 2.2). The resulting maps were separated by the Jenks natural breaks division into five zones: where zone 1 had the lowest radon potential, and zone 5 had the highest radon potential. The Nova Scotia roads network and the indoor database were added to help display the residential population distribution.

Map 4UW (Figure 2.4) was created by combining radon in till data, airborne radiometric equivalent uranium data, bedrock radon potential, and permeability in

surficial deposits. No weighting was used when multiplying the raster layers together to establish a baseline map to compare with the weighted map. Map 4W (Figure 2.5) was created using all four layers. After running an OLS regression on the data (with the indoor radon database as the dependent variable), the resulting equation was used to weigh the four layers. Map 2UW (Figure 2.6) was produced by multiplying the bedrock radon potential and the airborne radiometric equivalent uranium potential layers. These were the two statistically correlated variables (correlation seen in Table 2.9) to the indoor radon database; the layers were not weighted. Map 2W (Figure 2.7) was generated by multiplying the only two significantly correlated variables to indoor radon: airborne uranium potential and bedrock radon potential. Using the results of an OLS regression, both layers were multiplied by a weighting factor.

2.4.2 Distribution of Indoor data within Zones

The logarithmic distribution of the indoor radon database can be seen in Figure 2.1. To examine the spatial distribution of the indoor points within each zone, the indoor points from each respective map were extracted. The variances of each map are presented in box and whisker plots (Figures 2.8,2.9, 2.10, and 2.11) to satisfy the second objective:'identify trends in the spatial distributions between potential environmental radon emissions and radon concentrations indoors'.

The median values extracted from Map 4UW (Figure 2.4) have a weak positive linear correlation with the respective Jenks zones (r= 0.444, where r is the correlation), and the averages were strongly correlated (r=0.824). The distribution can be seen in Figure 2.8. The indoor radon medians from Map 4W (Figure 2.5) were weakly correlated to the zones (r=0.215), as they were associated with r values of less than 0.5, and the averages were also weakly correlated (r=0.460) (Figure 2.9). Map 2UW's medians and averages (Figure 2.10) were both very strongly correlated with increasing radon potential zones (respectively: r=0.908, r=0.917). Similarly, Map 2W's medians and averages also had strong positive linear correlations with the increasing radon potential zone classifications (respectively: r= 0.846, r=0.881) (seen in Figure 2.11). The range of values in the distribution graphs are overall very large. The large 'whiskers' are a result of the high variation in indoor home radon concentrations measured. High indoor radon variability, regardless of the scale, has been documented

before (Miles and Appleton, 2005).

2.4.3 Comparison with Previous Work

The trends between this study's maps and the most recently published radon potential map of Nova Scotia (Figure 1.11) are generally similar: the west side of the HRM had the highest radon potential, and the east side of the HRM had the lowest radon potential. This is potentially because of the underlying rock types - the west side of the HRM is underlain by the SMB, and the east side by the lower radon producing Halifax and Goldenville Groups (Goodwin et al., 2010).

O'Reilly (2008) described all of the SMB in the highest potential radon group. This study's maps (Figures 2.4, 2.5, 2.6, and 2.7) were able to show that the highest indoor radon potential occurs in areas underlain by the fine-grained leucomonzogranite phase of the SMB (Upper Tantallon region). That phase of the SMB has previously been documented to have the highest radon production within the HRM (Goodwin et al., 2010; O'Brien et al., 2011).

As the SMB is a granite enriched in uranium, the high regions are justified in having high radon values (Je, 1998a). Other areas of high indoor radon potential include the northeastern regions of Dartmouth (e.g. Figure 2.7). These regions correspond to other Early Devonian granitic intrusions (White, 2002), and were also categorized in the highest risk category by O'Reilly (2008).

2.5 Discussion

2.5.1 Indoor Trends

As seen from all the box and whisker plots (Figures 2.8, 2.9, 2.10, and 2.11), the indoor home data were highly variable, making significant trends difficult to establish. Overall, the average radon potentials increased with increasing zones for Maps 4UW (Figure 2.8), 2UW (Figure 2.10), and 2W (Figure 2.11). For Maps 4UW and 4W (Figures 2.8 and 2.9), the potentials were more variable in the lower zones (i.e. 1-3), whereas in Maps 2UW and 2W (Figures 2.10 and 2.11), the potentials were more variable in the higher zones (i.e. 3-5).

The variability in the indoor dataset was potentially attributable to a number

of factors: 1) time of year (indoor radon concentrations are higher in the winter; Selinus et al. (2005)), 2) variations in radon sampling equipment, 3) sample duration (length in days), 4) construction and style of home, and 5) location of test in home (in basement or not). Because this study incorporated three different testing companies' datasets, both electret ion chambers and continuous radon monitors were used to measure radon-222. Sampling spanned the entire year; exposure time per sample ranged from one day to three months. Locations within homes also varied from bedrooms to living rooms to basements. All of these factors likely affected the average radon measured, and could possibly explain why the OLS regression could only predict 14.4 and 16.8% of indoor variance.

Though the averages and medians of all mapped zones correlated with indoor radon, the ANOVA analysis showed that only Maps 2UW (Figure 2.6) and 2W (Figure 2.7) had statistically significant differences in means. The statistical analysis of the number of zones in each map suggested that the fewer zones displaying the potential, the more variable the potential values were.

As Map 2W was the only statistically significant potential map, indoor trends should be considered only for it (Figure 2.7). In Maps 4UW (Figure 2.4) and 4W (Figure 2.5), the distribution in zone 5 was statistically no different from the zone 1; therefore they could not be used to establish spatial trends. Map 2W (Figure 2.7) was able to predict 14.4% of the indoor variance, and because the zones were statistically different, they could be used as statistically significant predictors of indoor trends. In the box and whisker plots for Maps 2UW (Figure 2.10) and 2W (Figure 2.11), the higher radon potential zones (4 and 5) had much higher variability than the lower radon potential zones (1 and 2). This was not the case for Maps 4UW (Figure 2.8) and 4W (Figure 2.9), and may reflect the lack of significantly different mean between zones for Maps 4UW and 4W (Table 2.2).

2.5.2 Maps

One of the main objectives of this study was to synthesize existing provincial datasets to create a series of radon potential maps of the HRM. In assessing the maps, the reader should note that the map represents the radon *potential* of a region, and not the absolute values of radon in indoor air. It is also important to emphasize that

the radon potential in certain regions is estimated with more certainty based on the increasing number of samples (n value) and the distribution of homes in that zone. For example, potential levels farther away from the roads (i.e. away from where the most housing developments and indoor data points) were less accurately predicted than potentials within highly populated and tested regions. For that reason, the reader should take caution in assessing the radon potential of a region that does not contain indoor data points. Because of the nature of the variability, it is suggested that homes should be tested for indoor radon.

The large variability in indoor home data meant that in each zone, there were likely homes exceeding the Health Canada guideline of 200 Bq m^{-3}. For that reason, the zones did not represent 'safe' or 'dangerous' zones; they simply suggest a lower or higher potential for radon with respect to indoor air values. This variability could be due, in part, to the permeability of the underlying tills/bedrock. In areas where a home is built on fractured bedrock, the radon gas levels at the surface are likely higher given the higher permeability. This is an important issue that will be further addressed in Chapter 3.

In this study, bedrock geology and eU radiometric values were the only two layers that correlated to the indoor radon potential. In order for radon-222 gas to become a potential human health concern, the gas transport mechanisms (i.e. permeability and diffusivity) play important roles as well (O'Brien et al., 2011). Therefore, permeability is an important consideration as it is a control on the presence of radon gas at the surface. It is for this reason that the maps with all four layers (4UW and 4W) were included.

Within the study area, there were previously documented high radon regions; they acted as 'checks' to ensure the most accurate map were constructed (Figures 2.4, 2.5, 2.6, and 2.7). One of the important 'high' regions was Upper Tantallon; it had been previously documented as a uranium/radon high (O'Beirne-Ryan, 2006; Goodwin et al., 2010; O'Brien et al., 2011), and was indicated as a high region on all presented maps. Some known radon highs did not show up on the map, including the Harrietsfield area (seen on all maps) (as explained by Goodwin et al. (2008), and personal communications with Anne Marie O'Beirne-Ryan). In all four maps (Figures 2.4, 2.5, 2.6, and 2.7), the Harrietsfield region did not fall in the highest category of

radon potential. This could be due, in part, to the lack of data to document specific indoor potentials in that region, because it would then not be categorized in the higher zones of indoor radon potential. There was also large variability even within a 250 m grid cell. To avoid this problem in future mapping, it is recommended that the future indoor radon database be sampled on a grid to ensure an even distribution of points (e.g. 1 sample every 1 km^2 of measurements).

One of the main limitations of all four maps (Table 2.2) is that they are based on the radon potentials estimated from the multiple predictor layers. Though the potentials were justified by referencing published work, the values themselves could be refined more on the basis of better data control and sensitivity analyses. As such, the degree to which altering the potential values would affect the final maps is not quantified. Regardless of the technique used to interpolate, the accuracy of the resulting layer would be limited by the infrequency and spatial distribution of till geochemical data points. The 250 m grid cell was also potentially a limitation, especially when evaluating data from the Halifax Peninsula. The scale was better suited in regional areas, not city centers, as the scale was not refined enough for a high density population.

Map 4UW is a baseline map not derived from an indoor radon database. The bedrock geology units were not as apparent in Map 4UW (Figure 2.4) as they do in other maps (e.g. Map 2W, Figure 2.7). Regions on the west side of the HRM, over the SMB (east of Harrietsfield), that had been previously identified as having high radon potential (Goodwin et al., 2010), were classified as having the lowest radon potential. Also, the Halifax and Goldenville Groups were not highlighted on the east side of the map (from Dartmouth to Porters Lake). These trends suggested that in Map 4UW (Figure 2.4), bedrock geology did not determine indoor radon potentials. Regardless of the underlying probability and even though it is still recommended for residents to get their homes tested for indoor radon, the means of the zones were not significantly different; there was no difference between zones 1 and 5.

All four predictor layers were included in Map 4W (Figure 2.5) because they had all been previously reported as contributors (O'Reilly, 2008; Appleton and Miles, 2010), though statistically only bedrock and airborne radiometric equivalent uranium are significant predictors of radon in indoor air potential. Again, the lack of geologic

contacts seen in the NE part of the study area suggested that even after weighting, bedrock geology was not the dominant influence on radon potential. Though Upper Tantallon exhibited the highest radon potential area within the HRM study area, the regions surrounding Upper Tantallon had less radon potential compared to Map 4UW (Figure 2.4). Though the regression model significantly predicted 16.8% of indoor variance at the 95% confidence level, there was no statistical difference between the zones. Therefore, Map 4W (Figure 2.5) could not be used as a predictor of indoor radon, only as a predictor of the radon potential from geological factors alone.

Similar to Map 4UW (Figure 2.4), Map 2UW (Figure 2.6) was not weighted, and therefore represented the standard without influence from an indoor radon database. This map was created using only the bedrock geology and the airborne radiometric equivalent uranium. Without other influences such as till geochemistry or permeability, the eastern Meguma Group was spatially the most visible in this map relative to the other maps. The outline of the SMB was also very sharp in Map 2UW (Figure 2.6), suggesting that bedrock was a dominant influence on the potential values. This relationship has been confirmed in previous studies (Selinus et al., 2005). The means of the radon potential zones in Map 2UW (Figure 2.6) were significantly different from each other, therefore the potentials could be used to predict up to 14.4% at the 95% confidence level of indoor home variance.

Map 2W (Figure 2.7) is the best candidate for predicting radon potential because it is the only map where all of the layers significantly correlated with the indoor radon potential, and had significantly different zones. As such, it represented the most statistically significant map of the study, explaining 14.4% of the indoor radon variance. Similar to Map 2UW (Figure 2.6), both the SMB and Meguma Supergroup geology were clearly delineated. Because the co-efficients in the OLS regression were approximately equal (Equation 2.3), Map 2UW (Figure 2.6) and Map 2W (Figure 2.7) were spatially very similar. This suggests that bedrock and airborne radiometric uranium data are both equal predictors of indoor radon potential.

By running an OLS regression and significantly predicting 14.4% of indoor variance, the findings in this study agreed with previous work: there is a statistically significant, but low, correlation between bedrock geology and indoor radon (Shi et al., 2006). This relationship was also confirmed in the uni-variate stage of the statistical

analysis, as bedrock geology and indoor radon displayed a significant weak correlation (p=0.00, r=0.31). Maps 4UW (Figure 2.4) and 2UW (Figure 2.6) represent the distribution of radon in the HRM without taking into account the indoor radon data. In future work, by adding additional indoor data points and controlling the variables related to indoor radon measurements, the weighted maps may more closely resemble the un-weighted maps.

2.5.3 Comparison with Other Maps

Unlike the O'Reilly (2008) map, this study provides a statistical rationale for the all layers included in the final maps. Though Maps 4UW (Figure 2.4) and 4W (Figure 2.5) are those that best compare to the previous maps in terms of geologic trends, Map 2W (Figure 2.7) was the most statistically significant predictor of indoor radon to date, and with the current data is the closest match. Both O'Reilly (2008) map and the Chen et al. (2008a) map identified the SMB in the highest radon-producing potential category; the results of this study are comparable (Map 2W; Figure 2.7). In this study, at a larger scale, regions underlain by the SMB were refined in even more detail to predict the highest potential regions within the study region (i.e. Upper Tantallon). Though the O'Reilly (2008) map does not show the detailed radon potential breakdowns within the SMB, overall, the general trends between the 2008 map and the current study's maps are similar: bedrock geology is a significant predictor of indoor radon. The major contribution of this study, however, is that it suggests ways to create a GIS-based potential map with the optimal predictor layers based on the indoor radon database for the HRM (Table 2.2). By synthesizing the available data, and testing them against a collected set of radon in indoor air samples, this study has created a unique portrayal of the different ways to characterize the radon potential.

The statistical analysis in this chapter shows a different approach to radon potential mapping not previously done in Nova Scotia. The statistical approach has been executed in other places (Kemski et al., 2009; Borgoni et al., 2011; Appleton et al., 2011): Appleton and Miles (2010) ran a comparable analysis on the geogenic controls on indoor radon. The Appleton study was able to predict 25% of radon variation in England and Wales based on bedrock geology and surficial geology

(Appleton and Miles, 2010). One possible reason for the difference between the variation predicted in the 2010 study (25%) and the variation predicted in the current study (14.4%) is the number of indoor data samples. Appleton and Miles (2010) had more than 20,000 indoor radon points; the current study had 124 indoor radon points (Figure 2.1). With a larger and more evenly distributed set of indoor data, the geology and surficial geology of the HRM might be better predictors of the indoor radon variation.

Another study using regression analyses to predict indoor radon variance, was executed in Northern Ireland (Appleton et al., 2011). This 2011 study showed that the most statistically significant predictors of indoor radon were airborne radiometric equivalent uranium and soil permeability. The 2011 study found, however, that not including bedrock geology in the potential map led to underestimates of the radon potential in some locations - perhaps beacuse the limited penetration depth of the eU (top 30 cm of soil) (Appleton et al., 2011). In the current study, the significant predictors of indoor radon were found to be bedrock geology and airborne radiometric equivalent uranium (see Table 2.2). Estimated permeability potentials are not as accurate as measured values would be. Previous studies concluded that permeability is a key contributor in the transport of radon gas (Washington et al., 1994; Neznal and Neznal, 2005); because it was not found to be a statistical predictor in the current study, the importance of permeability in radon gas movement through tills, as well as measurements through HRM till units, is considered further in Chapter 3.

2.6 Conclusions

Though several maps are presented in this study (Table 2.2), Map 2W (Figure 2.7) was the only map where all the indicators were significant predictors of indoor radon variance, and the zones were statistically different. The other maps were included to show that there are many ways to present a map, each with its advantages and disadvantages; no map is a perfect representation of a region.

Maps 4UW (Figure 2.4) and 4W (Figure 2.5) were created using all four indoor radon indicator layers (i.e. bedrock geology, surficial till, permeability of the till, and airborne radiometric equivalent uranium), as they had previously been shown to predict indoor radon (Appleton, 2007). The respective zones did not have significantly

different means from each other. Maps 2UW (Figure 2.6) and 2W (Figure 2.7) were created using the only two layers found, in this study, to be statistically significant predictors of indoor radon (i.e. bedrock geology and airborne radiometric equivalent uranium). The maps divided the radon potentials into 5 respective zones with statistically different means. The spatial distribution of indoor radon constrained the accuracy of the maps as predictors. The potentials closer to dense groupings of indoor data points were more accurate predictors than regions without nearby indoor data.

Based on the OLS regression analysis used to make the maps, the potential values only predict 14.4% (e.g. Maps 2UW and 2W) or 16.8% (e.g. Maps 4UW and 4W) of indoor air variance. There is therefore up to 85.6% of predicted radon in indoor air is unaccounted for. There are several sources that could comprise the other 85.6% of indoor variance: i) measurement factors - i.e. type of instrument used, duration of test, location of test within home, and / or calibration of instrument, ii) home factors - i.e. home age and construction, open vs closed windows, as well as cracks in any walls or foundation, and iii) weather conditions - i.e. the atmospheric pressure, temperature, and time of day and year. Both permeability and surficial geology have been documented as being radon gas predictors; however, they were not statistically correlated to the indoor radon database in this study. Because the permeability and till geochemistry were not used to predict the 14.4%, better constraints of these components might help to explain the significant portions of the 85.6%.

Within each map, some tested homes exceeded the indoor guideline of 200 Bq m^{-3} in every zone. Because of the high variability within zones, there is significant radon potential throughout the map area; it is recommended that all homes be tested for indoor radon. Though the presented maps attempt to predict the indoor radon potential in different regions, the main goal of the study is to provide a way of understanding how radon potential maps should be created by optimizing the predictor variables.

The highest potential regions within the HRM correspond to the highest HRM potentials of previous studies (Goodwin et al., 2010; O'Brien et al., 2011). The high-potential Upper Tantallon region agrees with previous Nova Scotia maps (Jackson, 1990; O'Beirne-Ryan, 2006; O'Reilly, 2008; Chen et al., 2008a; Chen, 2009), and acted

as a 'check' to ensure the accuracy of the map. Overall, the SMB stood out in most maps, and even the Meguma influence was visible in Maps 2UW and 2W, indicating bedrock geology has a strong influence on indoor radon.

Though the SMB rocks near Upper Tantallon are not the highest radon-producing rocks and tills in Nova Scotia, they are the highest-producing units surrounding the largest and most populous city: Halifax. Therefore, these maps are important in estimating the relative radon potential for human health. Although it is still better to characterize a building site with a direct measurement, these potential maps can be useful predictors for residents, city planners, and building inspectors.

The results of this study provide an overall procedure for creating a radon potential map for HRM based on statistical analysis. Except for indoor radon database, the maps were not created using new data. However, this study synthesized the data with respect to indoor radon, and in doing so, contributed to the knowledge and understanding of how a radon hazard map can be produced. As radon in indoor air can be a human health hazard above 200 Bq m^{-3}, this study helped to refine the statistical techniques used to create the most accurate maps with the indoor radon predictor layers by evaluating the optimal layers for consideration. It also highlighted uncertainties in understanding the role of permeability in assessing indoor radon potential. That uncertainty is addressed in Chapter 3.

2.7 Future Work

There are several recommended datasets or dataset protocols that should be re-evaluated for future radon risk potential mapping techniques:

1. There is a need for an updated indoor radon dataset with a set sampling density (e.g. 1 sample every 1 km^2). With a set sampling location and duration, and a more even grid distribution of indoor radon measurements there will not be a proximity bias in the maps.

2. In future indoor databases, it is recommended that there is a set sampling protocol for all companies to follow. If all indoor radon measurements are taken using the same technique (i.e. type of equipment used, length of test, location in home, and time of year), some of the variability in indoor home data

will be reduced.

3. A permeability catalogue for the till units across the HRM is also needed. That way, instead of using estimates of till permeability, measured permeability values (similar to eU in ppm) can be used. A future study should look at creating a continuous permeability dataset for Nova Scotia (or the HRM) with measured values in m^2.

4. As new datasets become available, a future project should include a radon potential map of Nova Scotia using these techniques and statistical analyses.

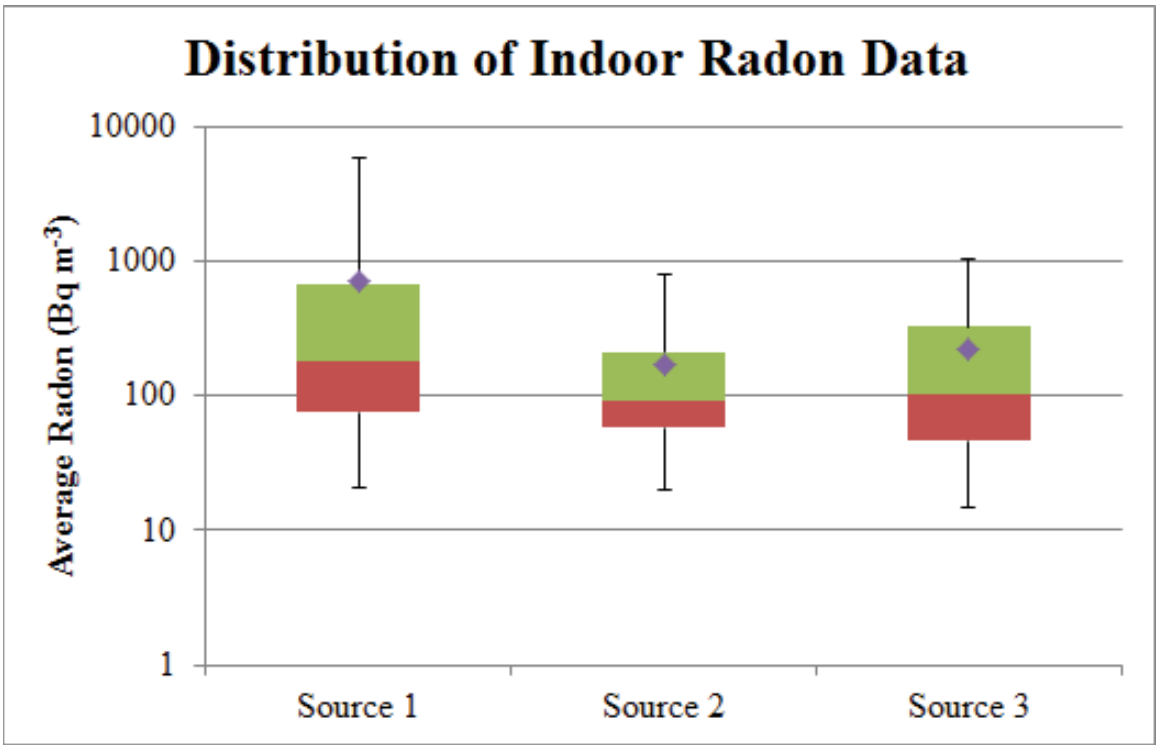

Figure 2.1: Box and whisker plots displaying the variance the indoor radon datasets acquired by source 1 (n=55), source 2 (n=35) and source 3 (n=34). The top and bottom error bars represent respectively the maximum and minimum values; the top box represents Q1; the bottom box represents Q3; the middle bar represents the median, and the diamond represents the mean. Note the logarithmic scale; 1000 Bq m^{-3} = 1 kBq m^{-3}.

Table 2.1: Descriptive statistics for the dependent (Y) and independent (X) variables of interest.

	Min	Max	Median	St. Dev.	Skewness	Kurtosis
Indoor (Y) (Bq m^{-3})	6	5844	141	818.8	4.5	26.1
Bedrock (X)	6	10	7	1.7	0.1	1.2
Till (X)	1	10	3	2.3	1.2	3.4
Airborne (X)	1	9	3	2.6	1.0	2.5
Permeability (X)	1.5	10	10	3.3	-1.4	3.0

Table 2.2: Detailed description of the predictor layers within the 4 maps.

Map	Contents	Weighting	Justification
4UW	Bedrock, Airborne, Surficial, Permeability	No	Standard
4W	Bedrock, Airborne, Surficial, Permeability	Yes	Statistically weighted layers
2UW	Bedrock, Airborne	No	Standard
2W	Bedrock, Airborne	Yes	Statistically significant weighted layers

Table 2.3: Radon potential values for the provincial bedrock geology layer (obtained from NSDNR), on a scale of 1 to 10. 1 is the lowest potential, and 10 is the highest potential. NA represents data that was unavailable.

Legend Description	Radon Potential Value
Early Carboniferous	NA
Cambro-Ordovician, Greywacke	6
Cambro-Ordovician, Slate	7
Intrusives	10

Table 2.4: Estimated indoor radon potential values for the three indoor radon databases: Sources 1, 2, and 3, on a scale of 1 to 10. 1 is the lowest potential, and 10 is the highest potential.

Overall Average Radon (Bq m^{-3})	Radon Potential Value
0 - 50	1
50.01 - 100	2
100.01 - 200	5
200.01 - 500	8
500.01 - 1000	9
> 1000	10

Table 2.5: Radon potential values for the surficial geology permeability (obtained from NSDNR), on a scale of 1 to 10. 1 is the lowest potential, and 10 is the highest potential.

Legend Description	Radon Potential Value
Lakes	1
Bedrock	1.5
Marine Deposits	3
Organic Deposits	3
Alluvial Deposits	5
Kames and Eskers	7
Hummocky Ground Moraine	8
Silty Drumlin	8.5
Silty Till Plain	9
Stony Drumlin	9.5
Stony Till Plain	10

Table 2.6: Re-classified radon potential values for the surficial geology permeability (obtained from NSDNR), on a scale of 1 to 10. 1 is the lowest potential, and 10 is the highest potential.

Legend Description	Radon Potential Value
Lakes	1
Bedrock	1.5
Marine Deposits	3
Organic Deposits	3
Alluvial Deposits	4
Silty Drumlin	6.5
Silty Till Plain	7
Hummocky Ground Moraine	8
Stony Drumlin	8.5
Stony Till Plain	9
Kames and Eskers	10

Table 2.7: Radon potential values for the till geochemistry (obtained from NSDNR), on a scale of 1 to 10. 1 is the lowest potential, and 10 is the highest potential. NA represents data that was unavailable.

Uranium (ppm)	Radon Potential Value
- 99	NA
0 - 0.5	1
0.501 - 5	3
5.01 - 10	6
10.01 - 20	9
$>$ 20	10

Table 2.8: Radon potential for the airborne radiometric uranium values (obtained from NRCan), on a scale of 1 to 10. 1 is the lowest potential, and 10 is the highest potential. NA represents data that was unavailable.

Uranium (ppm)	Radon Potential Value
< 0	NA
0 - 1	1
1.01 - 2	3
2.01 - 3	8
3.01 - 4	9
> 4	10

Table 2.9: Statistical correlation between OLS layers. r is the correlation co-efficient.

	Indoor	*Till*	*Airborne*	*Permeability*	*Bedrock*
Indoor	—				
Till	No	—			
Airborne	*Yes* r=0.35	No	—		
Permeability	No	No	No	—	
Bedrock	*Yes* r=0.31	*Yes* r=0.63	*Yes* r=0.55	No	—

Table 2.10: Results from both OLS regression models run, as well as VIF factors for each variable. β is the beta co-efficient, and ε is the residual.

Variable	OLS_1	VIF_1	OLS_2	VIF_2
Till	ß= -63.57664	1.76	—	—
Airborne	ß= 67.06051	2.37	ß= 80.09309	1.43
Permeability	ß= -14.4375	1.50	—	—
Bedrock	ß= 150.6077	1.02	ß= 84.27622	1.43
Residual	ε= -735.3522	—	ε= -607.0024	—

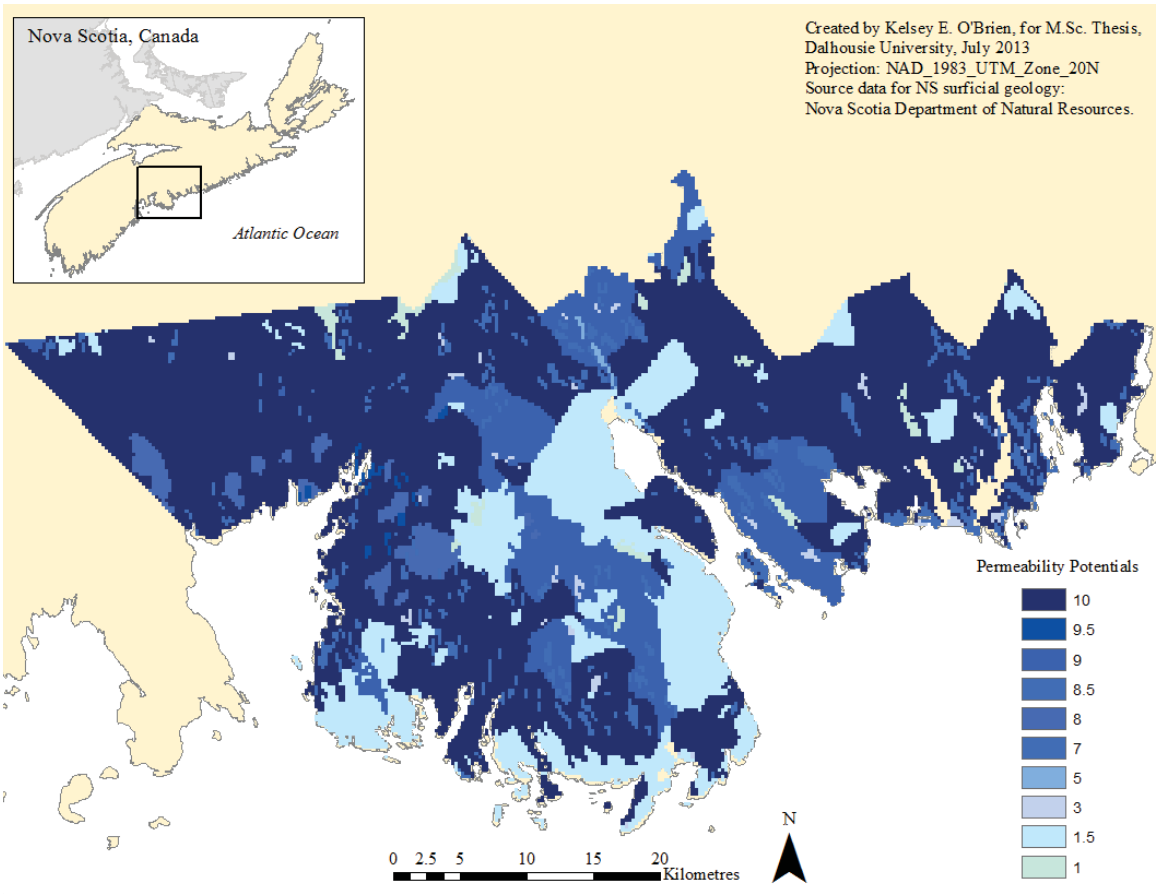

Figure 2.2: Original permeability potentials for the surficial geology layer, estimated from Stea et al. (1992).

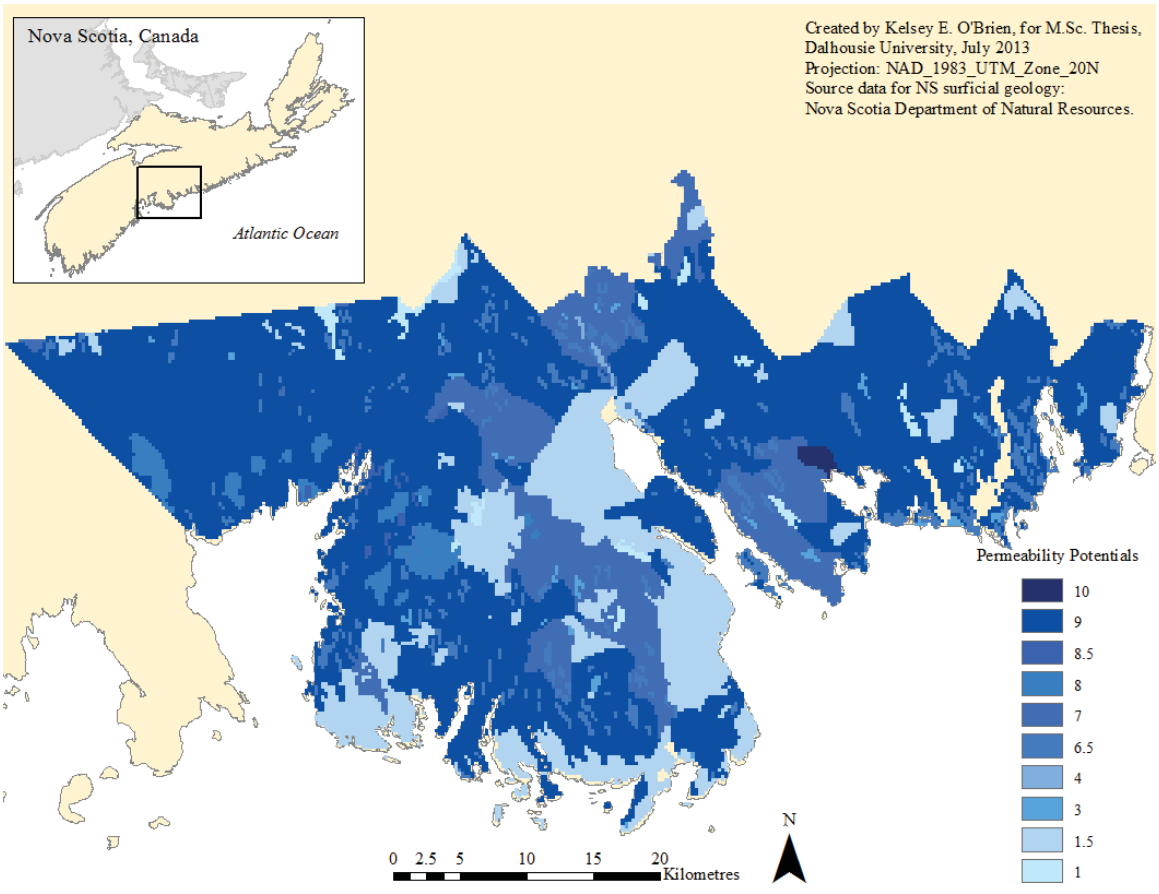

Figure 2.3: Re-worked permeability potentials for the surficial geology layer, estimated from Stea et al. (1992).

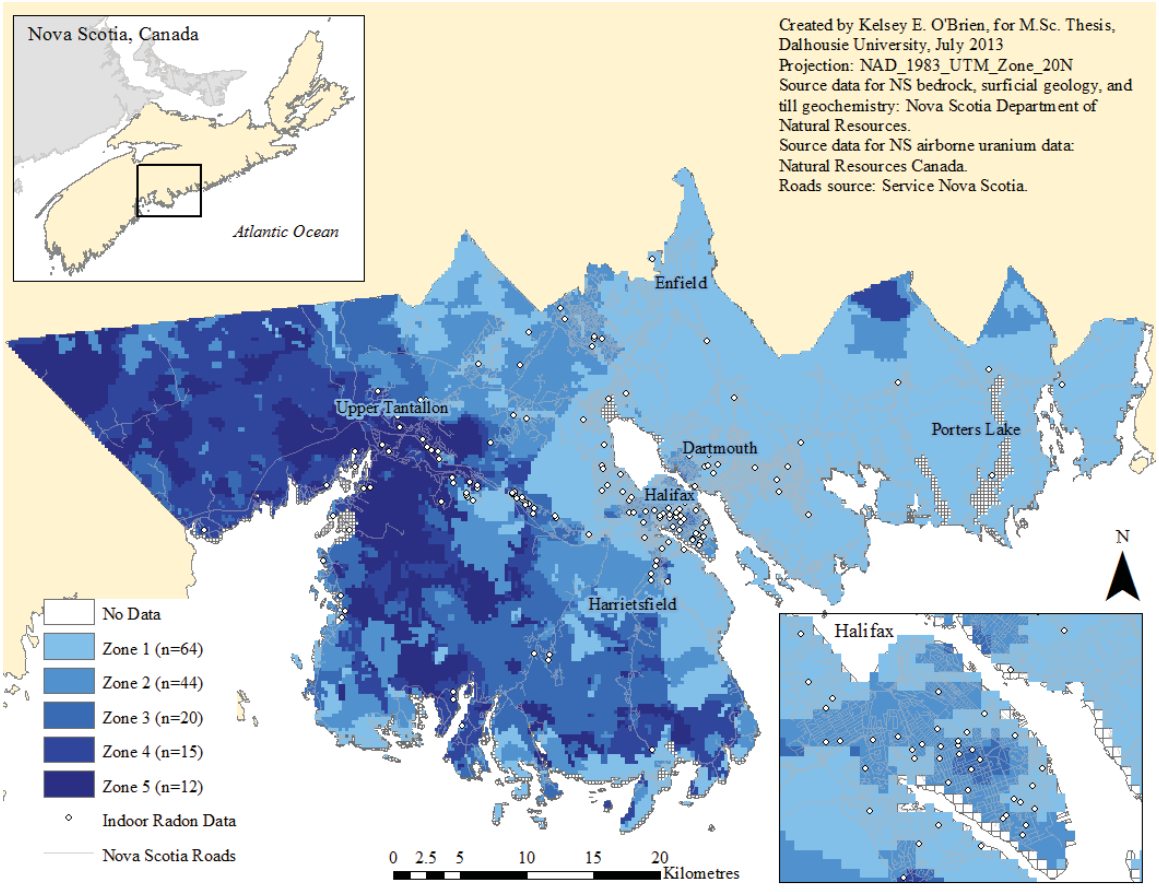

Figure 2.4: Map 4UW - Created using all four layers (*Till*, *Permeability*, *Bedrock*, and *Airborne*), un-weighted. Note the distribution of indoor radon data; the map is more accurate in regions with dense indoor radon data points.

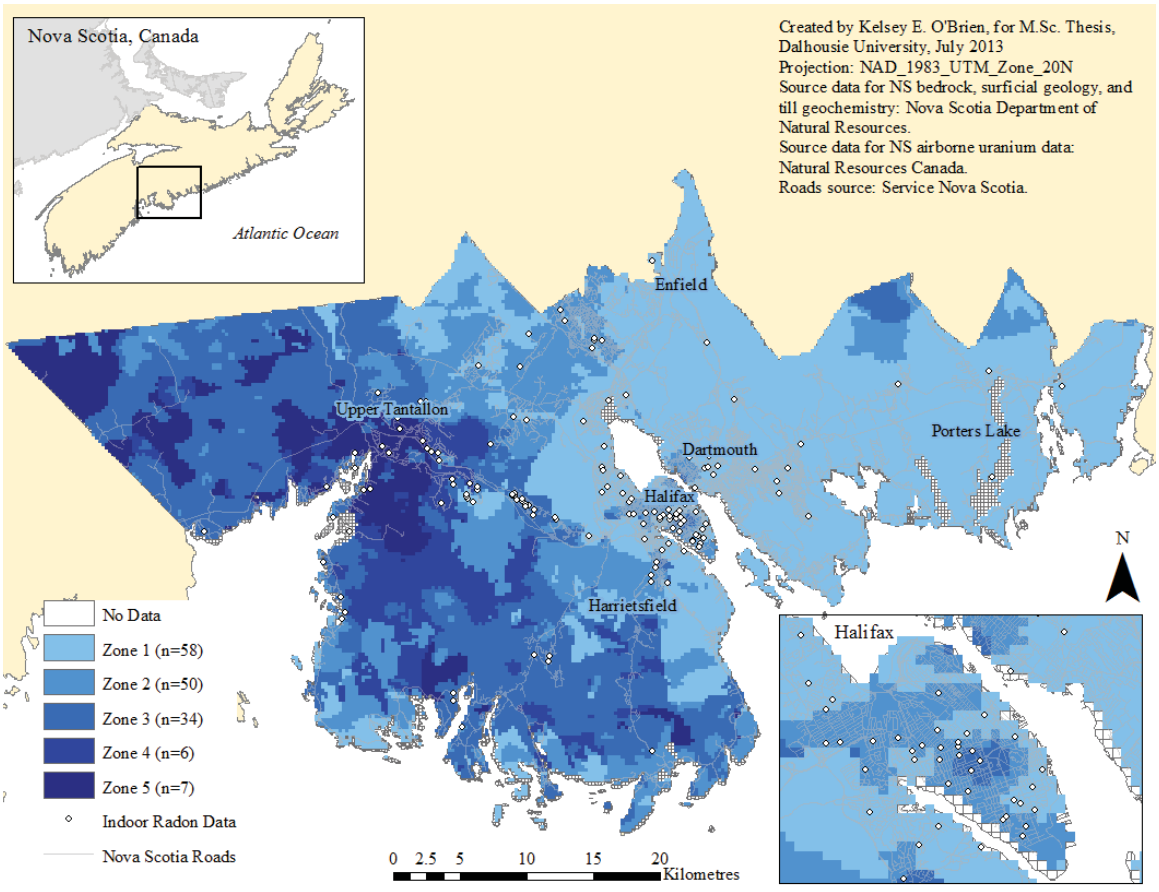

Figure 2.5: Map 4W - Created using all four layers (*Till*, *Permeability*, *Bedrock*, and *Airborne*), weighted using the OLS statistic regression. Note the distribution of indoor radon data; the map is more accurate in regions with dense indoor radon data points.

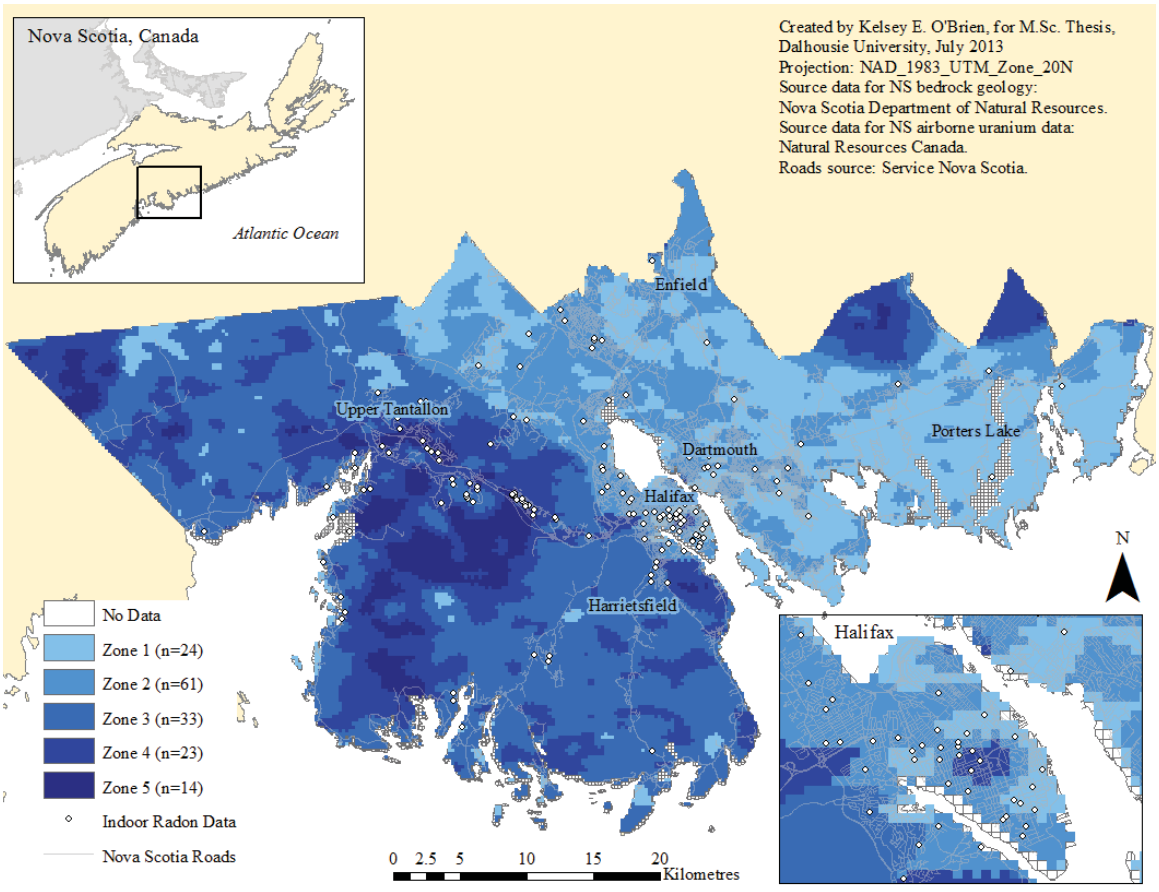

Figure 2.6: Map 2UW - Created using only two layers (*Bedrock* and *Airborne*), as they were the only significantly correlated layers to indoor radon. Both layers were un-weighted. Note the distribution of indoor radon data; the map is more accurate in regions with dense indoor radon data points.

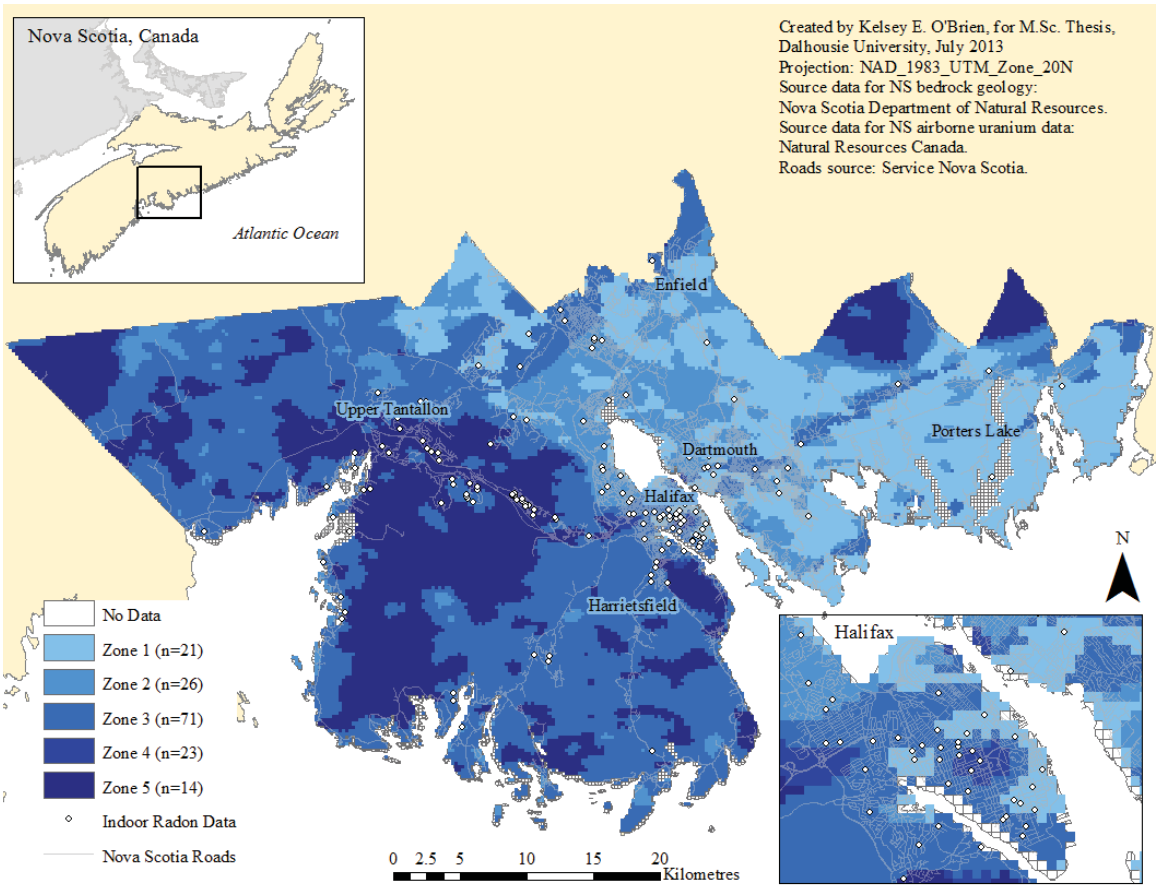

Figure 2.7: Map 2W - Created using only two layers (*Bedrock* and *Airborne*), as they were they only layers significantly correlated to indoor radon. Both layers were weighted using the OLS statistical regression. Note the distribution of indoor radon data; the map is more accurate in regions with dense indoor radon data points.

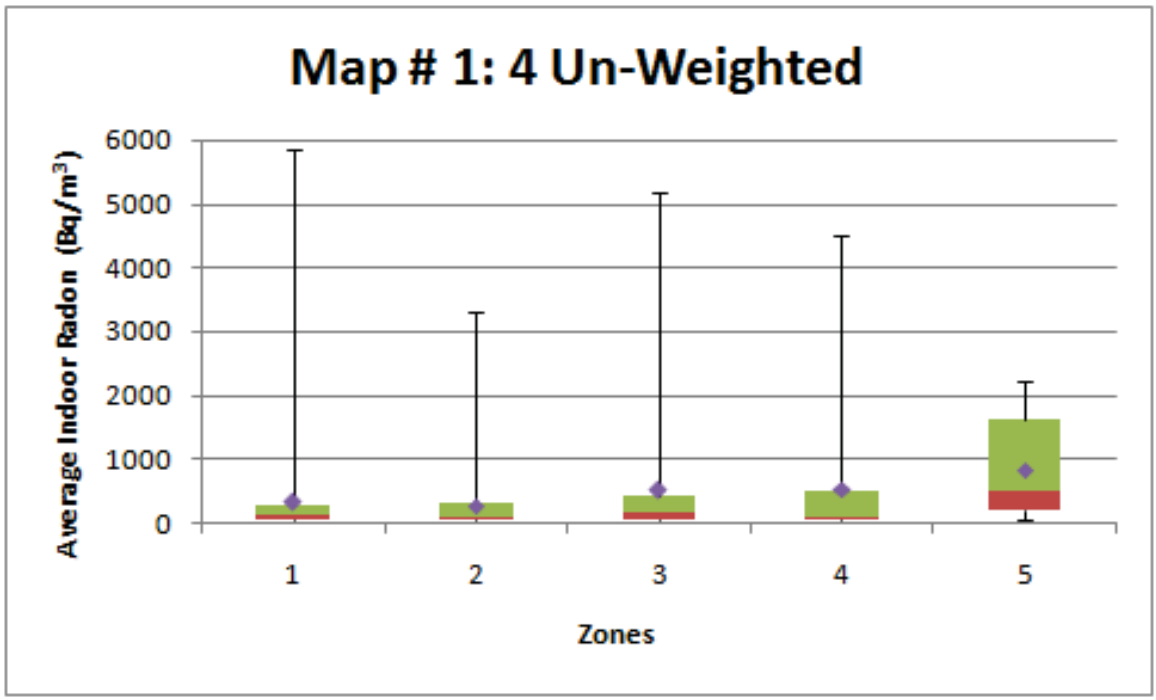

Figure 2.8: Box and whisker plots displaying the variance between each zone for Map 4UW. The top and bottom error bars represent respectively the maximum and minimum values; the top box represents Q1; the bottom box represents Q3; the middle bar represents the median, and the diamond represents the mean.

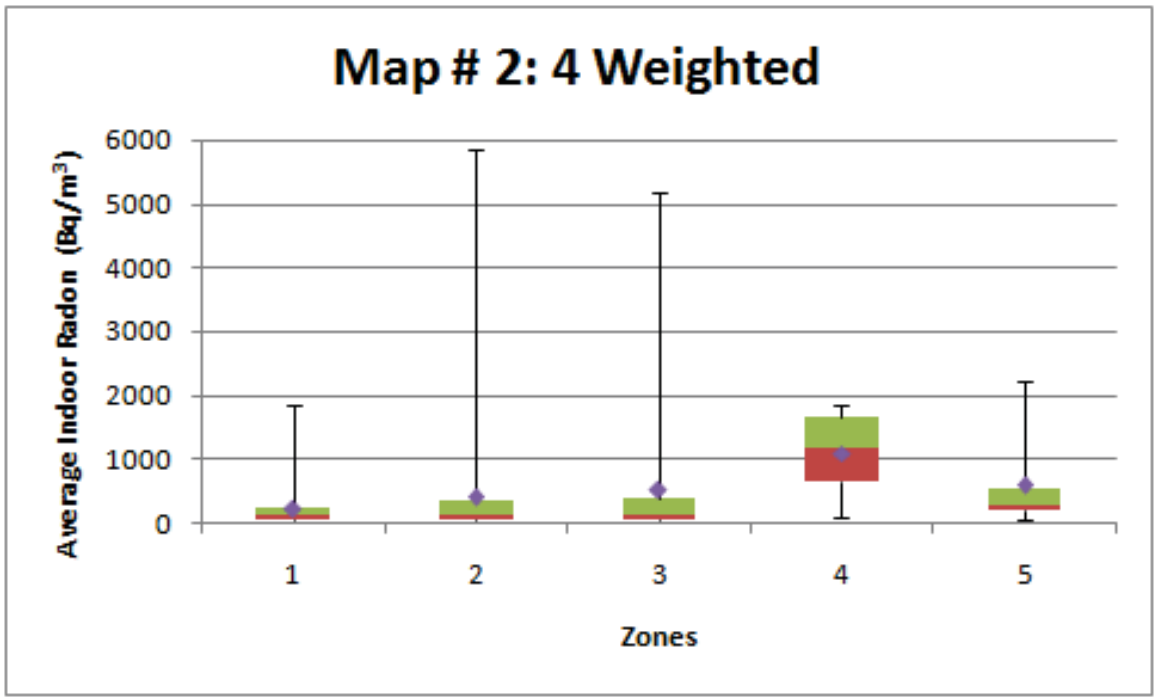

Figure 2.9: Box and whisker plots displaying the variance between each zone for Map 4W. The top and bottom error bars represent respectively the maximum and minimum values; the top box represents Q1; the bottom box represents Q3; the middle bar represents the median, and the diamond represents the mean.

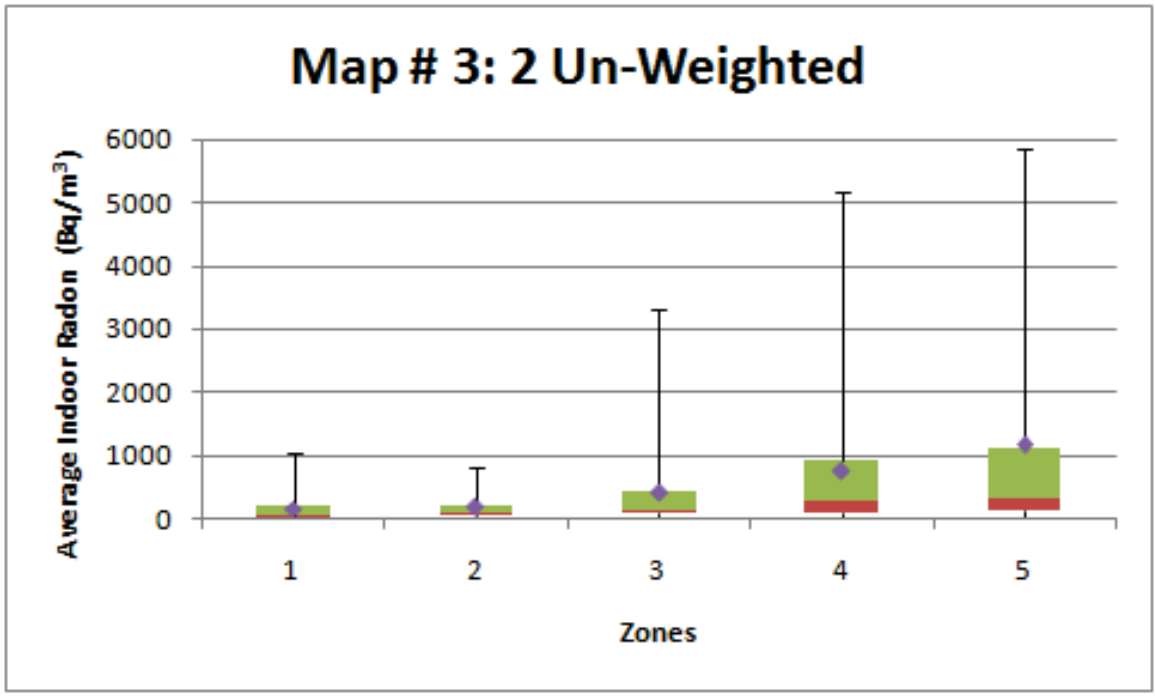

Figure 2.10: Box and whisker plots displaying the variance between each zone for Map 2UW. The top and bottom error bars represent respectively the maximum and minimum values; the top box represents Q1; the bottom box represents Q3; the middle bar represents the median, and the diamond represents the mean.

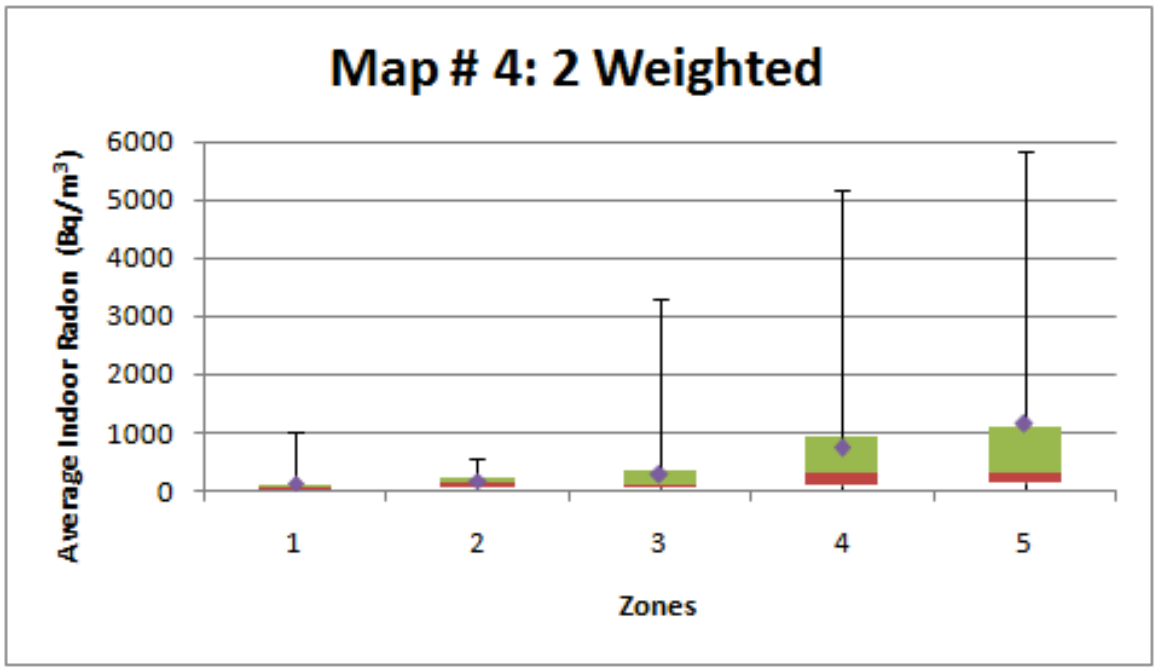

Figure 2.11: Box and whisker plots displaying the variance between each zone for Map 2W. The top and bottom error bars represent respectively the maximum and minimum values; the top box represents Q1; the bottom box represents Q3; the middle bar represents the median, and the diamond represents the mean.

Chapter 3

Radon Soil Gas Migration and Transport through Halifax Tills and Bedrock, Nova Scotia

3.1 Preamble

This chapter has been submitted as a manuscript for publication to *Environmental Earth Sciences*. I was the primary author and investigator in this study, and did all the field work, apparatus building, gas sampling, analyses and writing. The three other contributing authors: Dave Risk, Daniel Rainham, and Anne Marie O'Beirne-Ryan all reviewed, edited, and collaborated on this project and the manuscript.

3.2 Introduction

Radon-222 is a naturally occurring, invisible, odourless, and colourless radioactive gas that is present in measurable quantities in all till and soil types across Nova Scotia (Goodwin et al., 2008). It is a daughter product of the ^{238}U series (See Figure 3.1), and decays to ^{218}Po, releasing a potentially harmful alpha particle in the process. Radon-222 has a half-life of 3.82 days, and can be found in water, till, and air.

Radon-222 gas produced in rock, till, or water becomes a potential health hazard when it accumulates in a home and is inhaled. When the radon daughter decay particles break down they can potentially damage the lung tissue. Long-term exposure to high radon concentrations through inhalation is the second leading cause of lung cancer next to smoking (EPA, 1993; WHO, 2005). The Health Canada guideline for indoor radon gas exposure is set at 200 Bq m^{-3} (HC, 2012).

Previous radon studies have identified radon risk regions based on geographic distributions (i.e municipal boundaries), and not the local geology (Letourneau et al., 1992; Wichmann et al., 2002; Espinosa and Gammage, 2003; Kemski et al., 2009; Chen et al., 2008a). A radon risk potential map of Canada (seen in Figure 1.8) previously identified Central Canada (Winnipeg, Manitoba) and Atlantic Canada

(regions of Nova Scotia) as high risk areas (Chen et al., 2008a; Chen, 2009). This was the first radon map identifying risk regions within Canada, (though there were previous uranium studies in Canada - examples from Nova Scotia include: Dyck et al. (1976); Grantham (1986)), and was compiled using field radon gas readings and indoor measurements. As Nova Scotia was identified as a high radon inhalation risk region, the area should be further studied as the region potentially poses a threat to human health.

3.2.1 Radon Occurrence in Nova Scotia

The bedrock geology of Halifax Regional Municipality, the most populous region within the province of Nova Scotia, has been previously described (MacDonald and Horne, 1987; Keppie, 2006; White et al., 2008; White, 2010). There are three dominant bedrock geology units - the Goldenville and Halifax Groups of the Meguma Supergroup, and the South Mountain Batholith (SMB) (Figure 3.2). In addition to bedrock units, there are two major glacial units within the HRM that provide potential sources of radon gas - the Lawrencetown Till, and the Beaver River Till (BRT) (Figure 3.2). The Cambrian-Ordovician Goldenville and Halifax Groups comprise mainly metasandstones (previously quartzite) and slates (White et al., 2008; White, 2010). The Late Devonian SMB is a granitic plutonic complex that intruded both the Goldenville and Halifax Groups. This pluton has been subdivided into three main phases based on its composition: an early monzogranite, coarse-grained leucomonzogranite, and late fine-grained leucomonzogranite (FGL) (MacDonald and Horne, 1987). High radon soil gas values in the HRM are typically associated with granites and slates (Je, 1998a). In the HRM, radon has been previously identified as having a high potential health risk (Lewis et al. (1998); O'Beirne-Ryan and Zentilli (2006); White et al. (2008), among others). Granites are uraniferous, and fractures in the slate can increase the potential for radon escape from the bedrock.

There are many regions within Nova Scotia that have naturally high radon; a region of geologic interest to this study is near Windsor, Nova Scotia (Figure 3.3), as it is underlain by uranium-enriched bedrock. The Windsor region is underlain by basement Meguma Terrane (Cambro-Ordovician metasediments of the Meguma Supergroup with Late Devonian granitoids) overlain by the sedimentary sequence

of the Maritimes Basin (Ryan et al., 2009). Within this basin, the Mississippian clastic fluvial-lacustrine rocks of the Horton Group, among others, are exposed (Ryan et al., 2009). The Cheverie Formation sandstones, siltstones, and conglomerates are enriched in uranium and its daughter products (Ryan and O'Beirne-Ryan, 2009), making the region geochemically significant to this study. The uranium mineralization on Green Street (colloquially referred to as the 'Green Street' occurrence; Ryan et al. (2009); Ryan and O'Beirne-Ryan (2009)) created a sandstone roll-front type deposit that is restricted to roughly 1 km of outcrop (Ryan and O'Beirne-Ryan, 2007). As such, the radon gas potential for this region is high as it is uranium-rich (Ryan and O'Beirne-Ryan, 2007).

Soil gas testing across the province of Nova Scotia has shown measurable quantities of radon in all tested field sites (Goodwin et al., 2008). From 72 field sites, the granite phase of the BRT returned the highest mean radon concentration of 48.5 kBq m^{-3}, followed by the slate till phase with 36.1 kBq m^{-3}, and the metasandstone till phase and Lawrencetown Till with 22.4 kBq m^{-3} and 19.3 kBq m^{-3} respectively (Goodwin et al., 2010). Though there is no soil radon guideline, these values are orders of magnitudes higher than the indoor radon gas guideline. Though most tills in the HRM are uranium-bearing, the BRT granite phase (as defined by Stea and Fowler (1981); MacDonald and Horne (1987); Utting (2009)) has consistently displayed the HRM's highest concentration unit. It is therefore crucial to understand the gas transport properties of this unit, as approximately 40% of the HRM study area is underlain by this U-bearing granite phase till.

The Lawrencetown Till is comprised mostly clay and clasts, and does not reflect the composition of the local bedrock (Lewis et al., 1998). It is found mostly in drumlins around the HRM, and has the lowest radon soil gas of all the till units in this area (Goodwin et al., 2010, 2009). The second major unit, the BRT, is a locally derived glacial unit. For this study, the fine-grained leucomonzogranite phase of the BRT was studied in detail as it contains the highest soil radon gas concentrations (Goodwin et al., 2010, 2009). This granite phase till is comprised of locally-derived, angular, leucomonzogranite clasts set in a sandy matrix (seen in Stea and Fowler (1981, 1979). This till underlies approximately 40% of the HRM, and ranges in thickness from $<$ 1 to 10 m.

3.2.2 Radon Transport in Tills - Regional Work and Theory

Assessing the dominant factor in the control of radon gas expression is critical for assessing health risk potential of homes built on bedrock versus till. Previous 1 dimensional numerical soil gas modeling (for Halifax's high radon soil gas unit, BRT granite phase) showed that, unless the till is less than 1.0 m thick above the bedrock, the radon produced from bedrock alone will not make it to the surface before it decays (O'Brien, 2010; O'Brien et al., 2011). Indeed, till may produce and transport more radon soil gas than bedrock.

Gaseous transport within soil is known to be controlled by two main processes: diffusivity (Equation 3.1) and convection (Hillel, 1998). Though both processes contribute to movement of gases in soil, diffusion rather than convection has been acknowledged as the more important mechanism of soil aeration (Keen, 1931; Penman, 1940; Russell, 1952; Ball et al., 1999). As the dominant mechanism, diffusion is described by Fick's first law (as seen in Hillel (2004)):

$$J = -D\frac{\partial \phi}{\partial x} \tag{3.1}$$

Where:

J is the diffusion flux (mol / m^2 s)

D is the diffusion co-efficient, or diffusivity (m^2 / s)

ϕ is the concentration (mol / m^3)

x is the position (m)

In radon soil gas literature, permeability (rather than diffusivity) is commonly the measured form of flux transport (Friske et al., 2010; Goodwin et al., 2010; Chen et al., 2009). With respect to soil gas transport, diffusivity and permeability are proportional (Washington et al., 1994). The diffusion co-efficient and the permeability co-efficient exhibit a strong empirical relationship, as logarithmically transformed values of bulk diffusion and gas permeability are related in a positive linear fashion, as described by Washington et al. (1994):

$$logD_{b,g} = 2.47 + 0.53logk - logM_g^{0.5} \tag{3.2}$$

Where:

$D_{b,g}$ is the bulk diffusion of any soluble gas (cm^2 / s)

k is the permeability (cm^2)

M_g is the mass of the gas of interest (g)

Given the strong linear relationship between permeability and diffusivity (Equation 3.2) (Washington et al., 1994), this study will follow standard radon soil gas literature (e.g. Goodwin et al. (2009)) and describe soil gas movement predominantly in terms of permeability. Diffusivity has also been measured and values will be included for comparison. Diffusion is a key component in radon gas transport (Ball et al., 1999). ^{222}Rn can be produced in, or diffuse into, the interstitial pores of the soil and travel to the soil surface (Silker et al., 2007).

Permeability is also a significant factor in the movement of gas, as sandy soils have higher permeability than clay rich soils (Freeze and Cherry, 1979; Neznal and Neznal, 2005). Gas can then move faster through the pore spaces to reach the surface.

Water has been shown to play an important role in the diffusion and amount of radon measured in a system. Holkko and Liukkonen (1992) showed that the diffusion rate increased in moist soils compared to dry soils. A study from North Carolina showed that radon concentrations increased with increasing moisture content in closed soil columns, as well as in gas-bag samples (Menetrez and Mosley, 1996).

Although the importance of diffusivity and permeability has been previously documented, there are few studies that quantify the importance of one over another, and none within Nova Scotia. Diffusivity has not been measured in HRM tills. The physical parameters of gas transport need to be measured in a controlled field-analogue system in order to understand the important influences on radon gas movement. The addition of water will aid in addressing the transport dynamics that affect radon movement through the till.

3.2.3 Gaps in Existing Research

There have yet to be controlled laboratory experiments that test the contribution from bedrock and the limitations of the permeability measurements. Understanding the movement of radon gas through the BRT granite phase FGL unit is important within Halifax, because the BRT makes up 40% of the till coverage, and it has been demonstrated to be the most important source of radon.

Though many risk prediction techniques combine the importance of soil gas permeability and radon soil gas concentration (e.g. Jiranke et al. (1999); Appleton et al. (2011), there is still a need to quantify the relative contribution of these factors in the surface expression of radon gas. Traditionally, geological maps are the first reference for identifying high radon regions (Je, 1998a). Work is in progress to create a radon potential map of Nova Scotia using bedrock geology, surficial geology, and airborne radiometric uranium (O'Reilly et al., 2009b). In Nova Scotia, no field diffusivity, and few permeability measurements have been taken (Goodwin et al., 2008, 2009, 2010). Till thickness is highly variable, particularly in the HRM region and it ranges from $<$ 1 m to 10 m thick. Because of this variability, as well as the composition and clast variability within the till, the transport mechanisms and concentrations of gas moving though various units need to be understood. This study will contribute to the limited permeability database, and fill in the knowledge gaps in understanding and quantifying gas movement through these radon-producing tills.

This study aims to test the following hypotheses:

1. Till permeability and diffusivity of the tills are controlling factors on the radon concentration measured at the surface.

2. The radon measured at the till surface is primarily produced in the overlying glacial deposits, and not the underlying bedrock.

3. There is a correlation between the permeability and diffusivity of the tills that can be identified using analogue models of field conditions.

The contribution of this study is to determine and quantify the controlling factors, and the dominant production source of the ^{222}Rn concentration observed at the till surface.

In order to address these hypotheses, four different columns were constructed as analogue models of field conditions. Using a combination of field methods and laboratory experiments, ^{222}Rn concentration profiles were measured from 0.6 m depth to the column surface using combinations of granite or high-radon sandstone bedrock source, and granite phase till or inert sands. Described below are how the tills and bedrock samples were collected, as well as the column construction, and measurement collection.

3.3 Methods

3.3.1 Method A: Field Work

Till Sample Collection

Field sites were located within the HRM, and focused around the SMB FGL phase bedrock and till (as defined by Stea and Fowler (1981); MacDonald and Horne (1987)) (Figure 3.3).

A total of 12 sites were sampled with 47 x 2 kg till samples collected over a period of 2 months (July and August, 2011). Field sites were chosen based on existing road networks and property permission access, which resulted in the majority of sites being located within and around the Jerry Lawrence Provincial Park (Figure 3.3). The park is entirely underlain by the FGL bedrock; sampling permission was granted by the Nova Scotia Parks and Recreation Division. Another sample location within the FGL phase included a region where whole rock geochemistry data had previously been collected and analyzed by the Nova Scotia Department of Natural Resources (Fisher, 2006). The analyses showed high bedrock U concentrations of 13 and 20 parts per million (ppm) at sites less than 0.6 km from where samples were collected for this study. Finally, a FGL till sample was collected less than approx. 1.0 km from Tantallon Elementary School in Upper Tantallon (Figure 3.3). This school had previously been identified by the Nova Scotia Department of Environment as having 13 rooms testing above the 200 Bq m^{-3} Health Canada indoor radon guideline (NSDPE, 2009); it has since been mitigated.

Sample sites were located within recently undisturbed forests, away from any evident form of human contamination (ie. soil re-working, or foot paths), and were typically on upper slopes away from low-lying regions and bodies of water to avoid sampling below the water table. The sampling procedure was modeled after previous HRM till investigations (Goodwin et al., 2010; Friske et al., 2010). At each sample site, a 70 cm diameter soil pit was dug to a depth of at least 60 cm (Figure 3.4). The 60 cm sampling depth protocol was followed in this study to compare with previous work using the same sampling depth (Chen et al., 2009; Goodwin et al., 2009, 2010; Friske et al., 2010; O'Brien et al., 2011). In addition, it was shown that radon gas concentrations remained relatively constant deeper than 60 cm, and was therefore

unnecessary to sample at depths greater than 60 cm (Goodwin et al., 2008). Four 2 kg samples of the C horizon (the glacial till) were collected from each pit; on average, the C horizon began between 50-70 cm depth. No C horizon till was collected above 60 cm to remain comparable to previous studies. In addition, global positioning system (GPS) coordinates were taken at each location directly over each soil pit so sample locations could be cross referenced with geological maps (Figure 3.3). Till samples were sieved to determine grain size and distribution; results can be seen in Appendix C.

Bedrock Sample Collection

Bedrock samples were collected from two field locations (Figure 3.3) with elevated ^{238}U levels as registered on a GR-135+ spectrometer.

Sample one corresponded to the highest whole rock and till geochemistry uranium values (20 ppm and 16 ppm, respectively) previously collected and analyzed by the Nova Scotia Department of Natural Resources (Fisher, 2006). Field observations noted hemitization in the outcrop, indicative of late-stage fluid migration, possibly associated with uranium mineralization (as described by Ryan and O'Beirne-Ryan (2007)).

Sample two was collected within the Cheverie Formation of the Horton Group, near Windsor. The 'Green Street' sandstone outcrop is part of a roll-front uranium deposit (Ryan and O'Beirne-Ryan, 2009), with high uranium concentrations in the organic-rich (reducing) layer. As such, the organic-rich sandstone layer had a higher uranium (and subsequently, radon) content than the highest FGL granite outcrop in the HRM. This sample is used to mimic conditions that might exist in regions within the FGL granite bedrock with extensive or well developed fracture zones, where uranium concentrations are higher than average FGL concentrations (per. com., George O'Reilly). Because using a fractured bedrock source in the bottom of the column would affect the permeability, this enriched uranium sandstone was used to mimic the high concentrations emitted without compromising the permeability of the column.

Cutting Core

The two bedrock samples were cut into 15 cm diameter discs 2.5 to 6 cm thick. The discs were cut into five cores from the fine-grained leucomonzogranite phase of the SMB, and two cores from the Cheverie Formation sandstone from the Horton Group; 3 of the total 7 cores were used.

3.3.2 Method B: Lab Work

Building Soil Columns

Till samples from 8 (of 12) field sites were selected for pooling the tills to create a homogeneous 'representative sample' of the fine-grained leucomonzogranite till phase from the SMB. Individual samples were chosen based on the following criteria: (i) above the water table, (ii) confirmed C horizon till, (iii) near previously identified high indoor radon sites. All till samples were manually mixed until an assumed homogeneous medium was created.

Columns used in this study (Figure 3.5) were built out of low-uranium, 15 cm diameter 'schedule 40' polyvinyl chloride (PVC) pipe. The cleaned pipe was cut into 70 cm lengths, and 0.64 cm diameter holes were drilled up both sides of each column every 10 cm. Each column was packed manually, and aimed for a diffusivity of roughly 10^{-7} m, as dictated by previously calculated model conditions (O'Brien et al., 2011). Polyethylene tubing was inserted horizontally every 10 cm, to act as conduits for extracting radon soil gas and for permeability and diffusivity measurements. The middle 12 cm of each 30 cm long piece was perforated; the tubing was put in place as the till was packed up the column.

The soil column experiments were run in both an open system, and a closed system. When the columns were not capped, negligible concentrations of radon gas were measured, even directly above a bedrock source. In order to accumulate radon gas to see trends through the column, the experiments were capped (represented a closed system). Clamps were positioned to control the flow of the gas in and out of the columns. Leak tests were performed on all columns to ensure a trivial amount of gas was escaping.

The columns were left to equilibrate for two months (at least ten times the

estimated transit time, per. com. Dave Risk, 2013) before gas sampling started (Figure 3.6). As the half-life of radium is 1590 years, the soil columns were not in secular equilibrium (see section 1.4); the radium in the system has been building up for much longer than the radon (half-life 3.82 days)

Diffusivity

A 1D diffusive profile of the soil columns was generated using manually created CO_2 (by holding air in the lungs and exhaling into a syringe) gas as a tracer. 150 mL syringes of CO_2 were introduced at the 10 cm (back) and 10 cm (front) heights on all columns, for a total of 8 slugs of CO_2. A needle was then connected to a 3-way valve, in order to extract the gas from the column into a 3 mL flushed and evacuated vial.

Concentrations of CO_2 in the individual vials were measured using the Shimadzu GC-14A gas chromatograph machine (sensitivity of 40000 mV mL/mg). The machine was calibrated using triplicates of Matheson TriGas MicroMat10 CO_2 in 100 ppm (diluted with He), 1000 ppm (diluted with He) and 1% (diluted with N). The oven temperature was 50°C, N (carrier) gas was pressurized to 140 PSI, the current was 80 nA, and the polarization was 2%. Individual 3 mL samples were injected into the coil while 3 mL of triply de-ionized water was simultaneously pushed into the vials; this ensured atmospheric air was not being drawn into the machine.

Leak Test

To ensure the accuracy (i.e. gas trends seen are a result of diffusion, not leakage) of the gas measurements, and to help explain potential outliers from sampling results, a leak test was developed and performed on all four columns.

Slugs of CO_2 were introduced throughout the columns and left to equilibrate. Samples of air were then extracted every 2 days using the same procedure as for the diffusivity tests. Repetitions indicated the overall concentration of CO_2 in the columns diminished minimally with time.

Permeability

Using the protocol developed by the NAGLP project (Friske et al., 2010) and previous HRM field work (Goodwin et al., 2009, 2010), gas permeability was measured in

each column apparatus (Figure 3.5) using the RADON JOK portable permeability machine.

Permeability values were measured in sextuples at the 10 cm mark (60 cm depth); the timed values were then used to calculate permeability using the equation presented in the user's manual and used in previous work (Equation 1.4) (Friske et al., 2010; Goodwin et al., 2009).

Radon Soil Gas

The Durridge RAD7 was used to measure radon soil gas as it is accurate over a large range of concentrations (kBq m^{-3} to Bq m^{-3}), and has been validated in several studies (Chao et al., 1997; Yu et al., 2002; Groves-Kirkby et al., 2006). The RAD7 tested gas samples every 10 cm up the columns, measuring the radon daughter product (Po-218). A 45 micron filter capped the intake valve of the RAD7, and a Drierite drying tube was connected in series between the columns and RAD7 to minimize moisture.

Several precautions ensured that the gas samples were evenly drawn throughout the column without disturbing the tills beneath it: (i) gas samples were taken from perforated tubing that ran horizontally across the column, to minimize the vertical sphere of influence taken when gas was drawn from the column, (ii) the outlet valve of the RAD7 fed back into the same depth in the column (but the opposite side from the intake), (iii) radon concentrations were measured in triplicate from both the top down and the bottom up. The results presented in the next section show the average radon value calculated from a pool of six numbers at each depth (three top-down, and three bottom-up readings).

These methods also established the efficacy of a 5-minute purge technique used for eliminating memory effects within the Durridge RAD7. Replicates showed that when the instrument was not purged for 5 minutes between each reading, a false *hot spot* was measured; this build-up of *old* radon occurring within the machine could have potentially affected the readings.

3.4 Results

Column 1 simulated a home built on a drumlin (FGL T); column 2 simulated a potential building on bedrock with a thin till cover (FGL T and FGL B); column 3 simulated a building on bedrock with inert sands (FGL T and IS); column 4 simulated a home built on 'fractured' bedrock (i.e. simulated by extremely high uranium concentrations, FGL T and GS) (Figure 3.5). The average radon concentrations for column 1 (Figure 3.7) were 4,164 Bq m^{-3} and 7,495 Bq m^{-3}, respectively for dry and wet conditions; the dry and wet standard deviations were 1,279 Bq m^{-3} and 1,168 Bq m^{-3}. Both wet and dry conditions displayed increasing average radon concentration with increasing depth; the slopes of the lines of best fit are nearly identical.

Column 2 (Figure 3.7) had average radon concentrations of 5,247 Bq m^{-3} and 9,529 Bq m^{-3}, respectively for dry and wet conditions; the dry and wet standard deviations were 588 Bq m^{-3} and 1,481 Bq m^{-3}. Though both dry and wet trials showed increasing radon with depth, the radon/depth profile was steeper for the dry till sample. Similar to column 1, the wetted tills showed a significant increase in average radon concentration over the dry radon concentrations.

The average radon concentrations for column 3 (Figure 3.7) were 491 Bq m^{-3} and 486 Bq m^{-3}, respectively for dry and wet conditions; the dry and wet standard deviations were 99 Bq m^{-3} and 88 Bq m^{-3}. There was no significant trend between radon concentrations and depth; there was also no statistically significant difference between the radon concentrations for either moisture condition, perhaps because the sands could not retain moisture. The measured data were scattered with lower values than both columns 1 and 2.

Column 4 (Figure 3.7) had measured average radon concentrations of 72,148 Bq m^{-3} and 74,460 Bq m^{-3}, respectively for dry and wet conditions; the dry and wet standard deviations were 15,611 Bq m^{-3} and 27,341 Bq m^{-3}. The same positive correlation was displayed here, however, at such high concentrations, the difference between wet and dry was low. The radon/depth profile is shallower for wet conditions, a result also seen in column 2 results. All radon gas data can be seen in Appendix C.

The average diffusivity values for columns 1 and 2 were within the 10^{-8} m^2 range for both dry and wet tills, with the dry tills more diffusive than the wet (Table 3.1). Column 4 also showed this same gas transport trend where dry tills were more diffusive

than wet, though there was a much greater difference between the two. Column 3, however, showed an opposing trend of dry sand being less diffusive than wet.

The average permeability values for the FGL till were all within an order of magnitude (Table 3.2). Column 3 (silica sand unit) had average permeability values on the order of 10^{-12}. As expected, the sand unit was more permeable than the till unit.

An important trend identified was the permeability change with difference moisture content. In all four columns, the dry tills were more permeable than wet tills, as expected. Columns 1, 2, and 4 were near saturation with the addition of water, column 3 was not. The permeability contrast between dry and wet sand was the least well defined in column 3.

Overall, the dry tills were more diffusive and more permeable than the wet (as they had less water-filled pore spaces); the silica sand was more permeable than the FGL till. The average permeability values calculated from CO_2 had the strongest positive linear correlation with the average diffusivity values (Figure 3.8). This correlation may be weak as a result of some outliers originating from column 3. Diffusivity and permeability are positively correlated with an r value of 0.371. Table 3.3 shows the calculated transit times and speeds in the columns. The average transit time was 3.69 days, with a standard deviation of 1.70 days. The average transit speed for FGL till was 0.19 m day^{-1}; the standard deviation was 0.08 m day^{-1}. Because the transit time for the FGL till is less than the 3.82 day half-life, the radon was able to travel through the till before decaying completely.

The transit time was compared to a 3.82 half-life of ^{222}Rn, at which point 50% of the original concentration had decayed. If the transit time was longer than 3.8 days, it was considered 'slow', as more than 50% of the original radon decayed. Conversely, a transit time of less than 3.8 days describes a 'fast' time where less than 50% of the original concentration had a chance to decay before leaving the system.

3.5 Discussion

3.5.1 Radon

In the experiments presented here, the average dry radon concentration of the 3 FGL columns was 5,247 Bq m^{-3}, and the average wet concentration was 9,529 Bq m^{-3}. The radon values reported in this study are almost exactly one order of magnitude lower from those in previous literature, as might be expected, because the previous field measurements drew from a much larger radon 'sink' within the tills, both horizontally and vertically. Because the column experiments lack the horizontal sampling sphere, the exact concentrations are less important than the overall trends between the columns.

The radon soil gas results identified a positive correlation between gas concentrations and depth. In most cases with increasing moisture content, the radon gas concentrations also increase. When the tills are more saturated, some of the air-filled pore spaces become filled with water. This is also causes lower (resulting in slower) permeability and diffusivity rates. As radon is more soluble in air than water (Je, 1998b; Holkko and Liukkonen, 1992), the gas migrates when the pore spaces start to fill with water. The addition of water to the system changes the chemistry and transport dynamics; the remaining air-filled pore spaces therefore become enriched in radon.

This relationship is very important within the context of Nova Scotia, where the climate is wet. By adding the equivalent of a typical summer month's rain volume to the columns, the average radon gas concentrations doubled in columns 1, and 2. This relationship has been identified in recent literature (Menetrez and Mosley, 1996), however, it has now also been demonstrated in HRM tills. The lack of a clear permeability vs diffusivity trend in column 3 is attributed to the high permeability of quartz sand which therefore did not retain water.

A new result supported by the experiments in column 4 holds interesting implications for homes built on 'fractured' bedrock (i.e. represented with extremely high radon levels). With an extreme case of high radon-producing bedrock, not only did the radon produced in the till seem insignificant, but the moisture of the tills did not have a significant effect on radon concentration. Though the saturated tills did

have slightly more radon, the bedrock source was the dominant production source of radon. If the bedrock were fractured, the gaps would allow more rapid movement of gas, and potentially change the transport speeds and also the amount transported.

Another trend seen across the columns was the increasing variation with increasing radon concentrations. The average radon concentration trend was: column 4 > column 2 > column 1 > column 3. The standard deviations in column 4 were an order of magnitude higher than those in column 1 and 2, and two orders of magnitude higher than column 3, however there was the same percentage difference between the columns (20 - 30%). High standard deviations can be attributed to the variation within the soil column. Some of the variation can be attributed to, in part, to localized hot spots (^{238}U bearing clasts), and the natural heterogeneity of the till. It may also have been affected by the mixing of two different podzol (humic and ferric) profiles to approximate a homogeneous till.

3.5.2 Diffusivity

Diffusivity trends were identified in columns 1, 2 and 4; resulst from column 3 were difficult to interpret because of the high permeability. However, in mixed natural till samples, the dry FGL diffusivity derived from CO_2 had an average of 7.52 x 10^{-8} m^2 s^{-1} (st dev 2.51 x 10^{-8} m^2 s^{-1}), and the average wet FGL diffusivity was 3.37 x 10^{-8} m^2 s^{-1} (st dev 1.68 x 10^{-8} m^2 s^{-1}). The dry FGL average diffusivity calculated from ^{222}Rn measurements was 7.30 x 10^{-7} m^2 s^{-1} (st dev 5.05 x 10^{-7} m^2 s^{-1}); the average wet FGL diffusivity was 6.47x 10^{-7} m^2 s^{-1} (st dev 3.37 x 10^{-7} m^2 s^{-1}). These measured values were within an order of magnitude with the results calculated using a 1D model (10^{-7} 10^{-8} m^2 s^{-1}) (O'Brien et al., 2011). These results are the first diffusivity measurements for the BRT FGL till; as this till unit is the highest radon-producing unit within HRM, the findings here are vital in quantifying the gas movement by diffusion.

The diffusivity calculated from CO_2 (using Equation 4 from Risk et al. (2008)) values and transformed using Graham's Law of effusion, was likely an underestimate as it did not account for the radon decay. Graham's law is described by Solcova et al. (2001):

$$\frac{N_1}{N_2} = -\sqrt{\frac{M_2}{M_1}} \tag{3.3}$$

Where:

N_1 is the diffusion flux of gas 1 (m^2 s)

N_2 is the diffusion flux of gas 2 (m^2 s)

M_1 is the molar mass of gas 1 (g / mol)

M_2 is the molar mass of gas 2 (g / mol)

When radon concentrations were used to calculate diffusivity (using model fitting, per. com. Nick Nickerson), the radon measured at the surface was known to be no younger than the time (in days) calculated. Therefore, the diffusivity values calculated from CO_2 were the fastest possible diffusivity of the tills. It can be assumed that the diffusivity calculated from radon was slower than the 'true' value, and the diffusivity calculated from CO_2 was faster than the 'true' value. Because both methods have merit, the true diffusivity of the FGL in the columns was likely somewhere between the two (per. com. Dave Risk, 2013). However, it is not clear if the 'true' value is closer to diffusivity calculated from CO_2 or from Rn, therefore taking a basic mean of the two contrasting methods is too crude of an estimate.

3.5.3 Permeability

The radon soil gas and the permeability have both been shown to influence the concentrations of gas at the surface (Neznal et al., 2006); recent Halifax field studies hypothesized that permeability and radon concentration were both equally important determinants (O'Brien, 2010).

The permeability values measured in the laboratory columns were within an order of magnitude to those measured previously (Goodwin et al., 2010). The average field permeability value for the granite phase of the BRT had been previous measured as 5.77 x $^{-12}$ m^2; in the current study, the average permeability value of the FGL till was 7.50 x $^{-13}$ m^2 in the dry field tills, and 5.49 x $^{-13}$ m^2 in the wet tills (n=3; Table 3.2). The soil columns may have been less permeable because of the closed nature of the system, as opposed to field conditions, where it was an open system. This could affect the gas transport, and in turn, the radon gas concentrations. In the laboratory setting, the columns were capped, meaning that a negligible amount of gas

passed in and out of the column. In the field, there were other non-till units above the C horizon (F, H, Ae, Ah, Bf) that were less permeable, and therefore slowed the movement of gas to the surface. However, because the other soil units were more permeable than the column cap used in the experiments, the permeability of field tills was greater than that of laboratory tills. Another consideration was the packing; in the field, the tills could be packed tighter than the column experiments, meaning that the permeability of the columns were underestimates. The tills are less permeable than the sands, as expected, because there are more air-filled pore space in the sand units, than in the till.

A controlling factor on radon concentrations, permeability, and diffusivity was the influence of moisture. In the wet tills, radon concentrations were higher, and the tills were less diffusive and less permeable. These results are supported by radon gas literature; water plays an important role in the diffusion and abundance of radon gas in the system - with increasing moisture, radon concentrations increase and diffusivity decreases (Holkko and Liukkonen, 1992).

In the experiments, adding moisture equivalent to a heavy rain event (as expected in Nova Scotia's wet climate) increased the radon concentration in the tills, though they are less diffusive and less permeable. When additional moisture was added to the silica sand unit, the lack of clear response was likely a result of the high permeability of quartz sand.

The results of the diffusivity and permeability analyses (Figure 3.8) agree with previous work; the permeability and diffusivity of a medium are positively linearly correlated (Washington et al., 1994) (Equation 3.2). Though they are not identical, they are directly proportional to each other, and the transport information gained from both can be used as a reference for future HRM work. The permeability is a reasonable proxy for the diffusivity of the tills; though there is an order of magnitude difference between the absolute values, the proportions are similar.

3.5.4 Transit Time

Within columns 1, 2, and 4, the radon radioactive decay rate exceeded the transit time (Table 3.3). A transit time for column 3 could not be calculated; the high permeability overwrote any sort of trends, as the radon gas traveled straight through

the column without decaying significantly. This is potentially more problematic for building construction, as the soil gas could travel through the till to reach the basement foundation before it starts decaying.

In the two columns with FGL till and a bedrock source (2 and 4), the wet till conditions had slower transit times than the dry (Table 3.3). In the column with FGL till and no bedrock (3), the dry till conditions measured slower transit times than the dry. Though it is apparent that moisture can play an important role on the transit time, additional data is required to establish a clear trend. Assuming a homogeneous medium, uniform movement of gas, and no localized hot spots, with a less than 1 m thick till cover over bedrock, radon traveling through dry till will barely make it to the surface before it decays; radon from wet tills could decay in the medium before reaching the surface. These results are validated by previous modeling work, which predicted that unless the till is extremely thin above the bedrock (less than 1 m) radon would not have made it to the surface before decaying (O'Brien et al., 2011).

3.6 Conclusion

The importance of diffusivity in till has been previously documented; the results of this study contribute to the existing literature by quantifying the physical parameters of gas transport through HRM's highest radon-producing radon unit. None of the previous work on radon within the HRM till units had simultaneous permeability and diffusivity measurements in till, as diffusivity is difficult to measure in the field. By measuring the diffusivity in an experimental system, this study has contributed permeability data, and has also addressed a gap in diffusivity data.

The results showed that in areas of thin till cover (60 cm thick) over non-fractured bedrock, the radon concentration detected at the surface were produced in the till. However, with a 'fractured' bedrock source (i.e. with extremely high radon levels), the radon concentrations detected at the surface were being produced in the bedrock. The addition of moisture in the columns increased the average radon concentrations detected.

Further testing focused on open system columns with various cap materials (cement, clay, sand) could provide physical data to compare to calculated predictions.

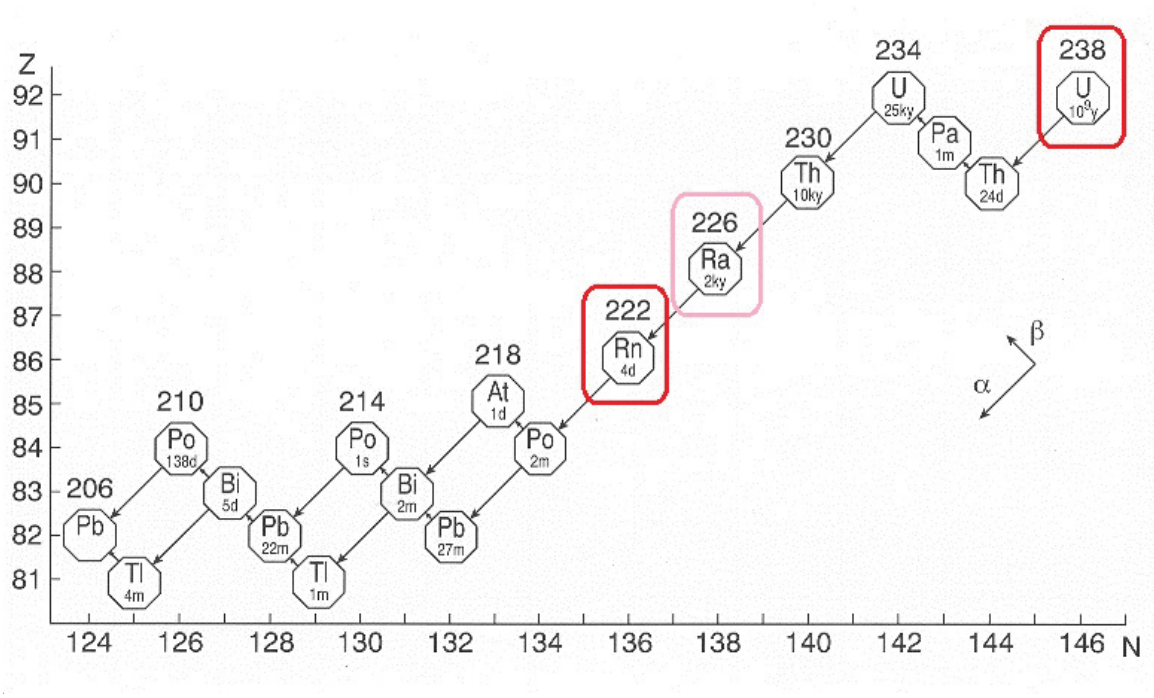

Figure 3.1: This figure depicts the uranium-238 decay chain, where Z is the atomic number and N is the number of neutrons. The half-life is also displayed in days (where 4d is equal to 3.82 days). Nuclides of interest are highlighted. Modified from the University of Maryland, Department of Physics. Source: `http://www.physics.umd.edu/lecdem/honr228q/notes/U238scheme.gif`.

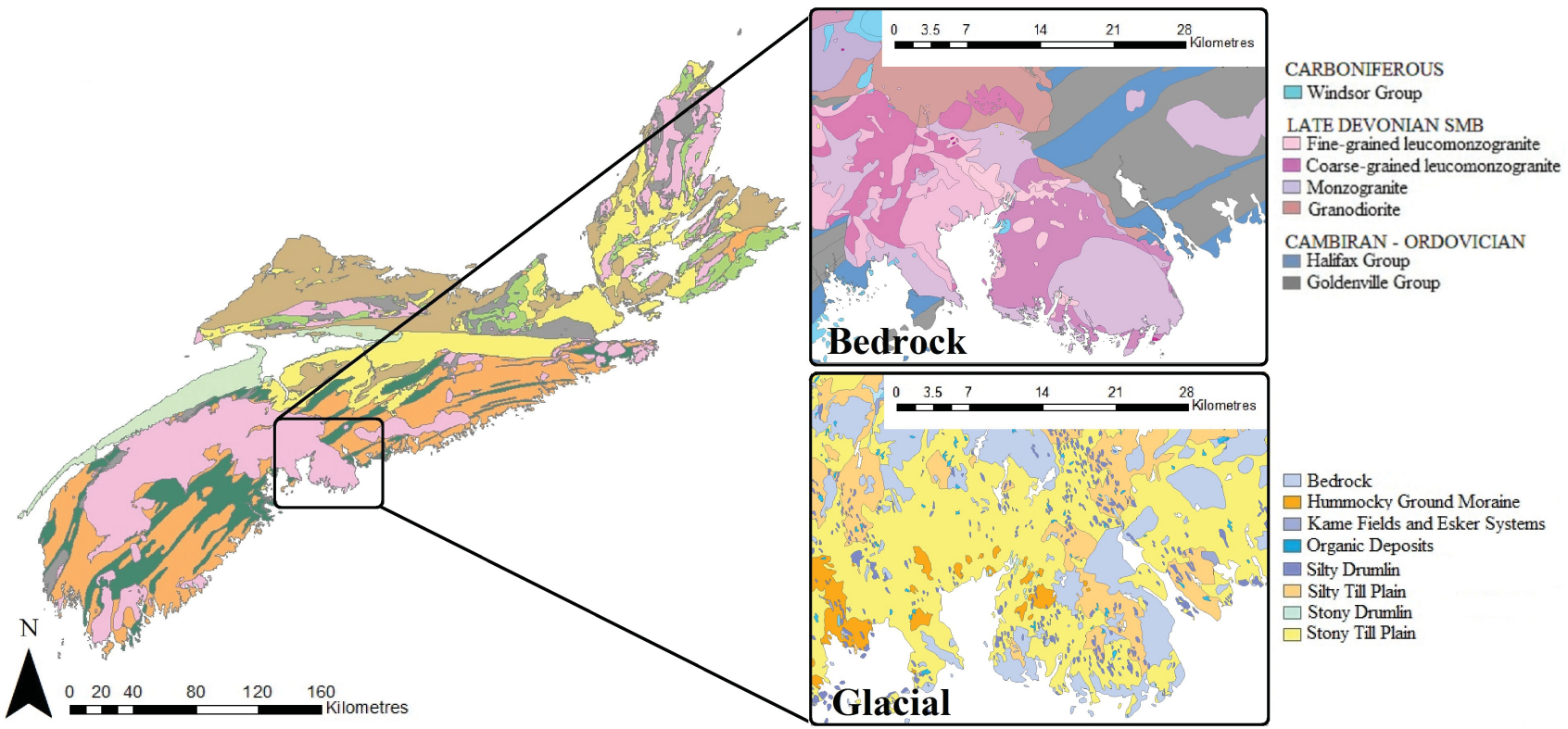

Figure 3.2: Geological map of Nova Scotia (modified after Keppie, 2000), with bedrock geology (modified after MacDonald and Horne, 1987) and glacial geology (modified after Stea and Fowler, 1981) inserts. The bedrock units of interest are highlighted in pink/purple shades; the glacial units of interests are highlighted in yellow/orange shades. The till plains within the glacial map can be further subdivided into the Lawrencetown Till, and the Beaver River Till (granite, slate, and metasandstone phase)

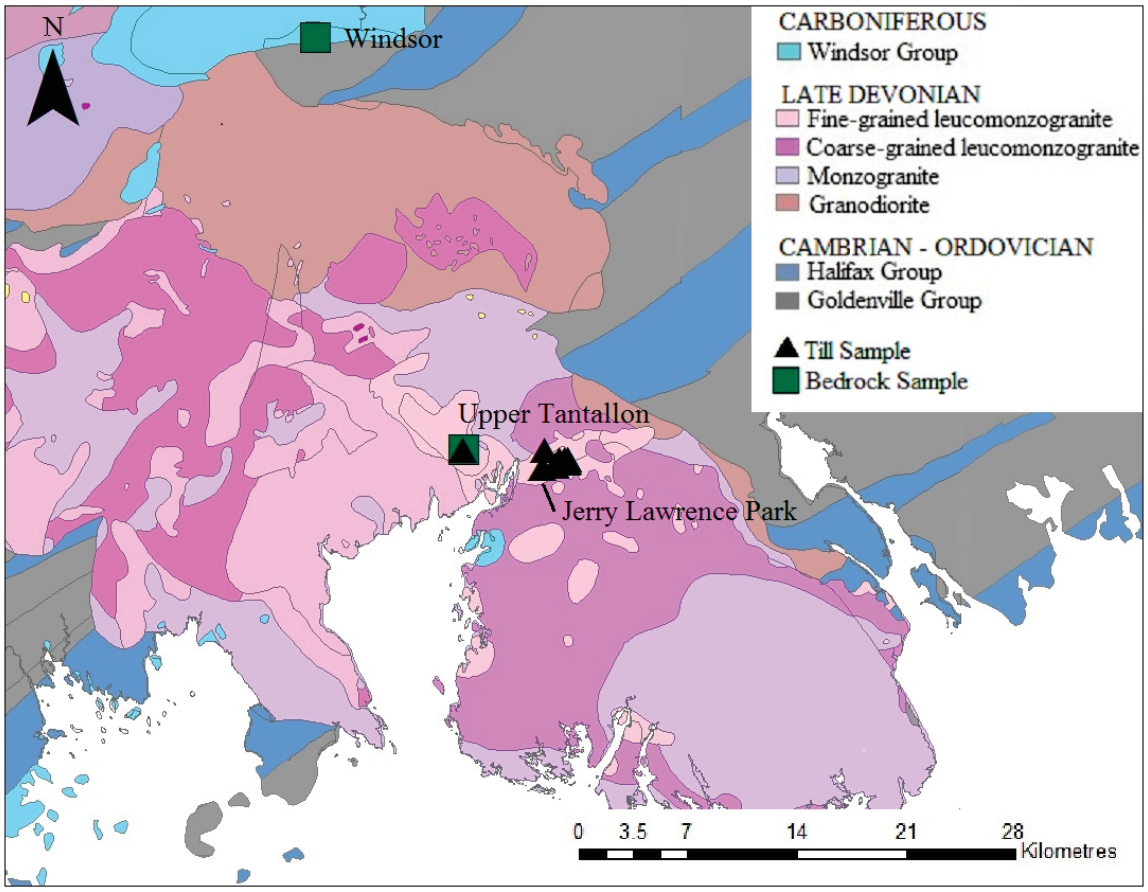

Figure 3.3: HRM till and bedrock sample locations (triangles and squares, respectively). Note all till samples and one bedrock sample are located within the fine-grained leucomonzogranite phase of the SMB. The second bedrock location is within the Windsor Group. Modified after Keppie 2000.

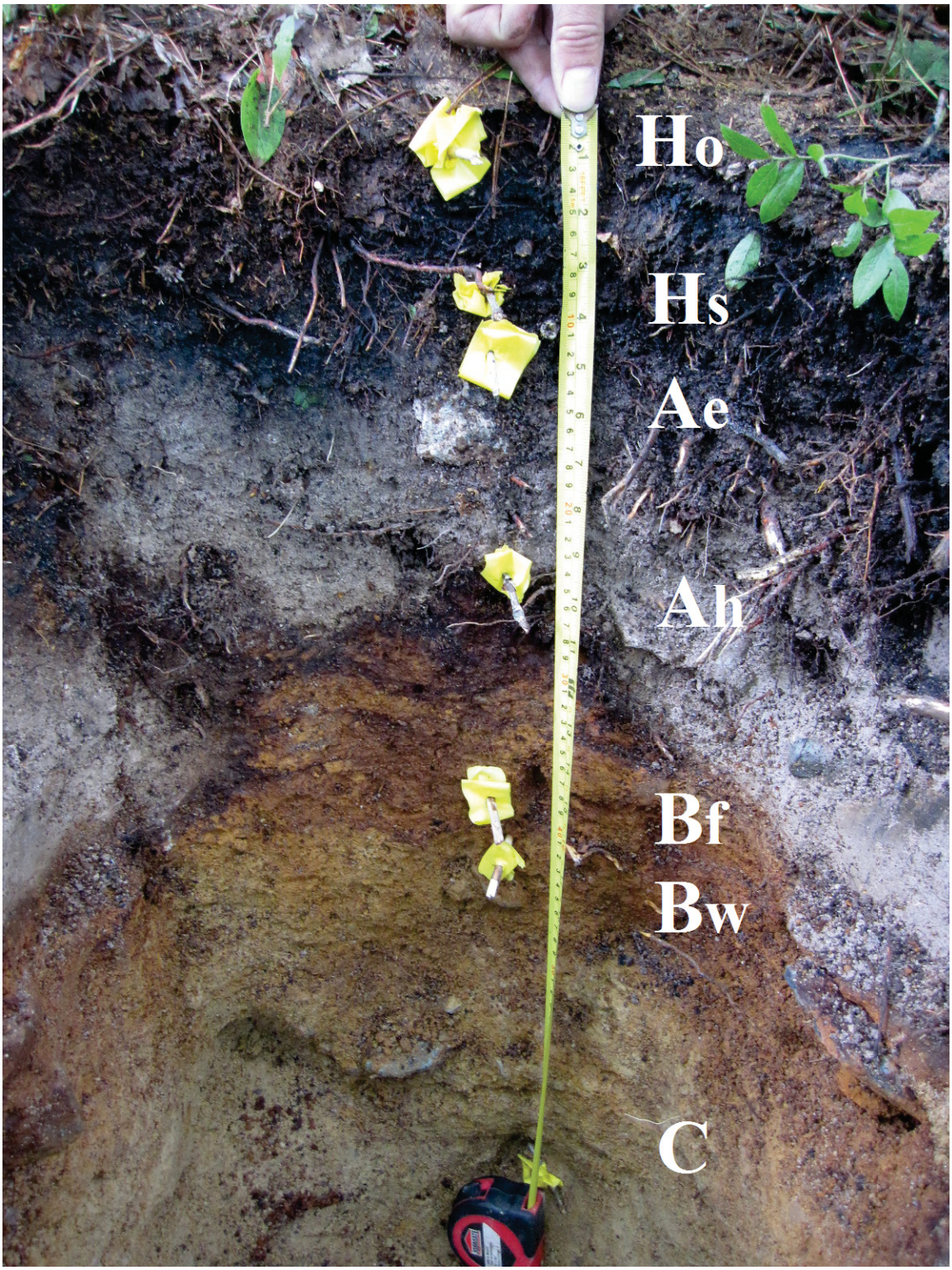

Figure 3.4: An example of a dug soil pit. Yellow flags mark the different soil horizons with depth, and a tape measure shows the depth of 60 cm.

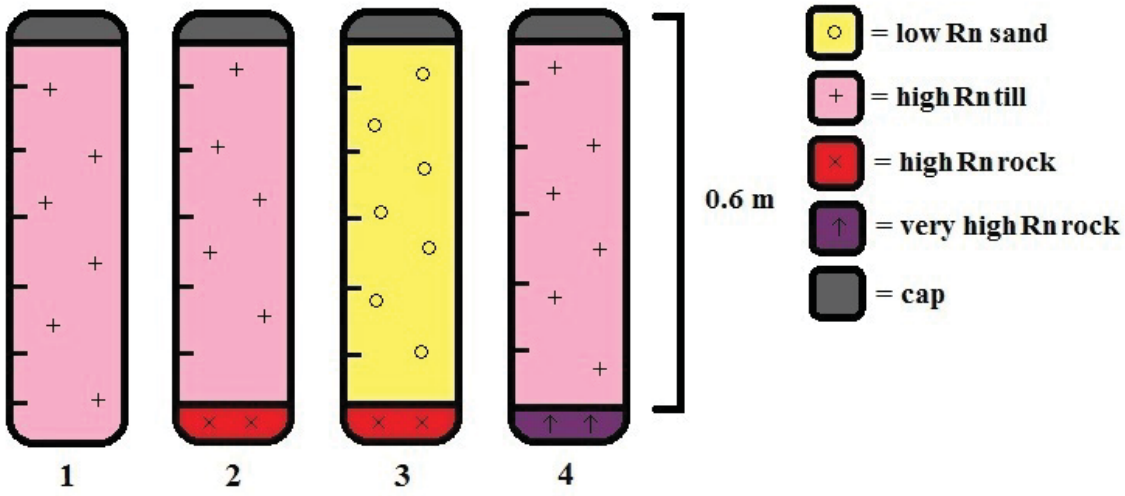

Figure 3.5: Schematic diagram showing how experimental soil columns were constructed, and the relative radon producing mediums within each. Fine-grained leucomonzogranite till = high Rn till, fine-grained leucomonzogranite bedrock = high Rn rock, inert sands = low Rn sand, and Green Street bedrock = very high Rn rock.

Figure 3.6: Columns 1 through 4 (left to right) filled with local tills and bedrock cores. Note the tubing extruding every 10 cm up the sealed columns. The cracks around the tubing holes were filled with Cole Parmer Very High-Peel Strength Epoxy. The height differences between the columns are a result of the thickness of the respective bedrock cores.

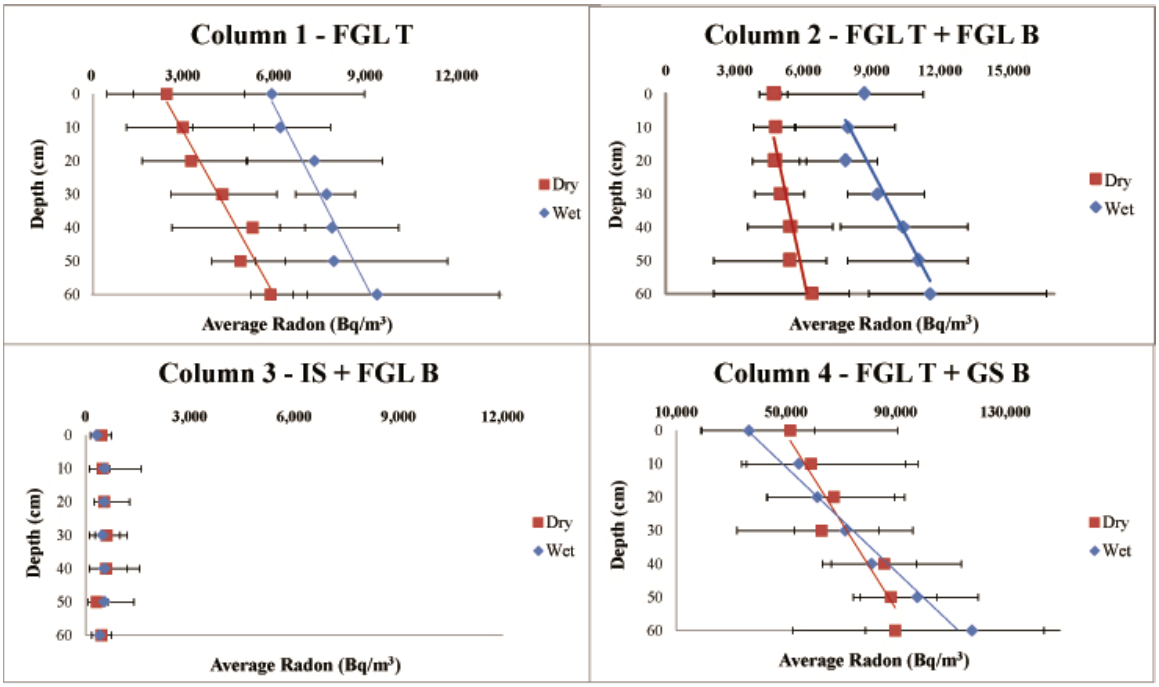

Figure 3.7: Average radon concentrations (Bq m^{-3}) for columns 1 through 4 in both wet and dry trials; note the changing radon scales across the x axis. FGL T= fine-grained leucomonzogranite till, FGL B= fine-grained leucomonzogranite bedrock, IS= Inert Sands, and GS B= Green Street Bedrock. Depth of 60 cm represents bedrock, and depth of 0 cm represents the surface.

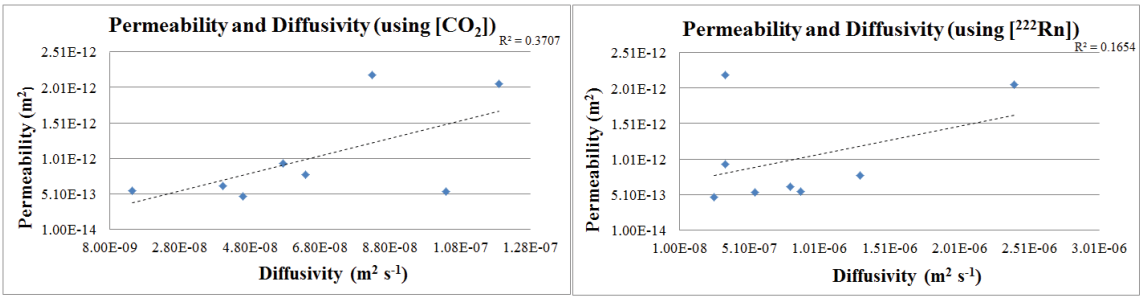

Figure 3.8: Figure displaying the average permeability values (m^2) to the average diffusivity values (m^2 s^{-1}) calculated from CO_2, and to the average diffusivity values calculated from ^{222}Rn. The p value (R^2) represents the correlation between the two, and the outliers are from column 3.

Table 3.1: Diffusivity calculated from CO_2 (m^2 s^{-1}), and the diffusivity calculated from ^{222}Rn (m^2 s^{-1}) for each column, with dry and wet till moistures. FGL T= fine-grained leucomonzogranite till, FGL B= fine-grained leucomonzogranite bedrock, IS= Inert Sands, and GS B= Green Street Bedrock.

		Diffusivity from CO_2 (m^2 s^{-1})	Diffusivity from ^{222}Rn (m^2 s^{-1})
Column 1	Dry	5.76E-08	3.40E-07
(FGL T)	Wet	4.03E-08	8.00E-07
Column 2	Dry	6.40E-08	1.30E-06
(FGL T + FGL B)	Wet	1.46E-08	8.80E-07
Column 3	Dry	8.29E-08	3.40E-07
(IS + FGL B)	Wet	1.19E-07	2.40E-06
Column 4	Dry	1.04E-07	5.50E-07
(FGL T + GS B)	Wet	4.61E-08	2.60E-07

Table 3.2: Average, minimum, and maximum permeabilities (m^2) for each column, with dry and wet till moistures; n is the number of samples. FGL T= fine-grained leucomonzogranite till, FGL B= fine-grained leucomonzogranite bedrock, IS= Inert Sands, and GS B= Green Street Bedrock.

		n	Average Permeability (m^2)	Min Permeability (m^2)	Max Permeability (m^2)
Column 1	Dry	6	9.39E-13	9.37E-13	9.41E-13
(FGL T)	Wet	6	6.21E-13	6.17E-13	6.26E-13
Column 2	Dry	6	7.75E-13	7.66E-13	7.82E-13
(FGL T + FGL B)	Wet	6	5.56E-13	5.53E-13	5.59E-13
Column 3	Dry	6	2.19E-12	2.17E-12	2.22E-12
(IS + FGL B)	Wet	6	2.06E-12	2.03E-12	2.08E-12
Column 4	Dry	6	5.37E-13	5.35E-13	5.38E-13
(FGL T + GS B)	Wet	6	4.70E-13	4.64E-13	4.78E-13

Table 3.3: % ^{222}Rn remaining in the system, the estimated and actual transit time (days), and the calculated transit speed. Column three was excluded because of a lack of clear trend. FGL T= fine-grained leucomonzogranite till, FGL B= fine-grained leucomonzogranite bedrock, IS= Inert Sands, and GS B= Green Street Bedrock.

		% Remaining in System	Estimated Transit Time (days)	Actual Transit Time (days)	Transit Speed (m/day)
Column 1	Dry	38.8	$>$ 3.82 (slow)	5.19	0.116
(FGL T)	Wet	63.1	$<$ 3.82 (fast)	2.52	0.238
Column 2	Dry	70.5	$<$ 3.82 (fast)	1.92	0.313
(FGL T + FGL B)	Wet	61.4	$<$ 3.82 (fast)	2.67	0.224
Column 3	Dry	N/A	N/A	N/A	N/A
(IS + FGL B)	Wet	N/A	N/A	N/A	N/A
Column 4	Dry	51.8	$<$ 3.82 (fast)	3.60	0.167
(FGL T + GS B)	Wet	31.9	$>$ 3.82 (slow)	6.26	0.096

Chapter 4

Conclusions

4.1 Conclusions and Implications from Chapters 2 and 3

This thesis aimed to address and satisfy the gaps associated with radon knowledge in Nova Scotia. There were several objectives, spread out over two chapters.

The main goal of Chapter 2, 'Optimizing the creation of radon potential maps using statistical analyses and GIS-based mapping of predictor layers', was to present a series of radon potential maps of the Halifax Regional Municipality (HRM) optimizing the indoor radon predictor layers. The aim of Chapter 3, 'Radon soil gas migration and transport through Halifax tills and bedrock, Nova Scotia' was to quantify the permeability, diffusivity, and radon concentrations through the FGL till under differing moisture conditions.

The four GIS-based maps created in this study (Figures 2.4, 2.5, 2.6, and 2.7) were compared to previous Nova Scotia radon potential maps. Overall trends from all four maps (Table 2.2) were similar to past radon mapping in Nova Scotia. The previous 2008 map identified the SMB in the highest radon potential category (O'Reilly, 2008). This same trend was seen across all maps in the current study. Regardless of which predictor layers were used, the geologic boundaries of the SMB could be seen, re-enforcing the importance of bedrock geology in estimating the indoor radon potential. Other areas of high indoor radon potential include the north eastern regions of Dartmouth (Figure 2.7, for example). These regions correspond to other Early Devonian granitic intrusions (described by (White, 2010)), and were also categorized in the highest risk category of the 2008 O'Reilly map (O'Reilly, 2008). As granites have been documented as having elevated uranium levels (Je, 1998a), the high regions are justified in having high radon values.

In addition to confirming previous radon potential studies, the present results are consistent with previous radon prediction studies. For example, Map 2W (Figure 2.7) was able to statistically predict 14.4% of indoor variance; a similar study by Appleton

was able to predict 25% of indoor variance using geologic predictors (Appleton and Miles, 2010). A likely reason for the difference was the number of indoor radon measurements; the Appleton study had over 20,000 samples, whereas this thesis had 134 samples.

The estimation techniques for radon prediction mapping could still be further refined; there were regions within the HRM that were known radon high regions such as Harrietsfield (per. com. Anne Marie O'Beirne-Ryan 2013) that did not show up on any of this study's maps (Figures 2.4, 2.5, 2.6, and 2.7). By refining the potential estimates in each layer, and using a more refined and more uniform grid for sample collection, some of these issues may be resolved in the future.

An important addition to consider for the radon potential maps is the inclusion of a layer representing bedrock geology structure. A layer mapping the major and minor faults, fractures, and joints in the bedrock throughout the HRM could help predict more than 14.4% of indoor radon variance. As fractures in the bedrock increase not only the permeability, but also radon gas concentrations (Je, 1998a), and these cracks could play a significant role in the potential indoor radon. It has been shown in this study that extremely high radon gas concentrations can be measured over a region underlain by bedrock concentrations mimicking fracture zones; therefore, a layer documenting the degree to which the bedrock is fractured should be included in future studies.

A contradictory finding from Chapter 2 was that the permeability was not found to be a statistically significant predictor of indoor radon (Table 2.9); in previous studies, permeability had been documented as a key predictor in indoor radon potential (O'Reilly, 2008; Appleton et al., 2011). The difference could potentially be because of the use of estimated potential values rather than actual measured values across the HRM in this study (seen in Table 2.5). Chapter 3 re-visited this issue to measure the permeability through the FGL till, however the focus was not on defining permeability for all the tills in the study area.

The radon gas results from Chapter 3 (Figure 3.7) showed that, unless an extremely high-radon producing bedrock source is present (such as a roll-front uranium deposit) the radon gas detected at the surface was likely largely produced in the tills. The measured radon gas values (Figure 3.7) provide a useful proxy for

the true radon concentrations in the HRM tills. Though the experimental column concentrations are field analogues, the key implications and overall trends between the columns can provide a very useful indicator for actual field tills. Based on the field analogues from this study, the dominant control on the measured concentration of radon gas is suggested to be the permeability/diffusivity of the tills and not the production of radon from the bedrock. This finding agrees with O'Brien et al. (2011), but carries the understanding further by using radon-active tills in lab experiments to understand till importance, rather than assumed inert tills in a 1D model system. This helps emphasize that this study is a step beyond, and new, whilst still delivering the quantitative measurements.

A valuable outcome of Chapter 3 was for homes built on 'fractured' bedrock (depicted in this study by *extremely* high radon production); the overlying surficial radon production and till moisture changes had little effect on the measured surface radon concentrations (seen in column four, Figure 3.7). This bedrock source (seen in column 4) was felt more strongly at a 0.6 m distance than the FGL SMB bedrock source (seen in column 2), suggesting that buildings built over these conditions be aware of the depth to bedrock and the higher potential for radon accumulation indoors, regardless of moisture conditions. If the bedrock was actually physically fractured, these gaps could allow more rapid movement of gas, and potentially change the transport rates (as described by Je (1998a)).

Experimental permeability and diffusivity values were established for both wet and dry tills through all four columns (Tables 3.1 and 3.2). In terms of gas transport potential, the silica sand unit had faster permeability (10^{-12} m^2, seen in Table 3.2) than the FGL till unit (10^{-13} m^2, seen in Table 3.2); the tills with low permeability also returned low diffusivity. The transit values (seen in Table 3.3) can be useful in predicting the distance radon gas could travel before decaying through tills. As previous modeling efforts used estimates of diffusivity (O'Brien et al., 2011), the actual values presented in this study will prove invaluable in future modeling efforts.

Moisture was found to be an important determinant of radon gas concentrations, which is important knowledge for a wet Nova Scotian climate. In local FGL tills (with or without a FGL bedrock source), in general the radon concentrations increased with increasing moisture. This moisture / radon gas relationship is well defined in columns

1 and 2 of Figure 3.7. However, when local FGL tills are overlaying a 'fractured' bedrock source, this relationship is somewhat modified (Figure 3.7). This would suggest that the till moisture / radon gas concentration is also related to the amount of U (and Rn) in bedrock, particularly when U levels are elevated.

The statistical analyses performed in Chapter 2 tested all the indoor radon predictor variables, and determined that permeability was not a statistically significant control on the radon in indoor air variance. However, because it had been previously documented as such (Appleton and Miles, 2010; Kemski et al., 2009; Mose et al., 1992), a focus in Chapter 3 was to determine the prominence of gas transport mechanisms on the radon gas levels measured. Chapter 3 tested the importance of the permeability in the transport of radon gas to the surface, through actual HRM field tills. Permeability was found to be a major control, re-enforcing the idea that gas transport mechanisms can be a dominant indicator for radon in indoor air. The results from Chapter 3 served as a validation for the permeability/diffusivity being included as an important predictor in the series of radon potential maps created. Future work on refining and extending permeability measurements in HRM tills should increase the predictive role of permeability in Rn at surface measurements.

The measured data from Chapter 3 was not included in Chapter 2, as it was an incomplete database. The Chapter 2 quantitative database was limited because it only measured diffusivity, permeability, and radon gas concentrations through depth for the fine-grained leucomonzogranite phase of the SMB. Because the map looked at all the till units within the HRM and not just FGL, the database was not a continuous layer of till permeability with quantitative concentrations.

The mapping portion of the thesis highlighted issues that needed to be further addressed, and a sampling program and experimental design was created around that those issues. Chapter 3 was an extremely informative study, as it showcased gaps in the mapping analysis. The column experiments were able to show that the permeability and till composition were in fact important constituents in the radon gas concentrations detected. This indicated that something was missing in the Chapter 2 predictions as these layers were not significantly correlated to indoor radon and the limitations of both chapters were more clearly understood.

The results show that even the most statistically accurate map (2W) may not

represent the true indoor radon potential, as it does not use till geochemistry, till permeability, or geologic structures as predictor layers. As such, the purpose of the mapping exercise in this thesis was to present a series of maps showing how to optimize the indoor radon predictors.

Overall this study provided valuable radon gas potential information for the HRM community. Larger scale conclusions can be drawn for homeowners and developers. The results from this study imply that building or home owners be aware of: the geology surrounding their structure, the infill type present, the depth to bedrock from their basement, the condition of the bedrock (fractured vs non fractured) in the region, and the aerating of the building after a heavy rainfall. All of these factors have been shown to help assess the radon gas concentrations that may be present near the till surface to potentially infiltrate a building. Developers should be aware that local blasting and construction may open radon migration pathways into buildings by fracturing the underlying bedrock. Municipal building codes should take this into account and appropriate blasting regulations should be put into place. This study could have practical implications, for example, where local till is used as an infill when building a community center. Knowing the radon production rate through the tills is extremely beneficial in estimating the potential of radon build-up within any structures in the region. This thesis has also shown that introducing lower permeability fill below basements may increase the transit time of radon gas, causing it to decay in the medium before reaching the surface. In planning new subdivisions, bylaws and building codes should use local radon potential maps to consider requiring mitigation measures in homes as they are being built.

4.2 Future Directions

The radon gas information presented in this study provides a solid foundation; however there is still essential future work that needs to be done to narrow down the radon potential values for the province. To more accurately predict these potentials, there is a requirement for an updated indoor radon dataset with a set sampling density (e.g. 1 sample every 1 km^2). With a more even grid distribution of indoor radon measurements, the proximity bias will be minimized. Within this needed indoor database, it is recommended that there is a set sampling protocol for all companies

to follow. If indoor radon concentrations are measured using the same technique (i.e. type of equipment used, length of test, location in home, and time of year), some of the variability in indoor home data would be reduced and outlying values would gain credibility.

As radon gas is a potential human health risk, there is also the need for expanded measurements of permeability, diffusivity, and radon gas through the other till units in the HRM. In the near future, this additional information will lead to the production of new radon potential maps with even more refined predictor layers.

Appendix A

Statistical Analyses

Hypothesis: Higher radon/uranium values in till, bedrock, and airborne uranium, as well as higher permeability regions result in high radon readings in homes.

Questions of interest: Are permeability, bedrock, airborne radiometric equivalent uranium, and/or till good predictors of indoor radon?

My variables of interest (VOI) were indoor radon (*Indoor*), bedrock geology (*Bedrock*), surficial geology (*Till*), permeability (*Permeability*), and airborne uranium (*Airborne*).

A.1 Characterizing the VOI

The geological uranium/radon potentials were the independent variables, because the indoor air was dependent on the presence of bedrock geology, surficial geology permeability and airborne radiometric equivalent uranium.

Dependent Variables: *Indoor*

Independent Variables: *Bedrock*, *Till*, *Permeability*, and *Airborne*.

The methods for the statistical analyses were determined with expert input from Yoko Yoshida (Dalhousie University).

A.2 Examining the Uni-Variate Distribution of the VOI

Indoor Air By looking at the histogram of *Indoor*, it was evident that the data was skewed to the right (skewness 4.5, kurtosis 26.07). Out of 155 points, the average indoor radon was 397.56 Bq m^{-3}, and the standard deviation was 818.75 Bq m^{-3}. Because the standard deviation was high compared to the mean, the mean was a less powerful representation of the observations. A five number summary helped describe where the central tendency lay: min=6, Q1=58, median=141, Q3=366, max=5844.

Till Potential: After plotting the *Till* data, the resulting histogram was again

skewed to the right, but only slightly (skewness 1.2, kurtosis 3.50). Out of 155 points, the average till potential was 3.84, and the standard deviation was 2.34; because the standard deviation was smaller than the mean, the mean was a powerful representation of the observations. The five number summary was as follows: min=1, Q1=3, median=3, Q2=3, and max=10.

Airborne Potential: The histogram of the 155 *Airborne* points showed slight right skewness (0.96), and a kurtosis of 2.48. The five number summary (min=1, Q1=3, median=3, Q2=3, max=9) showed a similar tendency as the Till variable. The mean was 3.95 and the standard deviation was 2.58. Because the standard deviation was smaller than the mean, the mean was a powerful representation of the observations.

Permeability Potential: Because the *Permeability* variable was more bimodal than normally distributed, the mean and standard deviations were not accurate representations: Q1 (9), the median (3), and Q2 (3) were the best ways to represent the data.

Bedrock Potential: After graphing the *Bedrock* variable, the histogram returned a left skewed trend (0.06 skewness, 1.18 kurtosis). The average bedrock potential was 8.16, and the standard deviation was 1.71. Because the standard deviation was smaller than the mean, the mean was a powerful representation of the observations. The five number summary showed the small range of values within this variable: min=6, Q1=7, median=7, Q2=10, max=10.

Because the above were uni-variate analyses, they do not combine variables to answer the hypothesized questions. It was however, a good preliminary look at the variables.

A.3 Bi-Variate Analyses Between VOI

In order to look at the uni-variate relationships between all predictors, a correlation matrix was calculated to determine the correlation co-efficients and their significance. The correlations between the Y variable (indoor air) and X variables were as follows:

1. H_0: p(rho)=0 (no correlation between indoor and till) H_a: p(rho)<0 (some correlation). 2. Decision rule =0.05. 3. p value was 0.4674. 4. (0.05)< p(0.4674), therefore we fail to rejected H_0 that there was no correlation, and lent support for the H_0: there was no association. 5. Based on the analysis, the association between

indoor air and till was not statistically significant, which lent support to the statement that 'Indoor air was not affected by till'.

1. H_0: p(rho)=0 (no correlation between indoor and airborne radiometrics) H_a: p(rho)<0 (some correlation). 2. Decision rule =0.05. 3. p value was 0.000. 4. (0.05)> p(0.000), therefore we rejected H_0 that there was no correlation, and lent support for the H_a: there was a correlation. 5. Based on the analysis, indoor and the airborne radiometrics were positively correlated, and the correlation was weak (r=0.3492).

1. H_0: p(rho)=0 (no correlation between indoor and permeability) H_a: p(rho)<0 (some correlation). 2. Decision rule =0.05. 3. p value was 0.2560. 4. (0.05)< p(0.2560), therefore we fail to rejected H_0 that there was no correlation, and lent support for the H_0: there was no association. 5. Based on the analysis, the association between indoor air and permeability was not statistically significant, which lent support to the statement that 'Indoor air was not affected by permeability'.

1. H_0: p(rho)=0 (no correlation between indoor air and bedrock) H_a: p(rho)<0 (some correlation). 2. Decision rule =0.05. 3. p value was 0.0001. 4. (0.05)> p(0.0001), therefore we rejected H_0 that there was no correlation, and lent support to H_a: there was a correlation. 5. Based on the analysis, indoor air and the bedrock were positively correlated, and the correlation was weak (r=0.3147).

Next, the correlations between only the X variables were explored: 1. H_0: p(rho)=0 (no correlation between airborne radiometrics and till) H_a: p(rho)<0 (some correlation). 2. Decision rule =0.05. 3. p value was 0.057. 4. (0.05)< p(0.057), therefore we fail to rejected H_0 that there was no correlation, and lent support for the H_0: there was no association. 5. Based on the analysis, the correlation between airborne radiometrics and till was not statistically significant, which lent support to the statement that 'Airborne radiometrics and till were not correlated'.

1. H_0: p(rho)=0 (no correlation between permeability and till) H_a: p(rho)<0 (some correlation). 2. Decision rule =0.05. 3. p value was 0.2142. 4. (0.05)< p(0.2142), therefore we fail to rejected H_0 that there was no correlation, and lent support for the H_0: there was no association. 5. Based on the analysis, the correlation between permeability and till was not statistically significant, which lent support to the statement that 'Permeability and till were not correlated'.

1. H_0: p(rho)=0 (no correlation between bedrock and till) H_a: p(rho)<0 (some

correlation). 2. Decision rule =0.05. 3. p value was 0.0000. 4. (0.05)> p(0.0000), therefore we rejected H_0 that there was no correlation, and lent support to H_a: there was a correlation. 5. Based on the analysis, the bedrock and the till were positively correlated, and the correlation was strong (r=0.6342).

1. H_0: p(rho)=0 (no correlation between airborne radiometrics and permeability) H_a: p(rho)<0 (some correlation). 2. Decision rule =0.05. 3. p value was 0.2717. 4. (0.05)< p(0.2717), therefore we fail to rejected H_0 that there was no correlation, and lent support for the H_0: there was no association. 5. Based on the analysis, the correlation between permeability and airborne radiometrics was not statistically significant, which lent support to the statement that ''Permeability and airborne radiometric equivalent uranium were not correlated'.

1. H_0: p(rho)=0 (no correlation between airborne radiometrics and bedrock) H_a: p(rho)<0 (some correlation). 2. Decision rule =0.05. 3. p value was 0.0000. 4. (0.05)> p(0.0000), therefore we rejected H_0 that there was no correlation, and lent support to Ha: there was an association. 5. Based on the analysis, the airborne radiometric equivalent uranium and the bedrock have a moderately strong positive correlation (r=0.5484).

1. H_0: p(rho)=0 (no correlation between permeability and bedrock) H_a: p(rho)<0 (some correlation). 2. Decision rule =0.05. 3. p value was 0.8548. 4. (0.05)< p(0.8548), therefore we fail to rejected H_0 that there was no correlation, and lent support to H_0: there was no correlation. 5. Based on the analysis, the permeability and the bedrock were not statistically correlated.

The main conclusions from the Y/X analyses were: indoor air and till were not correlated, indoor air and airborne radiometric equivalent uranium were positively correlated, indoor air and permeability were not correlated, and indoor air and bedrock were positively correlated.

The main conclusions from the X/X correlations were: airborne radiometric equivalent uranium and till were not correlated, permeability and till have no statistical correlation, bedrock and till were positively correlated, permeability and radiometric equivalent uranium were not correlated, airborne uranium and bedrock were positively correlated, and permeability and bedrock were not correlated,

A.4 Multiple Regression Analyses on VOI

A.4.1 OLS 1

Given the nature of the statistical analysis (i.e. the need for all four variables to have a correlation co-efficient to re-weight the radon potential map layers), all of the X variables were included in the regression. The Y variable was *Indoor*, which represented the indoor radon values. The X variables were *Till* (the radon potential of the till, X_1), *Airborne* (the airborne radiometric equivalent uranium potential, X_2), *Permeability* (the permeability potential of the surficial geology, X_3), and *Bedrock* (the radon potential of the bedrock, X_4).

The hypothesis was that: till, bedrock, permeability and airborne uranium would have a positive relationship with indoor radon values. In order to test this hypothesis, an ordinary least squares (OLS) regression model was used with a 95% confidence interval. Because the Y variable was not normally distributed, the OLS was used as it was suited for skewed variables.

The regression equation had the form: $Y=b_1X_1 + b_2X_2 + b_3X_3 + b_4X_4 + A$. Where b represented the co-efficients (betas) and A represented the constant (alpha). After running the OLS, the regression equation was: Y = -63.57664(*Till*) + 67.06051(*Airborne*) - 14.4375(*Permeability*) + 150.6077(*Bedrock*) - 737.3522. The indoor radon was predicted to decrease by 63.57664 (p=0.068) when the till went up by one, increase by 67.06051 (p=0.022) when the airborne radiometric equivalent uranium went up by one, decrease by 14.4375 (p=0.432) when the permeability went up by one, increase by 150.6077 (p=0.007) when the bedrock went up by one, and was predicted to be -737.3522 (p=0.044) when all X variables were zero.

1. H_0: p(rho)=0 (model did not significantly predict radon levels) H_a: p(rho)<0 (model significantly predicted indoor radon). 2. Decision rule =0.05. 3. p value was 0.0000. 4. (0.05)> p(0.0000), therefore we rejected H_0 that the model did not significantly predict radon levels, and lent support to H_a: the model significantly predicted indoor radon . The r value was 0.1677, meaning that the model predicted 16.77% of the indoor radon variance.

After the regression, a multi-co linearity analysis was run to determine if the X variables were too related. Variance inflation factor (VIF) was used as a check to see

if the beta's found in the regression were indicating inaccurate effects. The VIFs were as follows: *Till* (1.76), *Bedrock* (2.37), *Airborne* (1.50), and *Permeability* (1.02). A VIF of greater than 10 meant the beta estimates from the regression were less valid; as the VIF values were all less than 2.5, the beta estimates were valid.

A.4.2 OLS 2

The second multiple regression run used only the independent variables that were significantly correlated to the dependent variable. The Y variable used was *Indoor*, which represented the indoor radon values. The X variables were *Airborne* (the airborne radiometric equivalent uranium potential, X_1), and *Bedrock* (the radon potential of the bedrock, X_2).

The hypothesis was that: bedrock and airborne radiometric equivalent uranium would have a positive relationship with indoor radon values. In order to test this hypothesis, an ordinary least squares (OLS) regression model were used with a 95% confidence interval. Because the Y variable was not normally distributed, and was skewed, the OLS was used as it was more suited for skewed variables.

The regression equation had the form: $Y=b_1X_1 + b_2X_2 + A$. Where b represented the co-efficients (betas) and A represented the constant (alpha). After running the OLS, the regression equation was: Y= 80.09309(*Airborne*)+84.27622(*Bedrock*)-607.0024. The indoor radon was predicted to increase by 80.09309 (p=0.006) when the airborne radiometric equivalent uranium went up by one, increase by 84.27622 (p=0.052) when the bedrock went up by one, and was predicted to be -607.0024 (p=0.052) when both X variables were zero.

1. H_0: p(rho)=0 (model did not significantly predict radon levels) H_a: p(rho)<0 (model significantly predicted indoor radon). 2. Decision rule =0.05. 3. p value was 0.0000. 4. (0.05)> p(0.0000), therefore we rejected H_0 that the model did not significantly predict radon levels, and lent support to Ha: the model significantly predicted indoor radon. The r value was 0.1436, meaning that the model predicted 14.36% of the indoor radon variance.

After the regression, the VIF multi-co linearity analysis was run to determine if the X variables were too related. The VIFs were as follows: *Bedrock* (1.43), and *Airborne* (1.43); because the VIF values were all less than 2.5, the beta estimates

were valid.

Overall, the results of the statistical analyses helped come up with four different maps. To answer the original question of interest, not all four variables were good predictors of indoor radon. Statistically, only bedrock and airborne radiometric equivalent uranium were significant predictors based on the extracted potential pixels from the un-weighted map.

A.5 ANOVA Analyses on Map Zones

To determine the significance between the zones, an analysis of variance between groups (ANOVA) was run on each of the 12 maps (4 five zone maps, 4 four zone maps, 4 three zone maps). The ANOVA was chosen as the tool to run, as one variable was categorical and one was continuous; the ONEWAY tool was also run as a check of variance. This sensitivity analysis was done to ensure the maps represented zones with the most significance. Variable 1 was always the average indoor radon in Bq m^{-3}, and variable 2 was always the respective zones.

H_0= the means are equal in each group. H_a= At least one mean is not equal to the others. Alpha = 0.05 (95% confidence interval).

5 zones:

1. 4 uw: df=4, total=154 (df1:3, df2:150); F=1.43, P=0.2252. Different but not significant

2. 4w: df=4, total=154 (df1:3, df2:150); F=2.06, P=0.085. Different, but not significant

3. 2uw: df=4, total=154 (df1:3, df2:150); F=6.59, P=0.0001. Different and significant

4. 2w: df=4, total=154 (df1:3, df2:150); F=6.16, P=0.0001. Different and significant

4 zones:

1. 4uw: df=3, total=154 (df1:2, df2:151); F=1.92, P=0.1282. Different, but not significant

2. 4w: df=3, total=154 (df1:2, df2:151); F=2.29, P=0.0808. Different but not significant

3. 2uw: df=3, total=154 (df1:2, df2:151); F =9.15, P = 0.000. Different and significant

4. 2w: df=3, total=154 (df1:2, df2:151); F=7.28, P=0.001. Different and significant.

3 zones:

1. 4uw: df=2, total=154 (df1:1, df2:152); F=2.80, P=0.0642. Different but significant

2. 4w: df=2, total=154 (df1:1, df2:152); F=2.80, P=0.0642. Different but significant

3. 2uw: df=2, total=154 (df1:1, df2:152); F= 10.67, P=0.000. Different and significant

4. 2w: df=2, total=154 (df1:1, df2:152); F= 10.67, P=0.000. Different and significant

Overall conclusion: By running a sensitivity analysis on the zones, there was no statistically different variance between using 5, 4 or 3 zones. Therefore, the original 5 zones was kept, the maps with 4 layers (both weighted and un-weighted) had zonal means that were not significantly different from each other. The maps with 2 layers (both weighted and un-weighted) had zonal means that were significantly different from each other.

Figure A.1: Histogram of indoor radon readings (Bq m^{-3}).

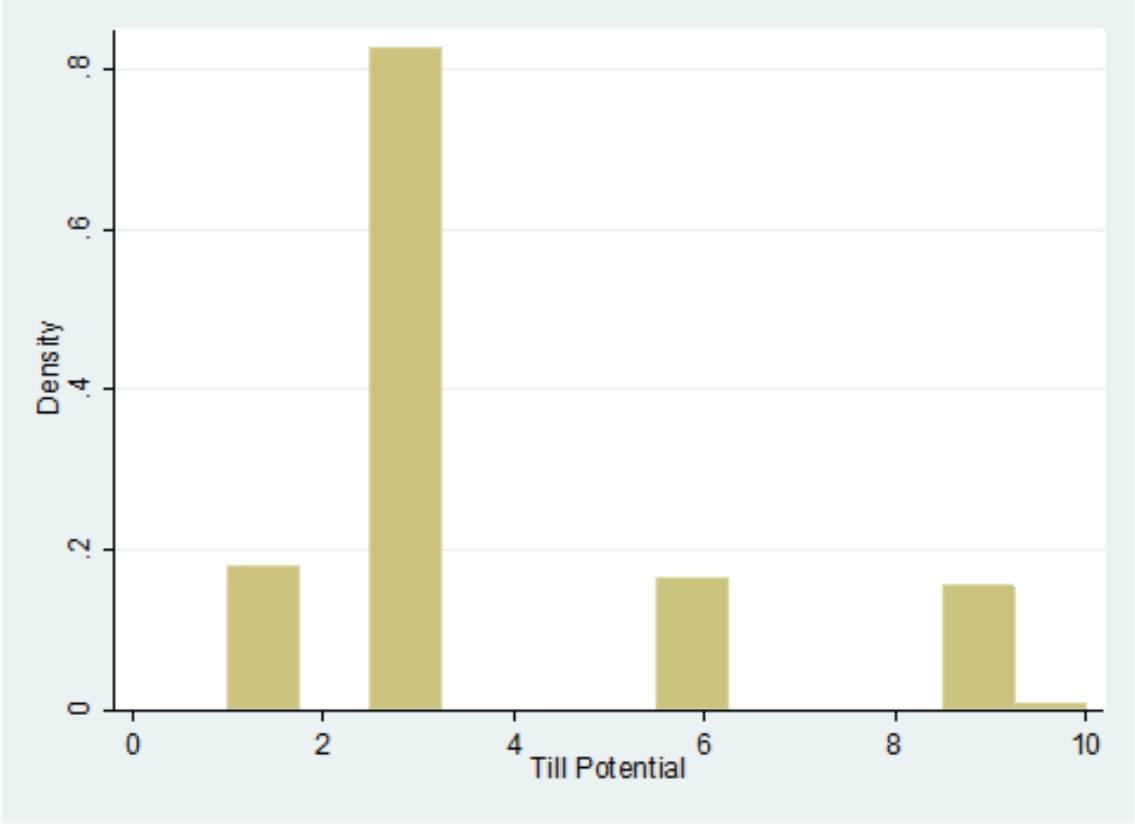

Figure A.2: Histogram of till potential values.

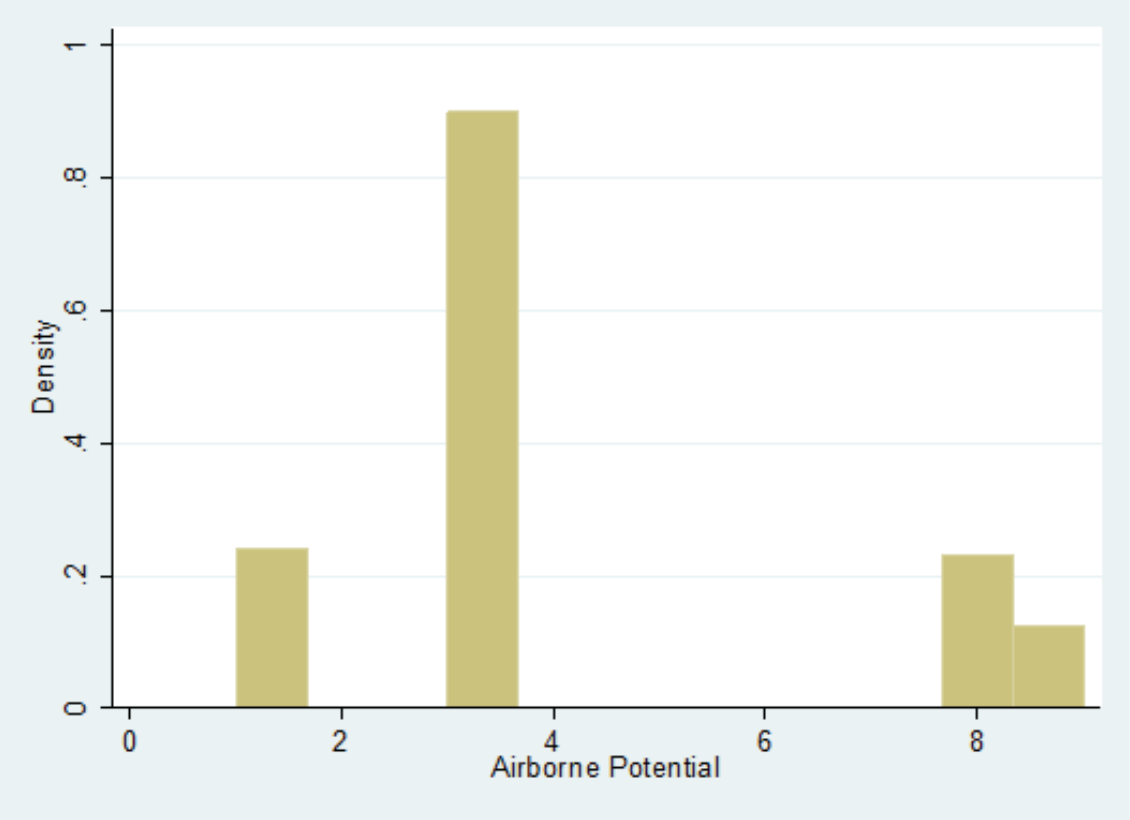

Figure A.3: Histogram of airborne radiometric equivalent uranium potential values.

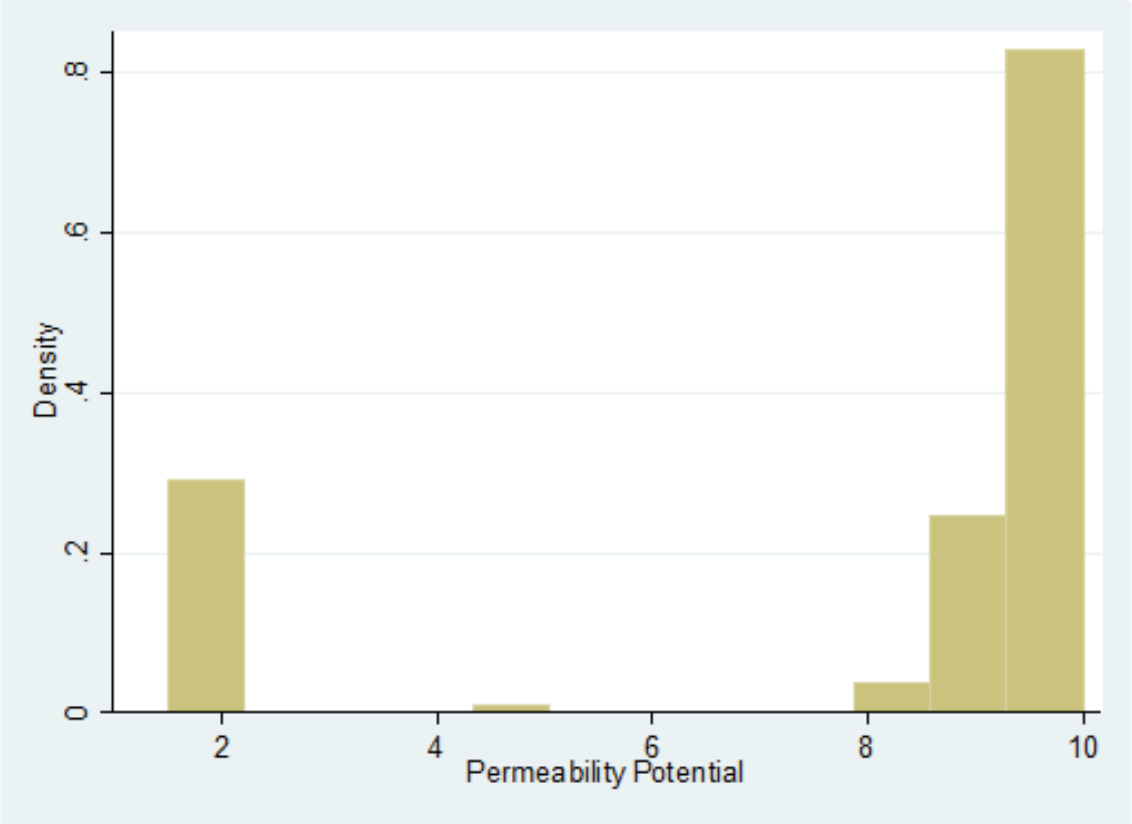

Figure A.4: Histogram of permeability potential values of the surficial geology.

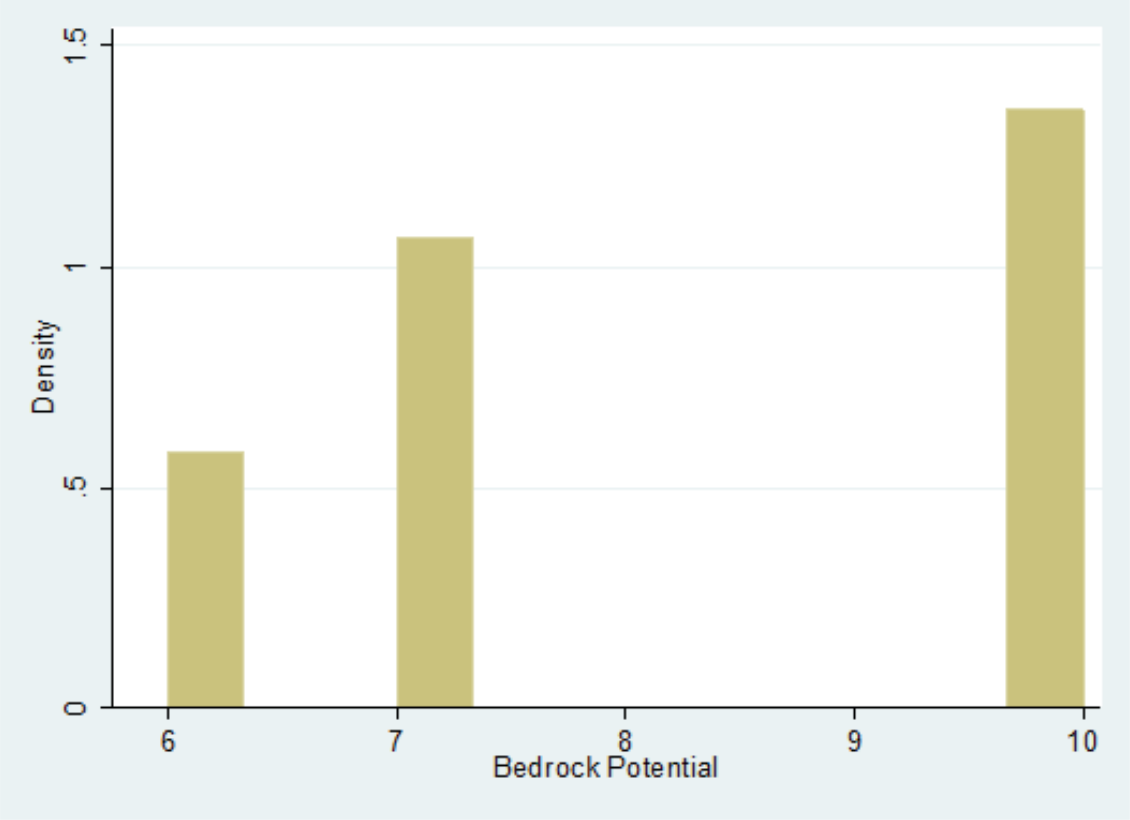

Figure A.5: Histogram of bedrock radon potential values.

```
. regress Indoor Till Airborne Permeability Bedrock
```

Source	SS	df	MS		
Model	17308407.5	4	4327101.88	Number of obs	= 155
Residual	85925140.5	150	572834.27	F(4, 150)	= 7.55
				Prob > F	= 0.0000
				R-squared	= 0.1677
				Adj R-squared	= 0.1455
Total	103233548	154	670347.715	Root MSE	= 756.86

Indoor	Coef.	Std. Err.	t	P>|t|	[95% Conf.	Interval]
Till	-63.57664	34.54509	-1.84	0.068	-131.8345	4.681195
Airborne	67.06051	28.93511	2.32	0.022	9.887474	124.2336
Permeability	-14.4375	18.30703	-0.79	0.432	-50.61046	21.73546
Bedrock	150.6077	54.81667	2.75	0.007	42.29517	258.9203
_cons	-737.3522	362.9982	-2.03	0.044	-1454.602	-20.10217

Figure A.6: Ordinary least squares regression of the Y variable (*Indoor*) and the X variables (*Till*, *Airborne*, *Permeability*, and *Bedrock*) (From Stata output).

```
. regress Indoor Airborne Bedrock
```

Source	SS	df	MS		
Model	14826266.7	2	7413133.34	Number of obs	= 155
Residual	88407281.4	152	581626.851	F(2, 152)	= 12.75
				Prob > F	= 0.0000
				R-squared	= 0.1436
				Adj R-squared	= 0.1324
Total	103233548	154	670347.715	Root MSE	= 762.64

Indoor	Coef.	Std. Err.	t	P>|t|	[95% Conf.	Interval]
Airborne	80.09309	28.46247	2.81	0.006	23.85996	136.3262
Bedrock	84.27622	42.94556	1.96	0.052	-.5710603	169.1235
_cons	-607.0024	309.8359	-1.96	0.052	-1219.143	5.138495

Figure A.7: Ordinary least squares regression of the Y variable (*Indoor*) and the correlated X variables (*Airborne* and *Bedrock*) (From Stata output).

Appendix B

Map Result Sensitivity Analyses

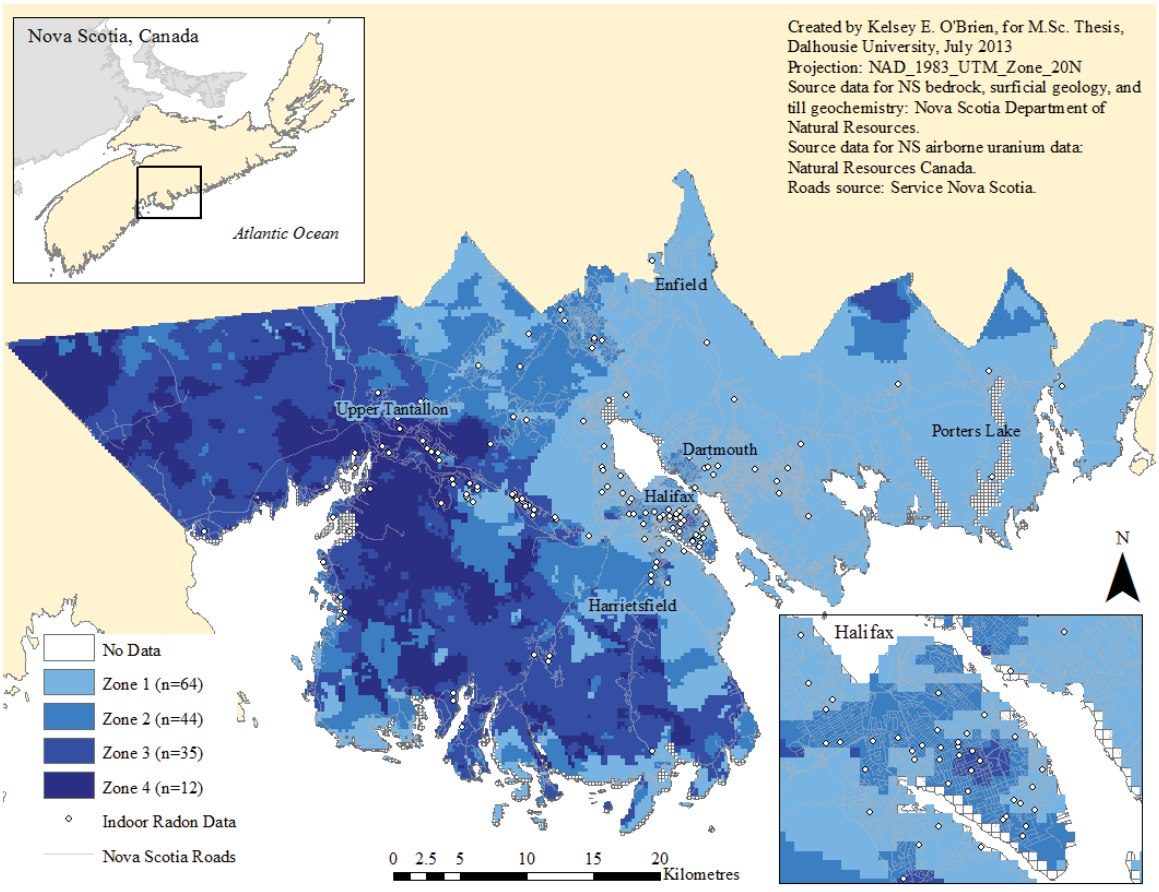

Figure B.1: Map 4UW(A) - Created using all four layers (*Till*, *Permeability*, *Airborne* and *Bedrock*), un-weighted; four zones.

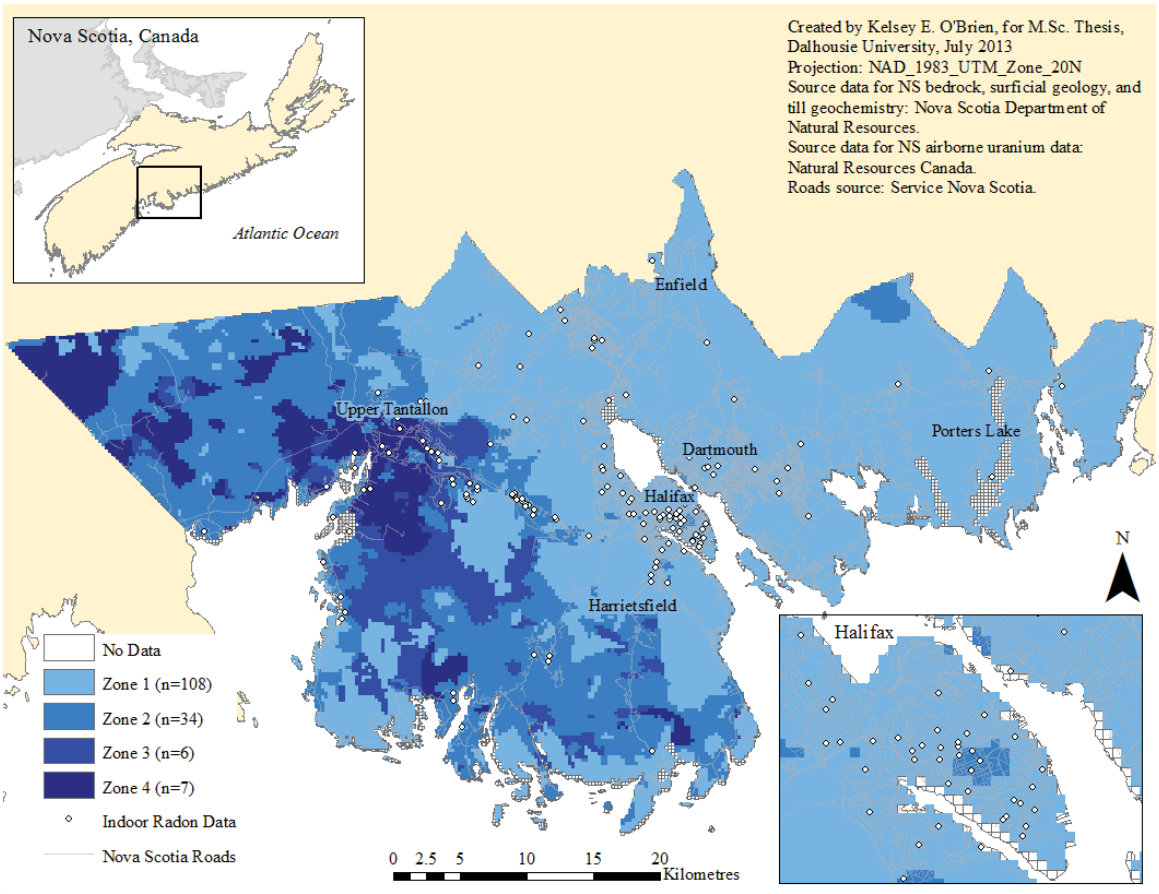

Figure B.2: Map 4W(A) - Created using all four layers (*Till*, *Permeability*, *Airborne* and *Bedrock*), weighted using the statistic regression; four zones.

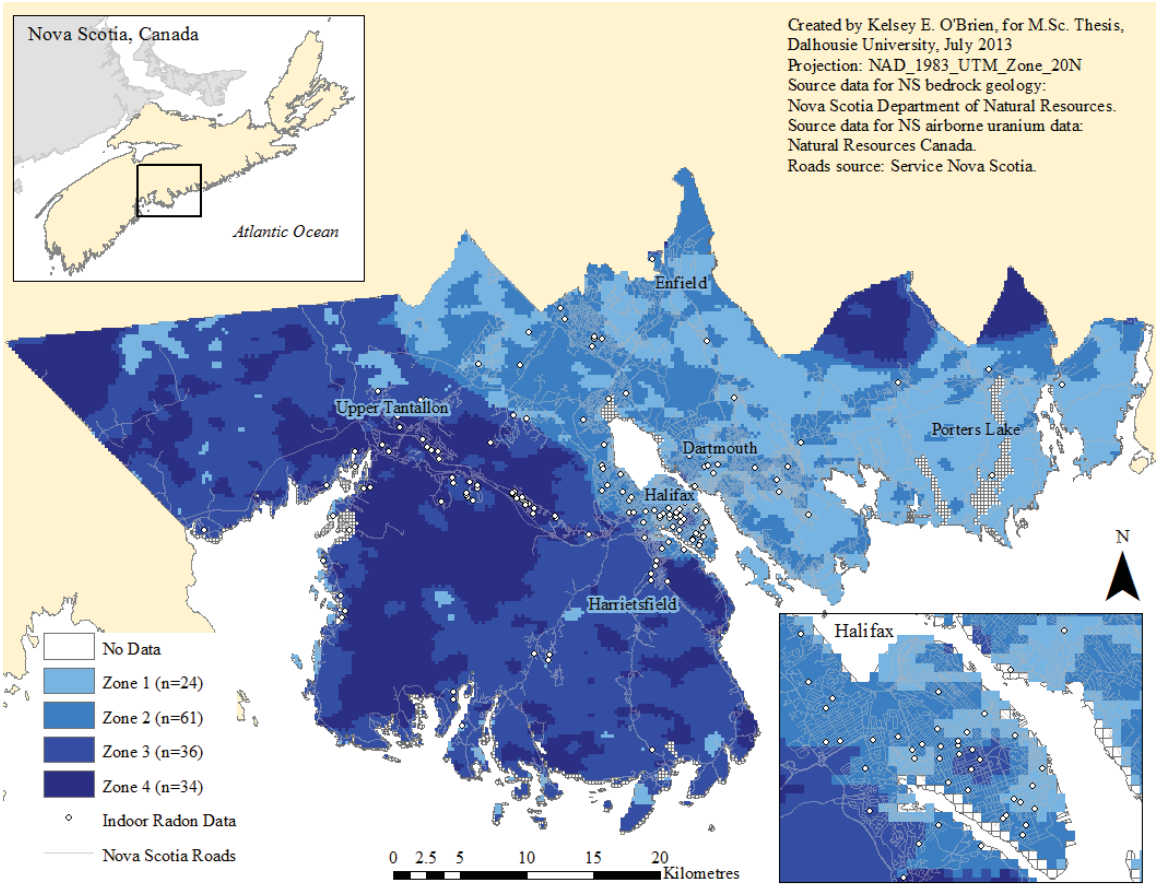

Figure B.3: Map 2UW(A) - Creating using only two layers (*Airborne* and *Bedrock*), as they were they only significantly correlated layers to indoor radon, four zones, un-weighted.

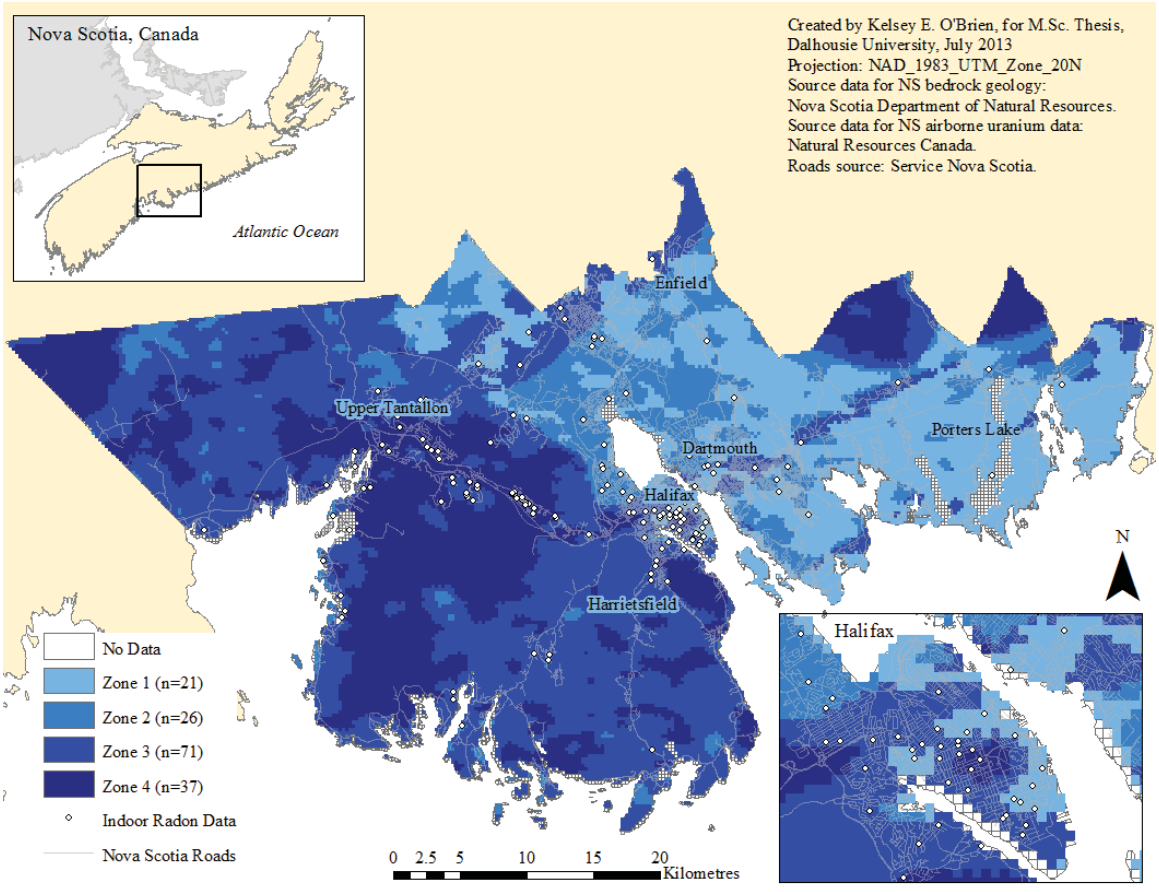

Figure B.4: Map 2W(A) - Creating using only two layers (*Airborne* and *Bedrock*), as they were they only significantly correlated layers to indoor radon. Both layers were weighted using the statistical regression, four zones.

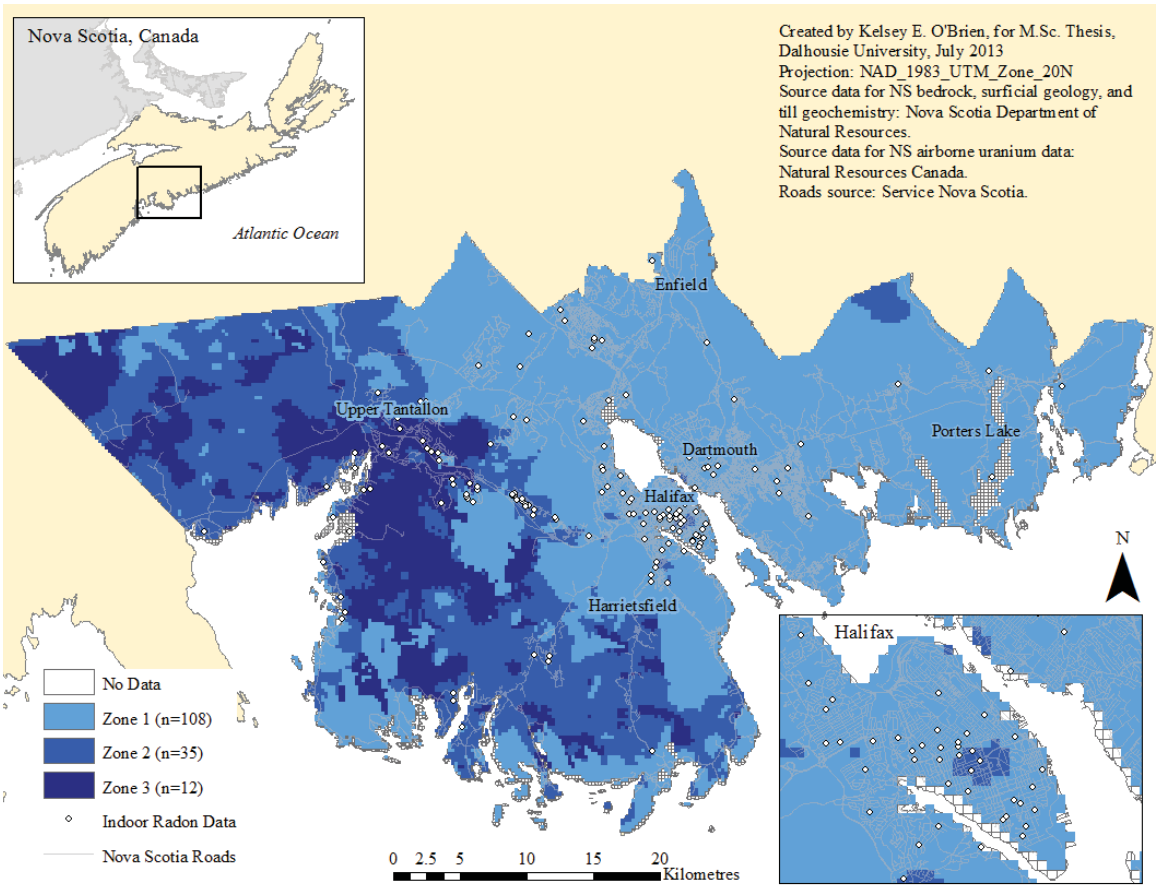

Figure B.5: Map 4UW(B) - Created using all four layers (*Till*, *Permeability*, *Airborne* and *Bedrock*), un-weighted; three zones.

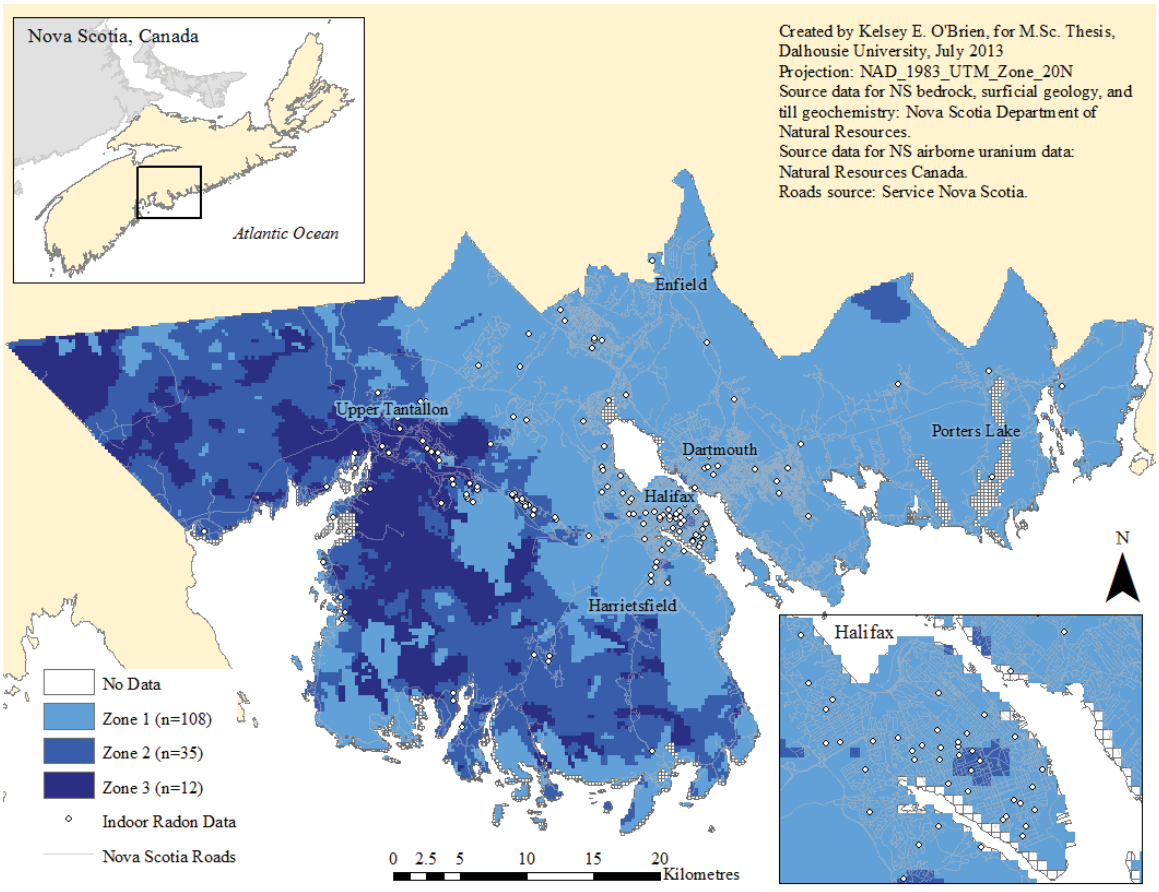

Figure B.6: Map 4W(B) - Created using all four layers (*Till*, *Permeability*, *Airborne* and *Bedrock*), weighted using the statistic regression; three zones.

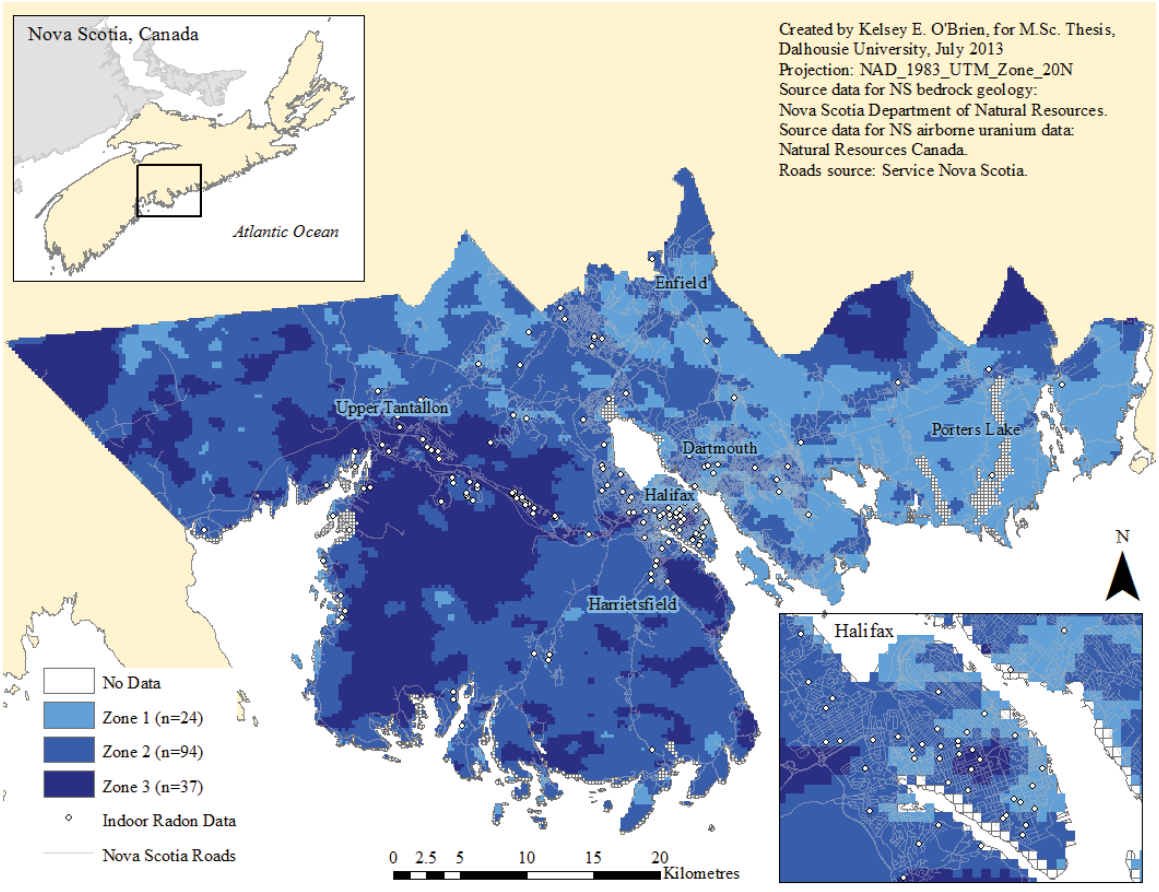

Figure B.7: Map 2UW(B) - Creating using only two layers (*Airborne* and *Bedrock*), as they were they only significantly correlated layers to indoor radon, three zones, un-weighted.

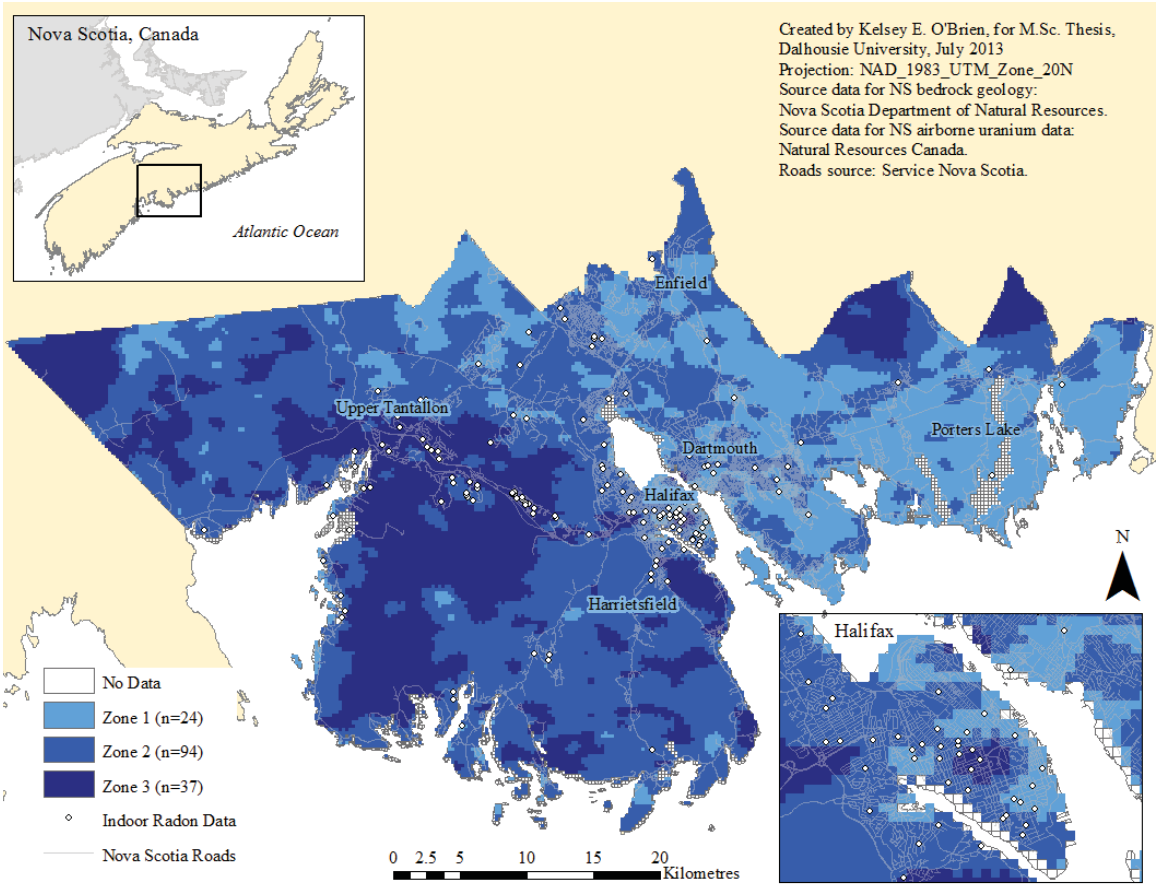

Figure B.8: Map 2W(B) - Creating using only two layers (*Airborne* and *Bedrock*), as they were they only significantly correlated layers to indoor radon. Both layers were weighted using the statistical regression, three zones.

Appendix C

Soil Column Additional Data

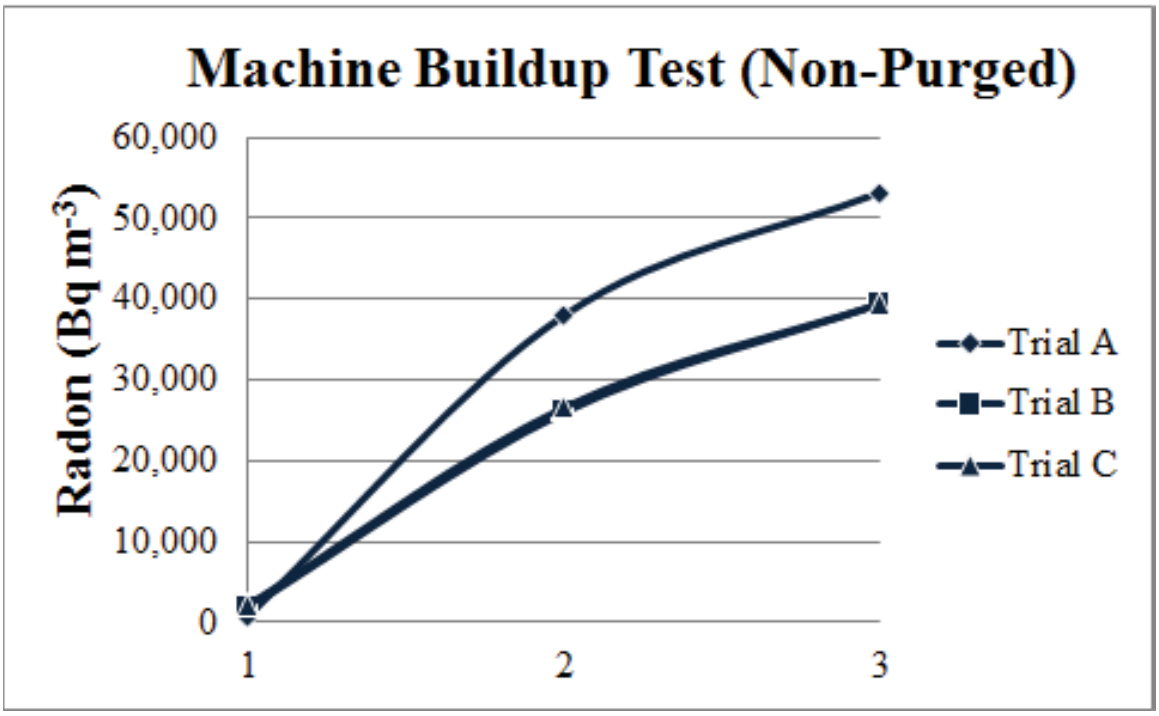

Figure C.1: Test of the RAD7 radon concentration buildup. Where 1 is a high radon zone, 2 is a low radon zone, and 3 is the same high radon zone. Results show three trials without purging the RAD7 for 5 minutes between each sample.

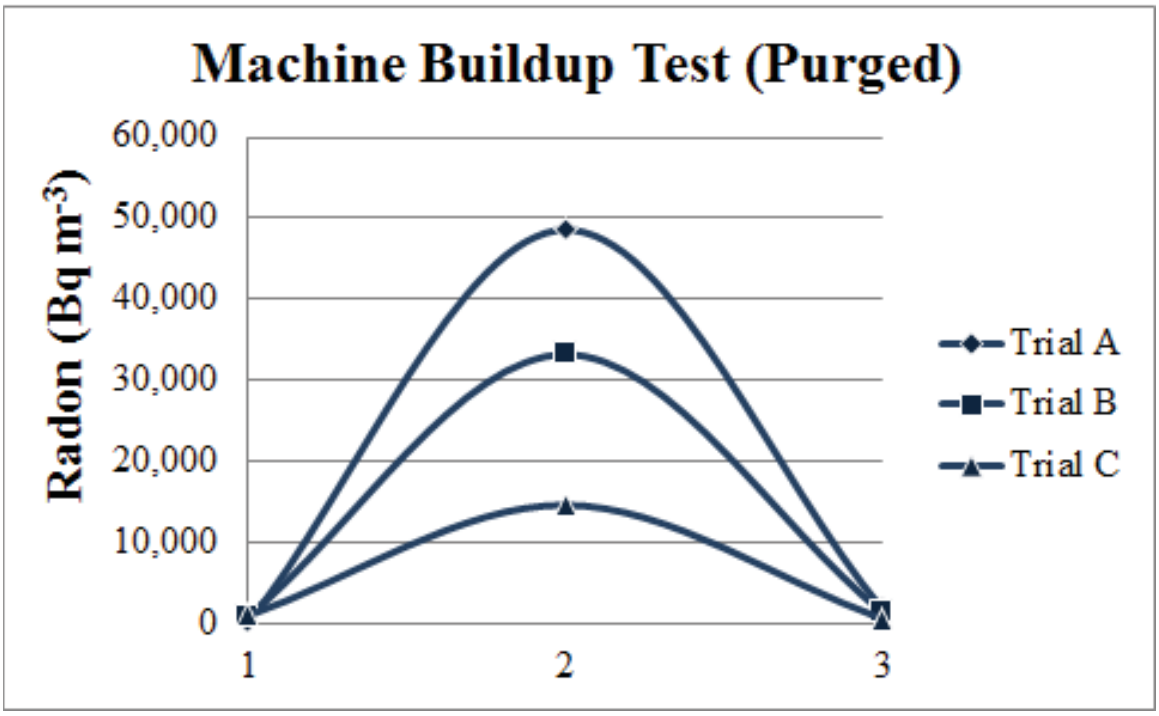

Figure C.2: Test of the RAD7 radon concentration buildup. Where 1 is a high radon zone, 2 is a low radon zone, and 3 is the same high radon zone. Results show three trials with purging the RAD7 for 5 minutes between each sample.

Table C.1: Determining moisture content of the dry tills. Baked 3 replicates of each column for 24 hours at 105 °C.

Column	Mass Lost (g)	Mass Lost (%)	Average % Lost per Column
1-A	0.7822	3.74	Col 1: 3.98
1-B	0.7901	4.09	—
1-C	0.8140	4.10	—
2-A	0.6891	4.48	Col 2: 4.28
2-B	0.8416	4.03	—
2-C	0.9951	4.32	—
3-A	0.0041	0.03	Col 3: 0.03
3-B	0.0035	0.03	—
3-C	0.0040	0.03	—
4-A	0.6482	4.84	Col 4: 4.34
4-B	0.5410	3.96	—
4-C	0.7716	4.21	—

Table C.2: Determining moisture content of the wet tills. Baked 3 replicates of each column for 24 hours at 105 °C.

Column	Mass Lost (g)	Mass Lost (%)	Average % Lost per Column
1-A	2.4449	10.04	Col 1: 11.15
1-B	2.7616	11.64	—
1-C	2.8044	11.78	—
2-A	2.8891	12.04	Col 2: 12.60
2-B	3.8441	14.31	—
2-C	2.7165	11.45	—
3-A	0.3375	1.46	Col 3: 1.57
3-B	0.3941	1.63	—
3-C	0.2646	1.61	—
4-A	2.7700	11.79	Col 4: 11.47
4-B	3.4114	10.29	—
4-C	2.5117	12.32	—

Table C.3: The measured CO_2 (ppm) detected in the columns at 10 cm (back) in the dry soils over a day to be used to calculate diffusivity. After calibration.

Hour	Column 1 CO_2 (ppm)	Column 2 CO_2 (ppm)	Column 3 CO_2 (ppm)	Column 4 CO_2 (ppm)
Background in Column	228.30	453.28	224.65	217.03
Initial Concentration	9,843.94	9,182.57	6,411.86	10,160.37
Hour 1	5,579.19	5,103.38	3,119.95	4,223.99
Hour 2	8,048.71	6,464.21	3,865.47	3,690.52
Hour 3	5,115.97	4,690.85	2,324.72	3,232.60
Hour 4	4,743.87	4,578.20	1,916.50	2,849.90
Hour 5	4,521.54	4,552.35	2,121.60	2,984.76

Table C.4: The measured CO_2 (ppm) detected in the columns at 10 cm (back) in the wet soils over a day to be used to calculate diffusivity. After calibration.

Hour	Column 1 CO_2 (ppm)	Column 2 CO_2 (ppm)	Column 3 CO_2 (ppm)	Column 4 CO_2 (ppm)
Background in Column	436.38	2,373.95	670.98	934.02
Initial Concentration	7,000.43	13,567.20	9,526.83	7,229.96
Hour 1	4,567.16	11,069.64	3,892.60	9,726.36
Hour 2	2,484.63	10,004.21	3,366.12	7,516.39
Hour 3	2,181.83	7,422.47	2,643.62	5,680.92
Hour 4	2,134.29	8,026.89	2,289.39	5,318.89
Hour 5	5,367.99	7,444.68	1,619.89	8,805.11

Table C.5: Granite replicate 1 of 3: breakdown of soil sieving. Where aggregates represent sediments still stuck together. Corr. Wt. is the corrected weight, Cum. Wt. is the cumulative weight, Cum. Pct. is the cumulative percent, and Ind. Pct. is the individual percentage. Using the Cole-Parmer USA Standard Test Sieves for the dry sieving, and the RO-TAO RX-29 sieve shaker.

Mesh	Held On (mm)	Raw Wt. (g)	Aggregates (%)	Corr. Wt. (g)	Cum. Wt. (g)	Cum. Pct. (%)	Ind. Pct. (%)
10	2	12.27	2	12.03	12.03	29.16	29.16
18	1	5.29	0	5.29	17.32	42.00	12.84
35	0.5	5.26	1	5.20	22.52	54.62	12.62
60	0.250	4.54	0	4.54	27.06	65.62	11.00
120	0.125	5.01	0	5.01	32.07	77.77	12.15
230	0.063	4.16	0	4.16	36.23	87.86	10.09
pan	< 0.063	5.00	0	5.00	41.24	100.00	12.14

Table C.6: Granite replicate 2 of 3: breakdown of soil sieving. Where aggregates represent sediments still stuck together. Corr. Wt. is the corrected weight, Cum. Wt. is the cumulative weight, Cum. Pct. is the cumulative percent, and Ind. Pct. is the individual percentage. Using the Cole-Parmer USA Standard Test Sieves for the dry sieving, and the RO-TAO RX-29 sieve shaker.

Mesh	Held On (mm)	Raw Wt. (g)	Aggregates (%)	Corr. Wt. (g)	Cum. Wt. (g)	Cum. Pct. (%)	Ind. Pct. (%)
10	2	9.31	3	9.03	9.03	22.62	22.62
18	1	5.71	1	5.65	14.69	36.77	14.16
35	0.5	5.47	0	5.47	20.15	50.46	13.68
60	0.250	4.65	0	4.65	24.81	62.11	11.65
120	0.125	5.16	0	5.16	29.97	75.02	12.91
230	0.063	4.45	0	4.45	34.41	86.15	11.13
pan	< 0.063	5.53	0	5.53	39.94	100.00	13.85

Table C.7: Granite replicate 3 of 3: breakdown of soil sieving. Where aggregates represent sediments still stuck together. Corr. Wt. is the corrected weight, Cum. Wt. is the cumulative weight, Cum. Pct. is the cumulative percent, and Ind. Pct. is the individual percentage. Using the Cole-Parmer USA Standard Test Sieves for the dry sieving, and the RO-TAO RX-29 sieve shaker.

Mesh	Held On (mm)	Raw Wt. (g)	Aggregates (%)	Corr. Wt. (g)	Cum. Wt. (g)	Cum. Pct. (%)	Ind. Pct. (%)
10	2	10.76	2	10.54	10.54	27.27	27.27
18	1	5.43	0	5.43	15.97	41.31	14.04
35	0.5	4.95	0	4.95	20.92	54.11	12.80
60	0.250	4.22	0	4.22	25.14	65.02	10.91
120	0.125	4.55	0	4.55	29.69	76.80	11.78
230	0.063	3.79	0	3.79	33.48	86.60	9.80
pan	< 0.063	5.18	0	5.18	38.66	100.00	13.40

Table C.8: Silica sand replicate 1 of 3: breakdown of soil sieving. Where aggregates represent sediments still stuck together. Corr. Wt. is the corrected weight, Cum. Wt. is the cumulative weight, Cum. Pct. is the cumulative percent, and Ind. Pct. is the individual percentage. Using the Cole-Parmer USA Standard Test Sieves for the dry sieving, and the RO-TAO RX-29 sieve shaker.

Mesh	Held On (mm)	Raw Wt. (g)	Aggregates (%)	Corr. Wt. (g)	Cum. Wt. (g)	Cum. Pct. (%)	Ind. Pct. (%)
10	2	0.01	0	0.01	0.01	0.02	0.02
18	1	0.07	0	0.07	0.07	0.18	0.16
35	0.5	10.54	0	10.54	10.61	26.29	26.10
60	0.250	16.63	0	16.63	27.25	67.49	41.20
120	0.125	9.70	0	9.70	36.95	91.52	24.03
230	0.063	2.81	0	2.81	39.76	98.50	6.97
pan	< 0.063	0.61	0	0.61	40.37	100.00	1.50

Table C.9: Silica sand replicate 2 of 3: breakdown of soil sieving. Where aggregates represent sediments still stuck together. Corr. Wt. is the corrected weight, Cum. Wt. is the cumulative weight, Cum. Pct. is the cumulative percent, and Ind. Pct. is the individual percentage. Using the Cole-Parmer USA Standard Test Sieves for the dry sieving, and the RO-TAO RX-29 sieve shaker.

Mesh	Held On (mm)	Raw Wt. (g)	Aggregates (%)	Corr. Wt. (g)	Cum. Wt. (g)	Cum. Pct. (%)	Ind. Pct. (%)
10	2	0.01	0	0.01	0.01	0.01	0.01
18	1	0.05	0	0.05	0.05	0.13	0.12
35	0.5	10.54	0	10.54	10.59	26.25	26.12
60	0.250	16.63	0	16.63	27.23	67.47	41.23
120	0.125	9.70	0	9.70	36.93	91.52	24.05
230	0.063	2.81	0	2.81	39.74	98.49	6.97
pan	< 0.063	0.61	0	0.61	40.35	100.00	1.51

Table C.10: Silica sand replicate 3 of 3: breakdown of soil sieving. Where aggregates represent sediments still stuck together. Corr. Wt. is the corrected weight, Cum. Wt. is the cumulative weight, Cum. Pct. is the cumulative percent, and Ind. Pct. is the individual percentage. Using the Cole-Parmer USA Standard Test Sieves for the dry sieving, and the RO-TAO RX-29 sieve shaker.

Mesh	Held On (mm)	Raw Wt. (g)	Aggregates (%)	Corr. Wt. (g)	Cum. Wt. (g)	Cum. Pct. (%)	Ind. Pct. (%)
10	2	0.04	0	0.04	0.04	0.15	0.15
18	1	0.04	0	0.04	0.08	0.33	0.18
35	0.5	5.96	0	5.96	6.04	26.01	25.68
60	0.250	9.41	0	9.41	15.45	66.56	40.55
120	0.125	5.63	0	5.63	21.08	90.82	24.26
230	0.063	1.80	0	1.80	22.88	98.56	7.74
pan	< 0.063	0.33	0	0.33	23.21	100.00	1.44

Table C.11: Radon concentrations through column 1 (wet). Where 1-3-A represent triplicates measured from the top down, and 1-3-B represent triplicates measured from the bottom up.

Trial	0 cm	10 cm	20 cm	30 cm	40 cm	50 cm	60 cm
1-A (Bq m^{-3})	13,400	10,300	8,420	6,980	5,070	3,320	1,380
2-A (Bq m^{-3})	11,900	11,700	10,100	8,670	7,160	6,500	5,060
3-A (Bq m^{-3})	9,050	8,400	8,810	7,570	5,780	5,160	3,940
1-B (Bq m^{-3})	6,640	5,380	6,200	8,010	9,570	7,850	8,810
2-B (Bq m^{-3})	8,500	6,260	7,290	8,430	9,290	7,640	7,400
3-B (Bq m^{-3})	6,850	5,780	6,640	6,710	7,090	6,780	8,980

Table C.12: Radon concentrations through column 1 (dry). Where 1-3-A represent triplicates measured from the top down, and 1-3-B represent triplicates measured from the bottom up.

Trial	0 cm	10 cm	20 cm	30 cm	40 cm	50 cm	60 cm
1-A (Bq m^{-3})	5,620	3,950	4,390	2,610	2,170	1,150	505
2-A (Bq m^{-3})	5,790	4,430	5,130	3,400	2,760	1,840	817
3-A (Bq m^{-3})	5,720	4,390	2,640	2,740	1,660	1,320	505
1-B (Bq m^{-3})	5,240	4,700	5,650	5,480	3,400	4,120	3,680
2-B (Bq m^{-3})	7,090	6,370	7,020	5,510	5,130	5,340	5,030
3-B (Bq m^{-3})	5,890	5,510	6,980	6,090	4,550	4,280	4,280

Table C.13: Radon concentrations through column 2 (wet). Where 1-3-A represent triplicates measured from the top down, and 1-3-B represent triplicates measured from the bottom up.

Trial	0 cm	10 cm	20 cm	30 cm	40 cm	50 cm	60 cm
1-A (Bq m^{-3})	16,600	13,200	13,200	10,800	9,220	8,390	6,090
2-A (Bq m^{-3})	10,900	9,830	11,000	11,300	9,100	10,000	8,960
3-A (Bq m^{-3})	9,570	7,920	7,640	7,960	6,020	5,920	10,000
1-B (Bq m^{-3})	8,840	10,900	11,300	8,330	8,740	8,080	11,200
2-B (Bq m^{-3})	12,500	13,100	11,000	9,000	8,240	9,690	10,700
3-B (Bq m^{-3})	10,800	11,300	8,260	8,100	5,820	5,680	5,030

Table C.14: Radon concentrations through column 2 (dry). Where 1-3-A represent triplicates measured from the top down, and 1-3-B represent triplicates measured from the bottom up.

Trial	0 cm	10 cm	20 cm	30 cm	40 cm	50 cm	60 cm
1-A (Bq m^{-3})	7,920	6,810	6,260	6,060	6,160	5,130	5,310
2-A (Bq m^{-3})	7,980	7,020	5,350	5,410	4,600	5,000	4,060
3-A (Bq m^{-3})	7,870	6,470	6,440	5,610	5,310	5,110	5,180
1-B (Bq m^{-3})	2,070	3,450	3,590	4,060	3,780	4,260	4,290
2-B (Bq m^{-3})	7,300	2,090	3,880	3,860	4,120	3,850	4,490
3-B (Bq m^{-3})	5,240	6,810	7,290	5,303	4,830	5,610	5,130

Table C.15: Radon concentrations through column 3 (wet). Where 1-3-A represent triplicates measured from the top down, and 1-3-B represent triplicates measured from the bottom up.

Trial	0 cm	10 cm	20 cm	30 cm	40 cm	50 cm	60 cm
1-A (Bq m^{-3})	745	1,390	1,560	1,190	1,260	1,600	749
2-A (Bq m^{-3})	472	707	745	711	842	610	237
3-A (Bq m^{-3})	404	539	606	573	404	371	135
1-B (Bq m^{-3})	337	202	135	236	236	371	337
2-B (Bq m^{-3})	337	202	101	135	269	236	269
3-B (Bq m^{-3})	168	202	135	101	236	101	202

Table C.16: Radon concentrations through column 3 (dry). Where 1-3-A represent triplicates measured from the top down, and 1-3-B represent triplicates measured from the bottom up.

Trial	0 cm	10 cm	20 cm	30 cm	40 cm	50 cm	60 cm
1-A (Bq m^{-3})	576	643	610	745	677	406	511
2-A (Bq m^{-3})	576	406	1190	987	545	685	513
3-A (Bq m^{-3})	303	404	1080	847	610	508	339
1-B (Bq m^{-3})	404	236	135	371	404	404	404
2-B (Bq m^{-3})	477	67.7	440	406	542	373	477
3-B (Bq m^{-3})	406	135	101	269	404	539	472

Table C.17: Radon concentrations through column 4 (wet). Where 1-3-A represent triplicates measured from the top down, and 1-3-B represent triplicates measured from the bottom up.

Trial	0 cm	10 cm	20 cm	30 cm	40 cm	50 cm	60 cm
1-A (Bq m^{-3})	159,000	94,000	77,200	62,200	52,500	37,800	19,400
2-A (Bq m^{-3})	125,000	91,100	72,400	61,500	51,400	39,600	25,700
3-A (Bq m^{-3})	106,000	74,600	66,500	52,900	43,200	35,500	24,200
1-B (Bq m^{-3})	125,000	110,000	97,600	96,200	89,600	93,700	60,600
2-B (Bq m^{-3})	113,000	120,000	80,000	91,100	78,500	66,700	47,300
3-B (Bq m^{-3})	79,000	97,700	93,300	66,200	53,700	54,600	41,800

Table C.18: Radon concentrations through column 4 (dry). Where 1-3-A represent triplicates measured from the top down, and 1-3-B represent triplicates measured from the bottom up.

Trial	0 cm	10 cm	20 cm	30 cm	40 cm	50 cm	60 cm
1-A (Bq m^{-3})	144,000	105,000	92,900	67,900	53,600	42,300	22,900
2-A (Bq m^{-3})	124,000	91,600	80,200	63,400	54,700	47,800	27,000
3-A (Bq m^{-3})	110,000	76,900	63,300	54,400	43,000	33,900	19,000
1-B (Bq m^{-3})	52,400	81,700	92,000	84,000	93,000	67,400	77,600
2-B (Bq m^{-3})	52,400	84,300	72,500	75,900	67,500	65,300	71,900
3-B (Bq m^{-3})	56,400	90,100	114,000	32,100	93,200	98,000	90,700

Bibliography

Appleton, J. (2007). Radon: Sources, health risks, and hazard mapping. *Royal Sweedish Academy of Sciences*, 36:85–89.

Appleton, J. and Miles, J. (2010). A statistical evaluation of the geogenic controls on indoor radon concentrations and radon risk. *Journal of Environmental Radioactivity*, 101:799–803.

Appleton, J., Miles, J., Green, B., and Larmour, R. (2008). Pilot study of the application of Tellus airborne radiometric and soil geochemical data for radon mapping. *Journal of Environmental Radioactivity*, 99:1687–1697.

Appleton, J., Miles, J., and Young, M. (2011). Comparison of Northern Ireland radon maps based on indoor radon measurements and geology with maps derived by predictive modelling of airborne radiometric and ground permeability data. *Science of the Total Environment*, 409:1572–1583.

ASTDR (2012). Toxicological profile for radon. From: US Department of Health and Human Services, Agency for Toxic Substances and Disease Registry.

Ball, B., Scott, A., and Parker, J. (1999). Field N_2O, CO_2 and CH_4 fluxes in relation to tillage, compaction and soil quality in Scotland. *Soil and Tillage Res.*, 53:29.

Ball, T., Cameron, D., Colman, T., and Roberts, P. (1993). The use of uranium exploration data for mapping radon potential in the UK - advantages and pitfalls. From: Proceedings of a technical Committee, International Atomic Energy Agency.

Boehner, R., Adams, G., and Giles, P. (2002). Karst geology in the salt-bearing Windsor Group evaporites and control on the origin of gypsum deposits in south-central Cape Breton Island, Nova Scotia. *Mineral Resources Branch, Report of Activities 2002; Nova Scotia Department of Natural Resources*, ME 2003-1:9–24.

Borgoni, R., Tritto, V., Bigliotto, C., and de Bartolo, D. (2011). A geostatistical approach to asses spatial association between indoor radon characteristics, geological features and building characteristics: The case of Lombarby, Northern Italy. *International Journal of Environmental Research and Public Health*, 8:1420–1440.

Bourdon, B. (2003). *Uranium-series Geochemistry*. Mineralogical Society of America.

Chao, C., Tung, T., and Burnett, J. (1997). Influence of ventilation on indoor radon level. *Build. and Environ.*, 32(6):527–534.

Chen, J. (2009). A preliminary design of a radon potential map for Canada: a multi-tier approach. *Environ. Earth Sciences*, 58:775–782.

Chen, J., Falcomer, R., Bergman, L., Wierdsma, J., and Ly, J. (2009). Correlation of soil radon and permeabiltiy with indoor radon potential in Ottawa. *Radiat. Prot. Dosim.*, 136:56–60.

Chen, J., Jiang, H., Tracy, B., and Zielinski, J. (2008a). A preliminary radon map for Canada according to health region. *Radiat. Prot. Dosim.*, 130:92–94.

Chen, J., Ly, J., Bergman, L., Wierdsma, J., and Klassen, R. (2008b). Variation of soil radon concentrations in Southern Ontario. *Radiat. Prot. Dosim.*, 131:385–389.

Damkjaer, A. and Korsbech, U. (1992). A small-diameter probe for in situ measurements of gas permeability of soils. *Radiat. Prot. Dosim.*, 45:85–89.

DPME (1982). Uranium in Nova Scotia: a background summary for the uranium inquiry, Nova Scotia. From: Nova Scotia Department of Mines and Energy Report 82-7.

Dubois, G. (2005). An overview of radon surveys in Europe. *European Commission*, pages 1–168.

Dyck, W., Chatterjee, A., Gemmell, D., and Murricane, K. (1976). Well water trace element reconnaissance, eastern Maritime Canada. *Journal of Geochemical Exploration*, 6:139–162.

EPA (1993). Environmental Protection Agency: Protocols for radon and radon decay product measurements in homes. *Office of Air and Radiation*, 6604J(402-R-93-003).

Espinosa, G. and Gammage, R. (2003). A representative survey of indoor radon in the sizteen regions in Mexico City. *Radiat. Prot. Dosim.*, 103:73–76.

Finck, P. and Graves, R. (1987). Glacial geology of Halifax and Sambro Nova Scotia. *Nova Scotia Department of Mines and Energy. Scale 1:50 000*, map 87-2.

Fisher, B. E. (2006). Regional till and rock geochemical surveys of the South Mountain Batholith by the Nova Scotia Department of Natural Resources over western Nova Scotia. *DP ME 137, Version 2.*

Ford, K., Carson, J., Grant, J., and Holman, P. (1998). Radioactivity map of Nova Scotia, equivalent uranium (ppm). *Geological Survey of Canada. Scale 1:500 000*, Map 35006G, sheet 3 of 9.

Ford, K., Savard, M., Dessau, J., and Pellerin, E. (2001). The role of gamma-ray spectrometry in radon risk evaluation: A case history from Oka, Quebec. *Geoscience Canada*, 28(2):59–64.

Freeze, R. and Cherry, J. (1979). *Groundwater*. Prentice-Hall, Inc., New Jersey.

Friske, P., Ford, K., Kettles, I., McCurdy, M., Mc-Neil, R., and Harvey, B. (2010). North American soil geo-chemical landscapes project: Canadian field protocols for collecting mineral soils and measuring soil gas radon and natural radioactivity. *Geol. Surv. of Can.*, Open File 6282:177.

Goodwin, T. (2002). Soil and till geochemistry of the Halifax Regional Municipality, Nova Scotia. *Nova Scotia Department of Natural Resources, Mineral Resources Branch, Report of Activities*, ME 2003-1:41–47.

Goodwin, T., McIsaac, E., Ford, K., and Friske, P. (2008). Radon soil gas in the Halifax Regional Municipality: Should we be concerned? *Nova Scotia Department of Natural Resources, Mineral Resources Branch, Report of Activities*, ME 2009-1:35–44.

Goodwin, T., O'Brien, K., Ford, K., and Friske, P. W. B. (2010). Radon soil gas in the Halifax Regional Municipality: Progress report on the 2009 sampling program. *Mineral Resources Branch, Report of Activities 2010, Nova Scotia Department of Natural Resources*, ME 2010-1:29–34.

Goodwin, T. A., Ford, K., Friske, P., and McIsaac, E. (2009). Radon soil gas in Nova Scotia. *Mineral Resources Branch, Report of Activities 2008, ed. D. R. MacDonald and K. A. Mills; Nova Scotia Department of Natural Resources*, ME 2009-1:25–34.

Grantham, D. (1986). The occurrence and significance of uranium, radium, and radon in the water supplies in Nova Scotia. *Nova Scotia Department of Health*, ME 1986-70.

Groves-Kirkby, C., Denman, A., Crockett, R., Phillips, P., Woolridge, A., and G.K, G. (2006). Time-integrating radon gas measurements in domestic premises: comparison of short-, medium- and long-term exposures. *J. Environ. Radioact.*, 86:92–109.

HC (2010a). Guidelines for Canadian drinking water quality. From: Health Canada Radiological Parameters.

HC (2010b). Health Canada cross-Canada survey of radon concentrations in homes year 1 interim report. Health Canada.

HC (2012). Health Canada: Radon. *Radiation Protection Bureau, Healthy Environments and Consumer Safety Branch, Health Canada*, H13-7/119-2012E-PDF.

Hicks, R., Jamieson, R., and Reynolds, P. (1999). Detrital and metamorphic $^{40}Ar/^{39}Ar$ ages from muscovite and whole-rock sample, Meguma Supergroup, southern Nova Scotia. *Can. J. Earth Eci.*, 36:23–32.

Hillel, D. (1998). *Environmental Soil Physics*. Academic Press, San Diego.

Hillel, D. (2004). *Introduction to Environmental Soil Physics*. Elsevier Science, California.

Holkko, J. and Liukkonen, S. (1992). Radon diffusion in Finnish glacial till soil. *Radiat. Prot. Dosim.*, 45(1):231–233.

Jackson, S. (1990). A survey to measure domestic concnetrations of radon gas in nova scotia. Nova Scotia Department of the Environment, unpublished report.

Jackson, S. (1992). Estimating radon potential from an aerial radiometric survey. *Health Physics Society*, 62(5):450–452.

Jamieson, R., Hart, G., Chapman, G., and Tobey, N. (2012). The contact aureole of the South Mountain Batholith in Halifax, Nova Scotia: geology, mineral assemblages, and isograds. *Can. J. Earth Sci.*, 49:1280–1296.

Je, I. (1998a). Bedrock structure control on soil-gas radon-222 anomalies in the Toronto area. *Environ. Eng. Geosci.*, 4:445–454.

Je, I. (1998b). Soil-gas radon-222 anomalies in the south central Ontario, Canada. From: M.Sc. Thesis, University of Toronto.

Jellick, G. and Schnabel, R. (1986). Evalutaion of a field methods for determining the gas diffusion coefficient in soils. *Soil Sci. Soc. Am.*, 50:18–23.

Jiranek, M. and Svoboda, Z. (2007). Numerical modelling as a tool for optimization of sub-slab depressurisation systems design. *Build. Environ.*, 42:1994–2003.

Jiranke, M., Neznal, M., and Neznal, M. (1999). Sub-slab depressurisation systems: efectiveness and soil permeability. *Radon in the Living Environ.*, pages 19–23.

Johner, H. and Surbeck, H. (2001). Soil gas measuremente below foundation depth improve indoor radon prediction. *Sci. of the Total Env.*, 272:337–341.

Keen, B. (1931). The physical properties of soil. *New York: Longman Greenand Company*, page 380.

Kemski, J., Klingel, R., and Siehl, A. (2009). From radon hazard to risk prediction-based on geologic maps, soil gas and indoor measurements in Germany. *Environ. Geol.*, 56:1269–1279.

Kemski, J., Klingel, R., Siehl, A., and Valdivia-Manchego, M. (2006). Radon risk prediction in Germany based on gridded geological maps and soil measurements. *Radon investigations in Czech Republic XI and the 8th international workshop on the geolocial aspects of radon risk mapping*, pages 139–156.

Keppie, J. D. (2006). Geological map of the province of Nova Scotia, scale 1:500 000. *Digital Version of Nova Scotia Department of Natural Resources Map ME 2000-1*, DP ME 043, Version 2.

Keppler, H. and Wyllie, P. (1990). Role of fluids in transport and fractionation of uranium and thorium in magmatic processes. *Nature*, 348.

Lavoie, D., Sangster, D., Savard, M., and Fallara, F. (1995). Multiple creccia events in the lower part of the Carboniferous Windsor Group, Nova Scotia. *Atlantic Geology*, 31:197–207.

Letourneau, E., Zielinski, J., Krewski, D., and McGregor, R. (1992). Levels of radon gas in Winnipeg homes. *Radiat. Prot. Dosim.*, 45:531–534.

Lewis, C., Taylor, B., Stea, R., Fader, G., Horne, R., MacNeill, S., and Moore, J. (1998). Earth science and engineering: urban development in the metropolitan Halifax region. *Urban Geology of Canadian Cities, Edited by. P.F. Karrow and O.L. White. Geologic. Assoc. Can.*, Special Paper 42:409–444.

MacDonald, M. (1994). Geological map of the South Mountain Batholih, western Nova Scotia. *Nova Scotia Depart. of Natural Resources, scale 1:250 000*, Map 94-01.

MacDonald, M. and Horne, R. (1987). Geological map of Halifax and Sambro (nts sheets 11 d/12 and 11 d/05), Nova Scotia. *Nova Scotia Depart. of Mines and Energy, scale 1:50 000*, Map 87-6.

MacDonald, M., Horne, R., Corey, M., and Ham, L. (1992). An overview of recent bedrock mapping and follow-up petrological studies of the South Mountain Batholith, southwestern Nova Scotia, Canada. *Atlantic Geology*, 28:7–28.

MacHattie, T. and O'Reilly, G. (2008). Timing of iron oxide-copper-gold (IOGC) mineralization and alteration along the Cobequid-Chedabucto fault zone. *Nova Scotia Depart. of Natural Resources, Report of Activities 2008*, ME 2009-1:63–69.

Menetrez, M. and Mosley, R. (1996). Evaluation of radon emanation from soil with varying moisture content in a soil chamber. *Environ. Int.*, 22(1):S447–S453.

Mersereau, H., Scott, A., and Whelan, K. (2013). Workplace indoor radon survey in Nova Scotia, Canada. *Environmental Health Review*, 56(1):13–18.

Miles, J. and Appleton, J. (2005). Mapping variation in radon potential both between and within geolocial units. *Journal of Radiological Protection*, 25:257–276.

Miles, J. and Ball, K. (1996). Mapping radon-prone areas using house radon data and geolocial boundaries. *Environment International*, 22:779–782.

Mose, D., Mushrush, G., and Chrosniak, C. (1992). Soil radon, permeability, and indoor radon prediction. *Environ. Geol. Water Sci.*, 19:91–96.

Nazaroff, W. (1992). Radon transport from soil to air. *Reviews of Geophysics*, 30:137–160.

Neznal, M. and Neznal, M. (2005). Permeability as an important parameter for radon risk classification of foundation soils. *Annals of Geophysics*, 48:175–180.

Neznal, M., Neznal, M., Matolin, I. B., Barnet, I., and Miksova, J. (2006). The new method for assessing the radon risk of building sites. *Czech Geol. Surv.*, 16:1–48.

NSDPE (2009). Nova Scotia Department of Education: Education department radon testing 2008. `http://www.gov.ns.ca/nse/airlandwater/docs/Radon-Results2008-06-Education.pdf`.

O'Beirne-Ryan, A. (2006). Weathering history of granitoids of the South Mountain Batholith, N.S., Canada: Mineralogy, geochemistry and environmental implications of saprolites. PhD Thesis, Dalhousie University.

O'Beirne-Ryan, A. and Zentilli, M. (2006). Weathering of Devonian monzogranites as recorded in the geochmistry of saprolites from the South Mountain Batholith, Nova Scotia, Canada. *Atlan. Geol.*, 42:151–157.

O'Brien, K. (2010). Radon soil gas within the Halifax Regional Municipality, Nova Scotia. Honours Thesis, St Francis Xavier University.

O'Brien, K., Goodwin, T., and Risk, D. (2011). Radon soil gas in the Halifax Regional Municipality, Nova Scotia, Canada. *Atlan. Geol.*, 47:112–124.

O'Reilly, G. (2008). Map showing potential for radon in indoor air in Nova Scotia. *NSDNR Mineral Resources Branch, Report of Activities*, ME 2009 1:111–113.

O'Reilly, G., Corey, M., and Ford, K. (1988). The role of airborne gamma-ray spectrometry in bedrock mapping and mineral exploration: case studies from granitic rocks within the Meguma zone, Nova Scotia. *Maritime Sediments and Atlantic Geology*, 24:47–60.

O'Reilly, G., Goodwin, T., and Drage, J. (2009a). Map showing potential for uranium and related radionuclides in groudnwater in Nova Scotia. *Nova Scotia Department of Natural Resources, Mineral Resources Branch. Scale 1:1 000 000*, ME 2009-7.

O'Reilly, G., Goodwin, T., and Fisher, B. (2009b). A GIS-based approach to producing a map showing the potential for radon in indoor air in Nova Scotia. *NSDNR Mineral Resources Branch, Report of Activities*, ME 2010-1:95–97.

Otton, J., Gundersen, L., Schumann, R., Reimer, G., and Duval, J. (1993). Uranium resource assesment and exploration data for geologic radon potential assesment in the United States. From: Proceedings of a technical Committee, International Atomic Energy Agency.

Parsons, A. (2007). Potential for uranium mobilization from weathered outcrops of uranium-bearing sedimentary strata, southern Nova Scotia. From: Honours Thesis, Dalhousie University.

Penman, R. (1940). Gas and vapour movement in soil: The diffusion of vapours thourgh porous solids. *J. Agric. Sci.*, 30:437–462.

Risk, D., Kellman, L., and Beltrami, H. (2008). A new method for in situ gas diffusivity measurement and applications in the monitoring of subsurface CO_2 production. *J. Geophys. Res.*, 113:1–9.

Rolston, D., Glauz, R., Grundmann, G., and Louie, D. (1991). Evaluation of an in situ method for measurement of gas diffusivity in surface soils. *Soil Sci. Soc. Am.*, 55:1536–1542.

Russell, M. B. (1952). *Soil aeration and plant growth, in Soil Physical Conditions and Plant Growth*. Academic, New York.

Ryan, R. and O'Beirne-Ryan, A. (2007). Preliminary report on the origin of uranium occurences in the Horton group of the Windsor area, Nova Scotia. *Nova Scotia Department of Natural Resources, Mineral Resources Branch, Report of Activities*, ME-2007-1:137–157.

Ryan, R. and O'Beirne-Ryan, A. (2009). Uranium occurences in the Horton group of the Windsor area, Nova Scotia and the environmental implications for the Maritimes Basin. *Atlan. Geol.*, 45:171–190.

Ryan, R., O'Beirne-Ryan, A., Finlayson, D., and Parson, A. (2009). Mobility of uranium and radon associated with uranium roll front occurences in the Horton group of the Windsor area, Nova Scotia, Canada. *Nova Scotia Department of Natural Resources, Mineral Resources Branch, Report of Activities*, ME 2010-1:162–165.

Selinus, O., Alloway, B., Centeno, J., Finkelman, R., Fuge, R., Lindh, U., and Smedley, P. (2005). *Essentials of Medical Geology: Impacts of the natural environment on public health*. Elsevier Avademic Press.

Shi, X., Hoftiezer, D., Duell, E., and Onega, T. (2006). Spatial association between residential radon concentration and bedrock types in New Hampshire. *Environ. Geol.*, 51:65–71.

Shives, R., Ford, K., and Charbonneau, B. (1995). Applications of gamma ray spectrometry / magnetic / vlf-em surveys. *Geological Survey of Canada*, Open File 3061:7.

Silker, W., Wogman, N., Thomas, C., Carr, D., and Hesler, P. (2007). Measurement of radon diffusion and exhalation from uranium mill tailings piles. *Environ. Sci. Technol.*, 13(8):962–964.

Solcova, O., Snajdaufova, H., and Schneider, P. (2001). Multicomponent counter-current gas diffusion in porous solids: the Graham's-law diffusion cell. *Chemical Engineering Science*, 56:5231–5237.

Stea, R., Conley, H., and Brown, Y. (1992). Surficial Geology Map of the Province of Nova Scotia. *DP ME 36, Version 2*.

Stea, R. and Finck, P. (2001). An evolutionary model of glacial disperal and till genesis in Maritime Canada. *Geological Society, London, Special Publication*, 185:237–265.

Stea, R. and Fowler, J. (1979). Pleistocene geology of the eastern shore region Nova Scotia (sheet 3). *Nova Scotia Department of Mines and Energy,Scale 1:100 000*, Map 79-3.

Stea, R. and Fowler, J. (1981). Pleistocene geology and till geochemistry of central Nova Scotia (sheet 4). *Nova Scotia Department of Mines and Energy,Scale 1:100 000*, Map 81-1.

Stea, R. and O'Reilly, G. (1982). Till geochemistry of the Meguma terrane in Nova Scotia and its metallogenic implications. *Institute of Mining and Metullurgy, London*, 5th Symposium on Prospecting in Glaciated Terrain:82–104.

UNSCLEAR (2006). Sources-to-effects assesment for radon in homes and workplaces. From: United Nations Scientific Committee on the Effects of Atomic Radiation 2006 Report Vol. II.

USEPA (1993). EPA's map of radon zones, national summary. *United States Environmental Protection Agency Air and Ratiation*, pages 1–48.

Utting, D. J. (2009). LiDAR-based glacial geology of the Halifax metropolitan area. *Mineral Resources Branch, Report of Activities 2008, eds. D. R. MacDonald and K. A. Mills*, ME 2009-1:129–137.

Washington, J. and Rose, A. (1990). Regional and temporal relations of radon in soil gas to soil temperature and moisture. *Geophysical Research Letters*, 17:829–832.

Washington, J., Rose, A., Ciolkosz, J., and Dobos, R. (1994). Gaseous diffusion and permeability in four soil profiles in central Pennsylvania. *Soil Sci.*, 157:65–76.

White, C. (2010). Stratigraphy of the Lower Paleozoic Goldenville and Halifax groups in southwestern Nova Scotia. *Atlan. Geol.*, 46:136–154.

White, C. E. (2002). Preliminary bedrock geology of the area between Chebogue Point, Yarmouth County, and Cape Sable Island, Shelburne Country, southwestern Nova Scotia. *Mineral Resources Branch Report of Activities 2002; Nova Scotia Department of Natural Resources*, ME 2003-1:127–145.

White, C. E., Bell, J. A., McLeish, D. F., MacDonald, M. A., Goodwin, T. A., and MacNeil, J. D. (2007). Preliminary bedrock geology of the Halifax map area (nts 11d/12), southern Nova Scotia. Mining Matters Report.

White, C. E., Bell, J. A., McLeish, D. F., MacDonald, M. A., Goodwin, T. A., and MacNeil, J. D. (2008). Geology of the Halifax Regional Municipality. *Mineral Resources Branch Report of Activities 2007. Edited by D. R. MacDonald; Nova Scotia Department of Natural Resources*, ME 2008-001:125–139.

WHO (2005). Radon and cancer. `http://www.who.int/media-centre/factsheets/fs291/en/index.html`. World Health Organization Fact Sheet No. 291.

Wichmann, H., Heinrich, J., Gerke, M., Kreuzer, M., Wellmann, J., Keller, G., and Kreienbrock, L. (2002). Domestic radon and lung cancer- current status including new evidence from Germany. *Internation Congress Series*, 1225:247–252.

Yu, K., Koo, V., and Guan, Z. (2002). A simple and versatile ^{222}Rn/^{220}Rn exposure chamber. *Nucl. Instrum. Methods Phys. Res., Sect. A*, 481:749–755.